University of Alberta

Disturbance Observer Design for Robotic and Telerobotic Systems

by

Alireza Mohammadi

A thesis submitted to the Faculty of Graduate Studies and Research
in partial fulfillment of the requirements for the degree of

Master of Science

in

Controls

Department of Electrical and Computer Engineering

Fall 2011

Edmonton, Alberta

To My Dearest Parents and Brother

Abstract

Employing disturbance observers is an effective way of enhancing the stability and performance of the control systems subject to disturbances. Disturbance observers have been extensively used for control of mechatronic systems since their introduction in the 1980s.

This thesis studies the design of nonlinear disturbance observers for robotic manipulators and their applications in the control of telerobotic systems. A novel framework is introduced, based on linear matrix inequalities, for the design of nonlinear disturbance observers for serial robotic manipulators. This design method removes the restrictions encountered in previous design methods.

In spite of the many applications of the disturbance observers in mechatronic systems, there are few studies that address the design of such observers for telerobotic systems. Moreover, these studies cannot guarantee the stability of telerobotic systems with time delay. This thesis presents a rigorous theoretical basis for the disturbance observer based control of telerobotic systems with variable time delays.

Acknowledgement

I would like to thank my supervisors, Dr. Horacio J. Marquez and Dr. Mahdi Tavakoli, for their inspiring guidance and invaluable support throughout my research.

I am greatly indebted to my parents and brother for their unfailing love and support. Without my parents' support my education would have been impossible. I wish to extend my gratitude to all my friends and colleagues at the Advanced Control Systems Lab and the Telerobotic and Biorobotic Systems Group at the University of Alberta for their help and support. I would also like to sincerely thank the Jakeway family for their friendship in the course of my studies at the University of Alberta in Edmonton.

Contents

List of Tables

List of Figures

List of Abbreviations

LTI Linear time invariant

DOF Degree of freedom

DOB Disturbance observer

NLDOB Nonlinear disturbance observer

SISO Single-input and single-output

MIMO Multiple-input and Multiple-output

LMI Linear matrix inequality

Chapter 1

Introduction

1.1 Intorduction

A profound concept in the systems and control literature is that of *observers*. An observer is a device used to reconstruct the states of a dynamical system from input-output measurements. Observers can be employed in numerous applications such as feedback control, system health monitoring, and fault detection [1].

In the late 1980s, a new type of observer referred to as "disturbance observer", was introduced for control of mechatronic systems [2, 3]. Unlike state observers that are used to reconstruct the unknown states of a system, disturbance observers are used to estimate the unknown inputs of a system [1]. Disturbance observers are used to estimate and suppress unknown disturbances acting on control systems and thus enhance their stability and performance. A disturbance observer may also be used to reduce the number of costly sensors needed in a control system [1]. Since their advent, disturbance observers have been employed successfully in applications such as control of direct drive motors [4], active car steering [5], control of DC servomotors [6], and current control of induction motors [7].

The disturbance observer concept has inspired a wide variety of applications in the robotics context as well as other fields of mechatronics. Disturbance observers are used to estimate unknown forces/torques in robotic manipulators. A typical disturbance observer that is used in a robotic system is shown in Figure 1.1. As it can be seen, the disturbance observer uses the known forces/torques applied to the robot and the measured output variables to estimate the unknown forces/torques that are exerted to the robot.

A considerable part of the existing literature on disturbance observer design for robotic applications uses linearized models or linear system techniques [8, 9, 10, 11]. Robotic manipulators, however, are nonlinear and coupled systems. There exists no

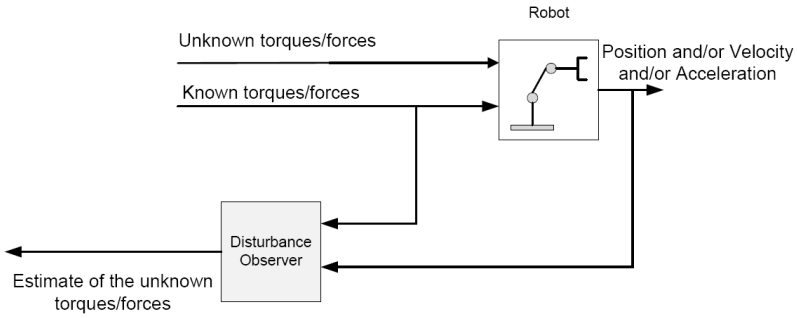

Figure 1.1: Block diagram of a typical disturbance observer used in a robotic system.

rigorous proof regarding the stability and performance of nonlinear robotic systems that use such linear disturbance observers [12, 13]. On the other hand, the proposed nonlinear disturbance observers in the literature assume certain restrictions on the configuration of the robotic manipulators. This serves as the motivation to seek a general framework for the design of disturbance observers for robotic manipulators.

A natural extension of the applications of the robotic disturbance observers is to use them in telerobotic systems [14]. Ability to reject disturbances is of great importance in distant environments where the remote robot is subject to unknown forces and disturbances and the human operator cannot easily access the remote robot. Teleoperation tasks, however, often involve time delays in the communication channel between the local robot and the remote robot [15]. The communication channel time delay can severely affect the stability and performance of the telerobotic system. Therefore, it is desirable to benefit from disturbance observers in telerobotic systems while the stability of the system is guaranteed in the presence of communication time delays.

1.2 Contributions of the Thesis

This thesis studies the design of nonlinear disturbance observers for robotic manipulators and their application in the control of telerobotic systems. The contributions of this thesis are twofold:

1. *Nonlinear disturbance observer design for robotic manipulators:* This thesis presents a general systematic approach, based on linear matrix inequalities (LMIs), to solve the disturbance observer design problem for serial robotic manipulators without the restrictions that have existed in the previous design methods. The proposed design method unifies the linear and nonlinear disturbance observers in a general framework.

2. *Disturbance observer based control of bilateral teleoperation systems with variable time delay:* This thesis presents a rigorous theoretical basis for the disturbance observer based control of teleoperation systems with variable time delays.

1.3 Organization of the Thesis

The rest of the thesis is organized in the following way:

- *Chapter 2. Background:* In this chapter, the applications of disturbance observers in robotic systems, and a brief literature review of disturbance observer design methods for such systems is presented first. Next, telerobotic (teleoperation) systems, their application, and an overview of the control of these systems is introduced. Lastly, the importance of disturbance observers in the control of telerobotic systems is described.
- *Chapter 3. Nonlinear Disturbance Observer Design for Single Robotic Manipulators:* This chapter starts by providing background information about the adynamic equations of robotic manipulators, their inherent properties, and the previous linear and nonlinear disturbance observers that have been proposed for robotic manipulators in the literature. Next, this chapter presents a general systematic approach, based on linear matrix inequalities (LMIs), to solve the disturbance observer design problem for serial robotic manipulators without restrictions on the number of degrees-of-freedom (DOFs), the types of joints, or the manipulator configuration. This chapter concludes with simulation studies to show the effectiveness of the proposed disturbance observer design method.
- *Chapter 4. Disturbance Observer Based Control of Bilateral Teleoperation Systems with Variable Time Delays:* In this chapter, a theoretical basis for disturbance observer based control of bilateral teleoperation systems with variable time delays is introduced. It is shown that bilateral teleoperation systems can be stabilized in the presence of disturbances and variable communication time delays when the disturbance observers, which are introduced in Chapter 3, are used in telerobotic systems with a slight modification. Simulation studies are performed to further demonstrate the efficiency of the proposed disturbance observer based teleoperation control scheme.
- *Chapter 5. Experiments:* The experimental setup and the developed software are presented in this chapter. We demonstrate the effectiveness of the proposed design methods developed throughout the thesis by performing experiments on popular and cost-effective PHANToM Omni® robotic arms.
- *Chapter 6. Conclusions and Future Directions:* Concluding remarks are presented and potential future research is discussed in this chapter.

Chapter 2

Background

2.1 Introduction

In this chapter, the applications of disturbance observers in robotic systems are introduced first. Next, a literature review of current disturbance observer design methods for such systems is presented. Thereafter, telerobotic (teleoperation) systems, their history and applications, and an overview of the control of these systems are introduced. Lastly, the importance and applications of disturbance observers in the control of telerobotic systems are described.

2.2 Disturbance Observers in Robotic Systems

This section briefly introduces applications of disturbance observers in robotic systems. The disturbance observer design methods that have been proposed in the literature are also presented in this section.

2.2.1 Applications of disturbance observers in robotic systems

The vast number of applications of disturbance observers in robotic systems can be categorized into two major groups, namely disturbance rejection and force sensing:

1. *Disturbance rejection:* Robotic manipulators are subject to different types of disturbances such as joint frictions and unknown payloads that adversely affect their performance such as positioning accuracy and repeatability. Employing disturbance observers is an effective way of suppressing these disturbances and improving the tracking performance. The idea behind disturbance observer based control of robotic manipulators is to lump all the internal and external disturbances acting on the manipulator into a single disturbance term,

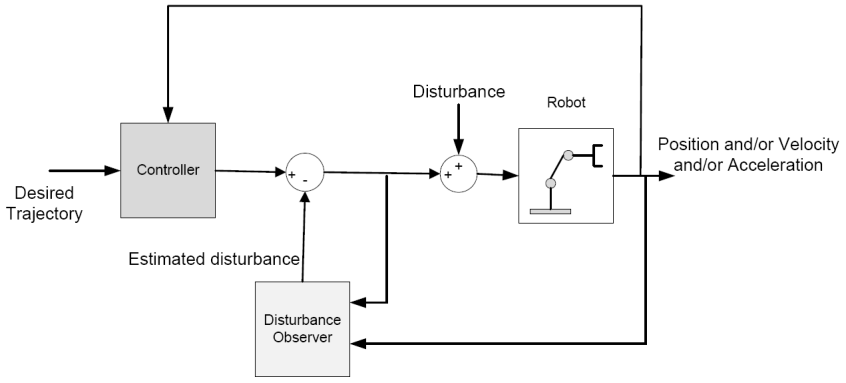

Figure 2.1: A disturbance observer used for disturbance rejection in a robotic control system.

estimate it, and then introduce feedforward compensation to cancel its effect. Figure 1 depicts a feedback structure including a disturbance observer (DOB) to control the position of a single robotic manipulator. If the disturbance is exactly estimated by the observer, disturbance will be cancelled out in the closed-loop system and it seems as if we are dealing with a robot with no disturbances, for which we can easily design a controller. Because of the feedforward nature of the compensation, disturbance observers can provide fast, excellent tracking performance and smooth control actions without the use of large feedback gains [16]. For instance, a disturbance observer might be used in independent joint control where joint couplings, load variations and dynamic uncertainties are collectively treated as the lumped disturbance term [17, 18, 19, 20]. Efficient suppression of these disturbances decouples the dynamics of the joints and allows for simple controllers to be designed independently for each degree of freedom (DOF). Another application of disturbance observers is in improving the manipulator tracking performance through friction estimation and compensation [21, 22]. An important aspect of disturbance observer based friction compensation schemes is that they are not based on any particular friction model [21].

2. *Force sensing:* In many robotics applications, the robot end-effector comes in contact with a compliant surface. In order to guarantee good system performance, a sensor is needed to measure these contact forces [23, 24]. Employing disturbance observers in these applications can eliminate the need for expensive force/torque sensors. Accordingly, disturbance observers have been employed successfully for sensorless force control [25, 26, 27]. It has been argued in [26] that noise-corrupted measurements and compliant mechanical structure of force sensors may destabilize the robot-environment interaction and thus using disturbance observers instead of force sensors is justified. This

justification is valid for micro/nano manipulation tasks, e.g., microinjection to introduce foreign materials into biological cells [28], where there is a lack of small enough force sensors with good precision and signal to noise ratio [29].

Lastly, industrial robots employ fault detection systems in order to determine if a fault such as a collision (i.e., an abrupt increase in reaction forces) has occurred in the system. Disturbance observers have been used for fault detection in a number of robotic applications [30, 31, 32].

2.2.2 Disturbance observer design methods

A considerable part of the existing literature on disturbance observer design for robotic applications uses linearized models or linear system techniques [8, 9, 10, 11]. However, robotic manipulators are nonlinear and coupled systems. There exists no rigorous proof regarding the stability and performance of nonlinear robotic systems that use such linear disturbance observers [12, 13]. In order to overcome the linear disturbance observer limitations for the nonlinear and coupled dynamics of robotic manipulators, Chen et al. proposed a nonlinear disturbance observer for nonlinear manipulators and designed it such that no acceleration measurement was needed [12]. However, the observer design problem was only solved for a 2-link planar serial manipulator with revolute joints. Later, Nikoobin et al. solved the design problem for n-link planar serial manipulators with revolute joints [13]. Despite these limitations in terms of the manipulator configuration, their design could not guarantee exponential disturbance tracking and merely ensured asymptotic disturbance tracking. However, in practice, a guaranteed minimum rate of decay of disturbance tracking error is highly desirable. Also, both [12, 13] used exact dynamic models of a particular class of manipulators to design their disturbance observers. Although these disturbance observers show promising results in disturbance estimation, their design is limited to planar, serial manipulators with revolute joints. However, industrial robots including 6-DOF articulated robotic arms such as EPSON C3 and PUMA 560 are non-planar. Moreover, some of the industrial arms such as SCARA manipulators have prismatic joints in addition to revolute joints.

Recently, a nonlinear disturbance observer based tracking control has been proposed for Euler-Lagrange systems in [33]. However, this method needs the exact Lagrangian of the mechanical system, while the exact values of parameters of a mechanical system are usually uncertain. Moreover, this method does not address the practical issues involved with the design of disturbance observers such as the tradeoff between the sensitivity to measurement noise and the rate of convergence of the disturbance tracking error. This serves as the motivation to look for a general disturbance observer design method for robotic systems that imposes minimum restrictions on the manipulator configuration and that does not require its exact dynamics.

2.3 An Introduction to Telerobotic Systems

Although there is slight difference between the meaning of *teleoperation* and *telerobotics*, many authors use these terms interchangeably (see, for example, [34, 35]). We will adopt the same convention, i.e., we will use *telerobotic system* and *teleoperation system* interchangeably.

In this section, we will first present the basic concepts of teleoperation. Next, we will have a brief overview of the history and applications of teleoperation. Then, we will introduce the problem of control of telerobotic systems.

2.3.1 Basics of teleoperation

Teleoperation involves indirect performance of a task in a remote environment and is used to extend a human operator's sensing and manipulation capability to a remote location [36]. The prefix *tele*, meaning distance, implies an existing barrier between the human operator and the task to be performed [37]. This barrier can be imposed by hazardous environments, large distances, or scaling to very small or very large environments.

Teleoperation systems have found applications in many fields such as handling hazardous materials [38], undersea and space explorations [39, 40], mobile robotics [41], and remote delivery of health care [42] including telesurgery [43]. For instance, the da Vinci Surgical System [44] developed by Intuitive Surgical, Inc. (Sunnyvale, CA), allows the surgical robot to be controlled by a surgeon from a console (user interface) and has been used in prostatectomy [45], cardiac valve repair [46], gynecologic surgical procedure [47], and many other procedures.

A teleoperation system consists of a master (local) robot (user interface), a communication channel, and a slave (remote) robot. A typical teleoperation system is depicted in Figure 2.3.1. As it can be seen, the human operator interacts with the master device, which might be a joystick, a mouse or a robotic arm located at the local side of the teleoperation system. Through this interaction, the operator applies his/her desired commands to the slave robot, which interacts with the remote environment. The slave robot then performs the human operator's desired commands at the remote side of the teleoperation system. Different types of information such as force, position, and visual/auditory data are exchanged between the remote and the local sides via a communication channel. If force feedback (haptic feedback) from the slave side to the master side is present, then the system is called a bilateral teleoperation system to distinguish it from a unilateral teleoperation system, in which no force is reflected to the user (i.e., there exists no haptic feedback). A bilateral teleoperation system is said to be *transparent* if the slave robot accurately follows the position of the master robot and the master robot faithfully displays the slave-environment contact force to the human operator. Haptic feedback has been

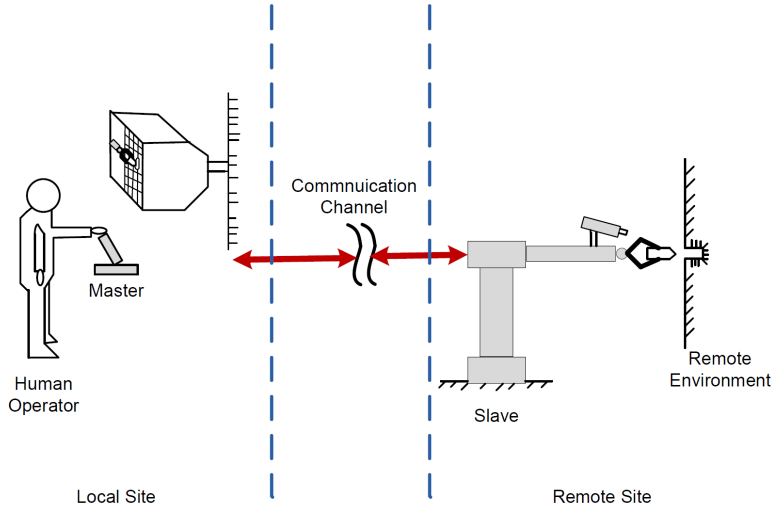

Figure 2.2: Diagram of a teleoperation system.

shown to enhance the human operator's performance in performing teleoperation tasks without time delay in terms of task success rate, completion time and economy of exerting forces [48, 49]. In [50], a study has been done to determine the effect of the presence of haptic feedback in teleoperation systems with time delay. It has been observed that haptic feedback helps reduce slave-environment contact forces at the cost of higher completion times.

2.3.2 A historical overview of teleoperation systems

In this section, we will present an overview of the history of teleoperation systems. For a complete review, the reader is referred to [15, 36, 37, 51].

Teleoperation has a rich and fascinating history. Raymond C. Goertz and his team developed the first mechanical master-slave teleoperator in 1945 [36]. This teleoperator was employed to handle hazardous materials. In 1954, Goertz improved his design by replacing mechanical tapes and linkages with electrical servomechanisms and adding closed-circuit television to the system [36].

In the 1960s, telemanipulators (teleoperators) were used to perform scientific undersea operations [36]. By 1980, teleoperation systems had become popular in offshore gas and oil industries and were used to perform undersea operations such as the monitoring the pipelines and well-head completion operations [36].

In the early 1960s, experiments were done to study the effect of time delay in space teleoperation [36]. Ferrell was a pioneer in these studies. In 1965, Ferrell found a quantitative relationship between the time delay and the time required by

the human operator to accomplish a certain task using a unilateral teleoperation system [15]. Later, Ferrell studied the effect of time delay on teleoperation when force reflection was present. He found that delays in the order of a tenth of a second could destabilize the system [52]. In 1967, Ferrell and Sheridan used supervisory control schemes to overcome the problem of time delay in teleoperation systems [15]. In supervisory control, high level commands such as 'move from point A to point B'or 'open/close the gripper 'is issued by the human operator at the local site and the remote robot which has a degree of autonomy executes these commands in the remote site [15, 53]. A breakthrough in space teleoperation was landing of Surveyor 1, the first lunar telemanipulator developed by NASA, on the surface of the moon in 1966 [36]. In 1970, Lunokhod 1, the first remotely-controlled lunar roving vehicle, landed on the moon [36].

In 1982, the M2 telerobotic system, which was the first telerobotic system that facilitated force feedback with separate master and slave electronics, was built at Oak Ridge National Laboratory [37]. Later, NASA used the M2 system to perform space truss assembly operation.

In 1990, Bejczy and Kim developed predictive display to tackle the problem of time delay in teleoperation systems [15, 54]. In a predictive display, the human operator can see the response of the remote system before it actually happens.

ROTEX, Robot Technology Experiment, was another breakthrough in the area of space teleoperation [37, 55]. ROTEX flew on board the Space Shuttle Columbia with Spacelab Mission-D2 in 1993. The system, developed by the German Aerospace Center (DLR), was used in different operational modes such as off-line programmed mode and on-line teleoperated mode to perform several prototype tasks such as assembling a truss structure and catching a floating object.

Using the Internet as the communication channel of teleoperation systems emerged in the mid 1990s [15]. Variable time-delay and loss of data packets are two major problems in the teleoperation over the Internet and have kept this field an active research area.

With the increasing power of computers in the 1980s and 1990s, teleoperation systems have found applications in medicine. An important development in medical teleoperation occurred in 2001. In this year, the first transatlantic telesurgery, Lindbergh Operation, was done successfully [37, 56]. In this minimally invasive telesurgery, the gallbladder of a patient in Strasbourg, France, was removed by a surgeon in New York, U.S., using a ZEUS telerobotic surgical system. Table 2.1 summarizes the most significant events in the history of teleoperation.

Table 2.1: Selected historical developments of teleoperation systems

1945	Goertz developed the first mechanical master-slave teleoperator.
1954	Goertz used electrical servomechanisms and closed circuit television in his teleoperator.
1965	Ferrell conducted first experiments to study the effect of time delay on the performance of teleoperation systems.
1966	NASA Surveyor 1 landed on the surface of the moon.
1967	Ferrell and Sheridan proposed first supervisory control schemes to overcome the problems caused by time delay in force reflecting teleoperation systems.
1970	Lunokhod 1, the first remotely controlled lunar roving vehicle landed on the moon.
1982	M2 telerobotic system was built at Oak Ridge National Laboratory.
1990	Bejczy and Kim used predictive displays to tackle the problem of time delay in teleoperation systems.
1993	DLR ROTEX was used successfully on board the Space Shuttle Columbia.
2001	Lindbergh Operation, the first transatlantic telesurgery, was done successfully between Strasbourg and New York.

2.3.3 Control of bilateral teleoperation systems

Teleoperation systems have long been a subject of interest within the control community. There exist several reasons for such interest [35]:

- Teleoperation systems are multiple-input/multiple-output (MIMO) nonlinear systems.
- Communication time-delay may exist between the master and the slave robots of a teleoperation system.
- Teleoperation systems physically interact with the human operator and the remote environment, which in general possess unknown, time-varying and nonlinear dynamics.
- The type of information exchanged in the communication channel between the local and the remote sites, affects the control as well as the system stability and performance.

From a control theoretic perspective, every teleoperation system should be able to achieve two main objectives [15, 34, 35]:

- *Stability*: The teleoperation system should be stable irrespective of the human operator, the communication channel, and the remote environment.
- *Telepresence (transparency)*: The human operator should be able to feel as

Table 2.2: Communication time delay of several space teleoperation tasks

Task	Round-trip delay (second)
Tasks in low earth orbit	0.4
Tasks on the moon	3
Tasks in earth orbitting space shuttles	6

if he/she is directly interacting with the remote environment while using the teleoperator to remotely act on the environment.

Literature review

Here, we will have a brief literature review of the control schemes that have been used in teleoperation systems with communication channel time delay. We will also present the disturbance observer based control schemes that have so far been proposed for teleoperation systems.

Communication channel time delay is inevitable in long-distance teleoperation. For instance, this delay is imposed by limits on the speed of radio transmission, and computer processing at sending and receiving stations and satellite relay stations in space teleoperation [53]. Table 2.2 shows the round-trip time delay for several such tasks [53]. As it can be seen, the communication time delay for teleoperation tasks done in earth orbitting space shuttles are larger than tasks done on the moon. This is because of multiple up-down links between the shuttle and the earth stations and signal buffering delays of the stations [53]. As another example, consider the case when the communication is done via an IP network. The communication delay in this case is caused by distance between the nodes (i.e., the computers in the network through which data flow), number of nodes traversed by the packet data, the speed and communication policy of each node, and the network load [57].

The problem of delay-induced instability in bilateral teleoperation systems was observed as early as 1966 by Ferrell [58] and solutions ranged from reducing the bandwidth of the communication channel to the supervisory control [15]. Yet, it was not before 1989 when Anderson and Spong developed a systematic solution to the delay-induced instability problem [52]. Inspired by the equations of lossless transmission lines, they used scattering theory to render a teleoperation system with a constant time delay in its communication channel passive and, therefore, stable. This scattering approach, however, implies a tradeoff between the stability and the performance of the teleoperation system [59].

The wave variable framework, which is a reformulation of the scattering transformation in [52], was another milestone in teleoperation control design [37, 60]. Readers are referred to [15] and [61] for a complete survey on the wave variable framework. In short, the wave variable framework has inspired many researchers to improve

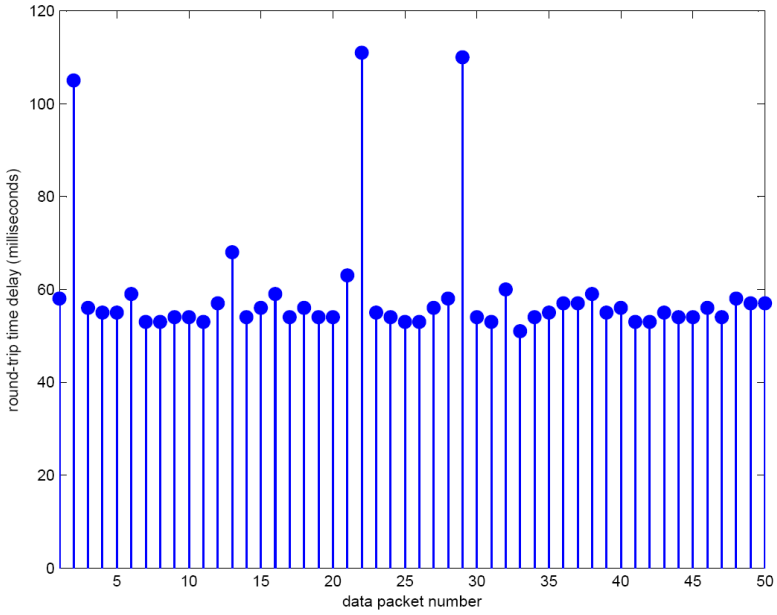

Figure 2.3: Round-trip communication time delay between a PC in Edmonton and the IP address 128.100.72.45.

the performance of time-delayed teleoperation systems while maintaining stability. Amongst these, we can refer to wave integral transmission [61], wave filtering [62], and wave prediction [63]. A widely-known problem of the classic wave-based teleoperation is the position drift between the master and the slave robots [59, 61]. In order to tackle this problem, solutions such as transmitting the master/slave position (in addition to velocities) [64], using symmetric PD-like controllers, and impedance matching [65] have been proposed.

One of the most critical problems involved in teleoperation over networks is the variable time delay– note that the passivity and wave formalisms are restricted to constant (albeit unknown) time delays. Variable time delays can cause severe instability and performance degradation in teleoperation systems. As an illustrative example of such variable time delay, consider Figure 2.3.3 that depicts the round-trip time delay for sending and receiving 50 consecutive packets of 32 bytes of data between a computer in Edmonton, AB and the IP address 128.100.72.45 (info.utcc.utoronto.ca). As it can be seen, the round-trip time delay varies between 51 milliseconds and 111 milliseconds.

Certain solutions have been proposed in the literature to tackle variable time-delays. In [66], communication management modules (CMM) were added to the bilateral teleoperation architecture to reconstruct the scattering variable while ensuring the passivity of the communication block. In [67], a time forward observer was used to ensure the passivity of a teleoperation system with variable time delay when there

were no model mismatches and the slave robot did not interact with hard surfaces in the remote environment. In [68], an energy balance monitoring mechanism was introduced that could ensure the system passivity. These solutions, however, are unable to ensure the boundedness of the position tracking error [59]. Recently, a theoretically rigorous approach by Nuno et al. has addressed the stability of variable time-delay teleoperation systems [59]. They proposed a general Lyapunov-like function candidate that can be employed to analyze the stability of teleoperation systems in the presence of constant and variable time-delays, and different control schemes, i.e, controllers with or without the scattering transformation, and controllers with or without position tracking capability.

Disturbance observers in telerobotic systems

A shortcoming of [59] and other prior art is that they do not consider the effect of disturbances on the teleoperation systems despite the fact that the master and the slave manipulators are subject to effects such as joint frictions and end-effector payloads, which can adversely affect the performance and stability of the teleoperation system. Employing disturbance observers is an effective way of suppressing such disturbances [3, 12, 16].

Disturbance observers have been used in telerobotic systems as well as the robotic systems. A disturbance observer based controller has been designed for bilateral teleoperation systems in [14]. In this work each joint of the master and the slave robots is treated as an independent single-input/single-output system and, thus, multiple disturbance observer based controllers need to be used for the multiple linear time-invariant (LTI) systems. This is in contrast to the fact that the dynamics of robotic systems are nonlinear and involve couplings among the manipulator's various degrees of freedom. In [69], disturbance observers were used as sensors for closed-loop force control of haptic interfaces. In [70], a disturbance observer was used to improve the performance of the master hand of a microsurgical telerobot system. In [71], a disturbance observer was used at the slave side of a unilateral teleoperation system in order to improve the position tracking between the master and the slave robot.

Disturbance observers have also been used in order to improve the telerobotic system performance under communication time delay [72, 73, 74]. In long-distance teleoperation, the position/force signals of the local and remote robots experience delays in the communication channel. The time-delayed position/force signals have been added to the output of the disturbance observer in order to provide the local and remote robots with estimations of undelayed position/force signals, in an effort to improve the teleoperation system performance [72]. In [75], a disturbance observer has been used to estimate the slave-environment contact forces and reflect the contact forces back to the human operator under variable communication time delay.

Although disturbance observers have been used to improve the performance of teleoperation systems in the presence of disturbances [72, 73, 74, 75] no rigorous analysis and design has been presented yet to guarantee the stability of the overall system in the presence of both variable time delays and disturbances. This serves as the motivation to seek a theoretical framework for disturbance observer based control of nonlinear bilateral teleoperation systems under variable time delays.

Chapter 3

Nonlinear Disturbance Observer Design for Single Robotic Manipulators

3.1 Introduction

In this chapter[1], we propose a general systematic approach, based on linear matrix inequalities (LMIs), to solve the disturbance observer design problem for serial robotic manipulators without restrictions on the number of degrees-of-freedom (DOFs), the types of joints, or the manipulator configuration. The proposed design method does not need the exact dynamic model of the serial robotic manipulator and unifies the previously proposed linear and nonlinear disturbance observers in a general framework.

The organization of this chapter is as follows. We first introduce the notation and several auxiliary theorems such as the Rayleigh Inequality and Schur Complement Inequality. Next, we introduce the dynamic equations and inherent dynamic properties of serial robotic manipulators. Then, we present the nonlinear disturbance observer (NLDO) structure and its modified version, which does not need joint acceleration measurements. Thereafter, we solve the design problem for nonlinear disturbance observers and provide sufficient conditions for global asymptotic and exponential disturbance tracking when the disturbances are slow-varying. When the disturbances are fast-varying, sufficient conditions for global uniform ultimate boundedness of the disturbance tracking error are provided. We will also formulate the observer design problem as a linear matrix inequality (LMI). Subsequently, the practical issues regarding the design of disturbance observers are discussed in this

[1] A version of this chapter has been submitted for publication in the Proceedings of the 2011 IEEE Conference on Decision and Control [76].

chapter. Lastly, simulation studies are presented for a 4-DOF SCARA manipulator to show the effectiveness of the proposed disturbance observer design method.

3.2 Mathematical Preliminaries

Notation. Let us adopt the following notation system:

- We denote the the set of real numbers by $\mathcal{R}$. We denote the set of n-tuples of real numbers $\mathbf{x} = [x_1, \ldots, x_n]^T$ and the set of $n \times m$ matrices with real entries by $\mathcal{R}^n$ and $\mathcal{R}^{n\times m}$, respectively.
- We represent the maximum and the minimum eigenvalues of a square matrix by $\lambda_{max}(.)$ and $\lambda_{min}(.)$, respectively.
- Throughout this chapter and the rest of this thesis, unless otherwise stated, by a vector norm we mean the vector 2-norm and by a matrix norm we mean the induced matrix 2-norm:

$$\mathbf{x} \in \mathcal{R}^n \Rightarrow |\mathbf{x}| = \sqrt{\mathbf{x}^T\mathbf{x}}$$
$$\mathbf{X} \in \mathcal{R}^{n\times n} \Rightarrow |\mathbf{X}| = \sqrt{\lambda_{max}(\mathbf{X}^T\mathbf{X})}$$

- By $\mathbf{A} \geq \mathbf{B}$, where $\mathbf{A}$ and $\mathbf{B}$ are square matrices, we mean that $\mathbf{A} - \mathbf{B}$ is a positive semi-definite matrix.

The following auxiliary theorems will be used to prove the main theorems in this chapter:

Rayleigh Inequality. *[77] Consider a nonsingular symmetric matrix $\mathbf{B} \in \mathcal{R}^{n\times n}$. Under these conditions and for any $\mathbf{x} \in \mathcal{R}^n$, we have*

$$\lambda_{min}(\mathbf{B})|\mathbf{x}|^2 \leq \mathbf{x}^T\mathbf{B}\mathbf{x} \leq \lambda_{max}(\mathbf{B})|\mathbf{x}|^2.$$

■

Schur Complement Inequality. *[78] Assume that $\mathbf{C}$ is a positive definite matrix. We have*

$$\mathbf{A} - \mathbf{B}\mathbf{C}^{-1}\mathbf{B}^T \geq 0 \Leftrightarrow \begin{bmatrix} \mathbf{A} & \mathbf{B} \\ \mathbf{B}^T & \mathbf{C} \end{bmatrix} \geq 0.$$

■

Now we define the concept of global uniform ultimate boundedness that will be used later in this chapter. For the sake of saving space, we will skip the global ultimate

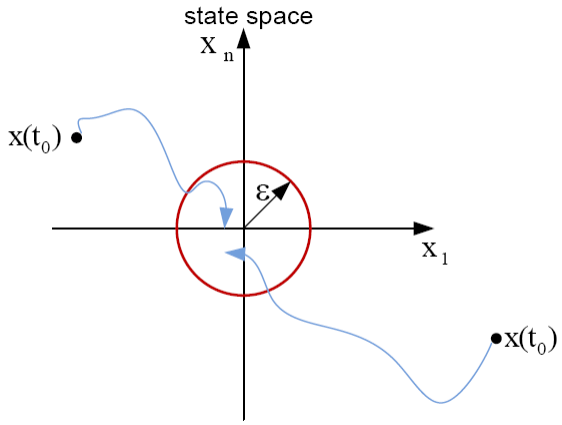

Figure 3.1: Global uniform ultimate boundedness concept.

boundedness theorems. The reader is referred to nonlinear control literature (see, for example, Theorem 5.1 and Corollary 5.1 in [79]).

Global Uniform Ultimate Boundedness. *[79] Consider the dynamic system* $\dot{\mathbf{x}} = \mathbf{f}(t, \mathbf{x})$*, where* $\mathbf{x} \in \mathcal{R}^n$ *and* t *represent the state vector of the system and time, respectively. The solutions of this system are said to be globally uniformaly ultimately bounded if for all initial conditions* $\mathbf{x}(t_0)$ *there exist positive constants* ϵ *and* T *such that*

$$|\mathbf{x}(t)| \leq \epsilon, \, \forall t \geq T.$$

The concept of global uniform ultimate boundedness in shown in Figure 3.1. As it can be observed, all the system trajectories will eventually converge to a ball with radius ϵ. The positive constant ϵ is sometimes called the ultimate bound.

3.3 Dynamics of Serial Robotic Manipulators

The following equation gives the dynamics of an n-DOF rigid serial manipulator [80]:

$$\mathbf{M}(\mathbf{q})\ddot{\mathbf{q}} + \mathbf{N}(\mathbf{q}, \dot{\mathbf{q}}) + \mathbf{F}(\dot{\mathbf{q}}) = \boldsymbol{\tau} + \boldsymbol{\tau}_{ext} \tag{3.1}$$

where

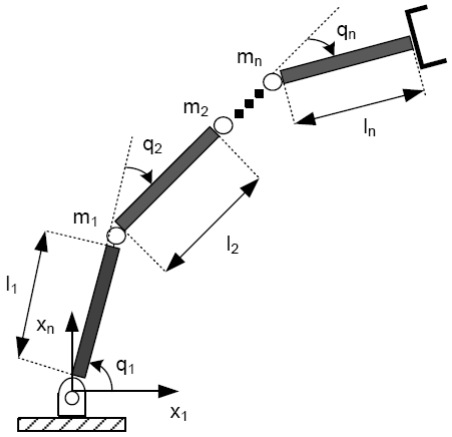

Figure 3.2: Schematic diagram of a typical n-DOF serial manipulator.

$$\mathbf{N}(\mathbf{q}, \dot{\mathbf{q}}) = \mathbf{C}(\mathbf{q}, \dot{\mathbf{q}})\dot{\mathbf{q}} + \mathbf{G}(\mathbf{q}) \tag{3.2}$$

and $\mathbf{q} \in \mathcal{R}^n$ is the vector of joint positions, $\mathbf{M}(\mathbf{q}) \in \mathcal{R}^{n \times n}$ is the inertia matrix, $\mathbf{F}(\dot{\mathbf{q}})$ is the vector of joint friction torques, $\mathbf{C}(\mathbf{q}, \dot{\mathbf{q}})\dot{\mathbf{q}} \in \mathcal{R}^n$ is the vector of Coriolis and centrifugal forces, $\mathbf{G}(\mathbf{q}) \in \mathcal{R}^n$ is the gravity vector, $\boldsymbol{\tau} \in \mathcal{R}^n$ is the vector of the control torques applied to the joints, and $\boldsymbol{\tau}_{ext} \in \mathcal{R}^n$ is the vector of the external disturbances exerted to the joints. Figure 3.2 shows a typical n-DOF serial manipulator where the parameters m_i and l_i, $i = 1, \ldots, n$ are the mass and the length of the i^{th} link of the robot, respectively.

In this chapter, we assume that the manipulator velocity vector lies in a bounded set, i.e.,

$$\dot{\mathbf{q}} \in D_{\dot{\mathbf{q}}} = \{\dot{\mathbf{q}} \in \mathcal{R}^n : |\dot{\mathbf{q}}| \leq |\dot{\mathbf{q}}|_{max}\}. \tag{3.3}$$

Note that the above assumption requires the input torque $\boldsymbol{\tau} + \boldsymbol{\tau}_{ext}$ to be bounded [13]. We also denote the set in which the robot joint variables vary (i.e., the robot workspace) by $D_{\mathbf{q}}$. We assume that $D_{\mathbf{q}}$ is a bounded set. This assumption ensures that the manipulator's prismatic joints do not extend to infinity, which is true in all physical manipulators.

Serial robotic manipulators have several inherent dynamic properties, which will be used when designing the disturbance observer later in this chapter. These properties are listed below.

Property 3.1. *The inertia matrix* $\mathbf{M}(\mathbf{q})$ *is symmetric and positive definite and its norm is bounded [80]:*

$$\mathbf{M}(\mathbf{q}) = \mathbf{M}^T(\mathbf{q}) > \mathbf{0} \tag{3.4}$$

$$\forall \mathbf{q} \in D_{\mathbf{q}},\ \nu_1(\mathbf{q}) \leq |\mathbf{M}(\mathbf{q})| \leq \nu_2(\mathbf{q}) \tag{3.5}$$

where $\nu_1(\mathbf{q})$ *and* $\nu_2(\mathbf{q})$ *are scalar functions of the joint position vector* $\mathbf{q}$*. Defining* $\nu_1 = \inf_{\mathbf{q} \in D_{\mathbf{q}}} \{\nu_1(\mathbf{q})\}$ *and* $\nu_2 = \sup_{\mathbf{q} \in D_{\mathbf{q}}} \{\sigma_2(\mathbf{q})\}$*, we get*

$$\nu_1 \leq |\mathbf{M}(\mathbf{q})| \leq \nu_2, \forall \mathbf{q} \in D_{\mathbf{q}}. \tag{3.6}$$

Property 3.2. *The matrix* $\dot{\mathbf{M}}(\mathbf{q}) - 2\mathbf{C}(\mathbf{q}, \dot{\mathbf{q}})$ *is skew-symmetric [80]:*

$$\begin{aligned} [\dot{\mathbf{M}}(\mathbf{q}) - 2\mathbf{C}(\mathbf{q}, \dot{\mathbf{q}})]^T &= -[\dot{\mathbf{M}}(\mathbf{q}) - 2\mathbf{C}(\mathbf{q}, \dot{\mathbf{q}})] \\ \Rightarrow \dot{\mathbf{M}}(\mathbf{q}) &= \mathbf{C}(\mathbf{q}, \dot{\mathbf{q}}) + \mathbf{C}^T(\mathbf{q}, \dot{\mathbf{q}}). \end{aligned} \tag{3.7}$$

Property 3.3. *The Coriolis/centrifugal matrix* $\mathbf{C}(\mathbf{q}, \dot{\mathbf{q}})$ *has an upper bounded induced 2-norm [81]:*

$$\forall \mathbf{q} \in D_{\mathbf{q}},\ \ |\mathbf{C}(\mathbf{q}, \dot{\mathbf{q}})| \leq C_b(\mathbf{q})|\dot{\mathbf{q}}|^2 \tag{3.8}$$

where $C_b(\mathbf{q})$ *is a scalar function of the joint position vector* $\mathbf{q}$*.*

Defining $\delta = \sup_{\mathbf{q} \in D_{\mathbf{q}}} \{C_b(\mathbf{q})\}$ *and using* (3.3)*, from* (3.8) *we get*

$$|\mathbf{C}(\mathbf{q}, \dot{\mathbf{q}})| \leq \delta |\dot{\mathbf{q}}|^2_{max}. \tag{3.9}$$

Also note that (3.7) *and* (3.9) *imply*

$$|\dot{\mathbf{M}}(\mathbf{q})| \leq 2\delta |\dot{\mathbf{q}}|^2_{max}. \tag{3.10}$$

Remark. If all joints of the manipulator are revolute, the scalar function $C_b(\mathbf{q})$ in (3.8) will become a constant and $\mathbf{C}(\mathbf{q}, \dot{\mathbf{q}})$ is said to be uniformly bounded. In this case, an upper bound of $C_b(\mathbf{q})$ is given as [81]:

$$\delta = \frac{3}{2} \sup_{\mathbf{q} \in D_{\mathbf{q}}} \{\sum_{i=1}^{n} |\frac{\partial \mathbf{M}(\mathbf{q})}{\partial q_i}|\}. \tag{3.11}$$

The above equation can be used efficiently to determine an upper bound of $|\dot{\mathbf{M}}(\mathbf{q})|$ for articulated robots.

$\diamondsuit$

Property 3.4. *The time derivative of the Coriolis/centrifugal matrix* $\mathbf{C}(\mathbf{q}, \dot{\mathbf{q}})$ *is bounded if the velocity and the acceleration of the robot are bounded [82].*

3.3.1 Effect of disturbances on robot dynamics

Assume that $\hat{\mathbf{M}}(\mathbf{q})$, $\hat{\mathbf{N}}(\mathbf{q}, \dot{\mathbf{q}})$, $\hat{\mathbf{C}}(\mathbf{q}, \dot{\mathbf{q}})$ and $\hat{\mathbf{G}}(\mathbf{q})$ are the estimates of the actual $\mathbf{C}(\mathbf{q}, \dot{\mathbf{q}})$ and $\mathbf{G}(\mathbf{q})$, and that $\Delta\mathbf{M}$, $\Delta\mathbf{C}$, $\Delta\mathbf{G}$ and $\Delta\mathbf{N} = \Delta\mathbf{C}\dot{\mathbf{q}} + \Delta\mathbf{G}$ are the corresponding additive uncertainties present in the model of the robot:

$$\mathbf{M}(\mathbf{q}) = \hat{\mathbf{M}}(\mathbf{q}) + \Delta\mathbf{M} \tag{3.12}$$
$$\mathbf{C}(\mathbf{q}, \dot{\mathbf{q}}) = \hat{\mathbf{C}}(\mathbf{q}, \dot{\mathbf{q}}) + \Delta\mathbf{C} \tag{3.13}$$
$$\mathbf{G}(\mathbf{q}) = \hat{\mathbf{G}}(\mathbf{q}) + \Delta\mathbf{G} \tag{3.14}$$
$$\mathbf{N}(\mathbf{q}, \dot{\mathbf{q}}) = \hat{\mathbf{N}}(\mathbf{q}, \dot{\mathbf{q}}) + \Delta\mathbf{N}. \tag{3.15}$$

Let us define the lumped disturbance vector $\boldsymbol{\tau}_d$ as

$$\boldsymbol{\tau}_d = \boldsymbol{\tau}_{ext} - \Delta\mathbf{M}\ddot{\mathbf{q}} - \Delta\mathbf{N} - \mathbf{F}(\dot{\mathbf{q}}). \tag{3.16}$$

By this definition, we lump the effect of all dynamic uncertainties, joint frictions and external disturbances into a single disturbance vector $\boldsymbol{\tau}_d$. From (3.1), we get

$$\hat{\mathbf{M}}(\mathbf{q})\ddot{\mathbf{q}} + \hat{\mathbf{N}}(\mathbf{q}, \dot{\mathbf{q}}) = \boldsymbol{\tau} + \boldsymbol{\tau}_d. \tag{3.17}$$

Inspired by the inherent dynamic characteristics of serial robotic manipulators, we choose our inertia matrix estimate $\hat{\mathbf{M}}(\mathbf{q})$ to satisfy the following properties:

- $\hat{\mathbf{M}}(\mathbf{q})$ is symmetric, positive definite and uniformly bounded. That is, we have:

$$\hat{\mathbf{M}}(\mathbf{q}) = \hat{\mathbf{M}}^T(\mathbf{q}) > \mathbf{0} \tag{3.18}$$
$$\forall \mathbf{q} \in D_{\mathbf{q}},\ \sigma_1\mathbf{I} \leq \hat{\mathbf{M}}(\mathbf{q}) \leq \sigma_2\mathbf{I} \tag{3.19}$$
$$\dot{\mathbf{q}}^T[\dot{\hat{\mathbf{M}}}(\mathbf{q}) - 2\hat{\mathbf{C}}(\mathbf{q}, \dot{\mathbf{q}})]\dot{\mathbf{q}} = 0 \tag{3.20}$$

  where σ_1 and σ_2 are two positive real constants. Also, $\mathbf{I}$ is the identity matrix.

- The 2-norm of $\dot{\hat{\mathbf{M}}}(\mathbf{q})$ is bounded. That is to say

$$\forall \mathbf{q} \in D_{\mathbf{q}},\ |\dot{\hat{\mathbf{M}}}(\mathbf{q})| \leq \zeta \tag{3.21}$$

where ζ is a positive real constant.

Remark. $\hat{\mathbf{M}}(\mathbf{q})$ can be any arbitrary matrix satisfying (3.18), (3.19) and (3.21). For instance, $\hat{\mathbf{M}}(\mathbf{q})$, can be a constant, positive definite and symmetric matrix. As another example, the estimated Denavit-Hartenberg (D-H) parameters[2] of a robot may be used to find the estimate of its inertia matrix. This is also true about the Coriolis matrix estimate $\hat{\mathbf{C}}(\mathbf{q}, \dot{\mathbf{q}})$ and the gravity vector estimate $\hat{\mathbf{G}}(\mathbf{q})$, i.e., when $\hat{\mathbf{M}}(\mathbf{q})$ is chosen to be a constant matrix, $\hat{\mathbf{C}}(\mathbf{q}, \dot{\mathbf{q}})$ is chosen to be zero (due to (3.20)), and when the D-H parameters are used to estimate the inertia matrix of the robot, the same D-H parameters will be used to estimate $\hat{\mathbf{C}}(\mathbf{q}, \dot{\mathbf{q}})$ and $\hat{\mathbf{G}}(\mathbf{q})$.

♢

3.4 Nonlinear Disturbance Observer Structure

In this section, we will first introduce a basic diturbance observer for robotic manipulators that needs joint acceleration measurements. Then, we will modify the disturbance observer in a way that acceleration measurement is no longer needed. We emphasize that disturbance observers are fundamentally different from state observers. While the state observers are used to estimate the unknown states of the robot such as the joint velocity (see, for example, the successful time delay and Nicosia state observers in [84, 85]), the disturbance observers are used to estimate the unknown inputs, such as unknown contact forces, exerted to the robot. Finally, while our simulations and experiments have to make choice on the robot control method, this chapter especially addresses the problem of the design of disturbance observers and not the design of controllers for robotic manipulators. Indeed, the proposed disturbance observers can be used in conjunction with any control scheme or state observer that has been proposed for robotic manipulators.

3.4.1 Basic disturbance observer structure

Assuming joint acceleration measurements are available, the following nonlinear disturbance observer has been proposed for the robot (3.17) by [12]:

$$\dot{\hat{\boldsymbol{\tau}}}_d = -\mathbf{L}\hat{\boldsymbol{\tau}}_d + \mathbf{L}\{\hat{\mathbf{M}}(\mathbf{q})\ddot{\mathbf{q}} + \hat{\mathbf{N}}(\mathbf{q}, \dot{\mathbf{q}}) - \boldsymbol{\tau}\} \tag{3.22}$$

[2]Denavit-Hartenberg convention is a commonly used convention for selecting frames of reference in robotics applications (see [80, 83] for a detailed discussion).

where $\mathbf{L}$ is the observer gain matrix. Defining $\Delta\boldsymbol{\tau}_d = \boldsymbol{\tau}_d - \hat{\boldsymbol{\tau}}_d$ as the disturbance tracking error and using (3.17), we have

$$\dot{\hat{\boldsymbol{\tau}}}_d = \mathbf{L}\Delta\boldsymbol{\tau}_d \tag{3.23}$$

or, equivalently,

$$\Delta\dot{\boldsymbol{\tau}}_d = \dot{\boldsymbol{\tau}}_d - \mathbf{L}\Delta\boldsymbol{\tau}_d. \tag{3.24}$$

3.4.2 Modified disturbance observer structure

The disadvantage of the disturbance observer (3.22) is the need for acceleration measurement. Accurate accelerometers are not available in many robotic systems. Unless robust differentiation techniques are employed [86], differentiating the noise-corrupted velocity signals is not a suitable option for deriving acceleration signals. It is possible to modify the disturbance observer, as in [12], in a way that no acceleration measurement is needed. For this purpose, let us define the auxiliary variable

$$\mathbf{z} = \hat{\boldsymbol{\tau}}_d - \mathbf{p}(\mathbf{q}, \dot{\mathbf{q}}) \tag{3.25}$$

where the vector $\mathbf{p}(\mathbf{q}, \dot{\mathbf{q}})$ can be determined from the modified observer gain matrix $\mathbf{L}(\mathbf{q}, \dot{\mathbf{q}})$:

$$\frac{d}{dt}\mathbf{p}(\mathbf{q}, \dot{\mathbf{q}}) = \mathbf{L}(\mathbf{q}, \dot{\mathbf{q}})\hat{\mathbf{M}}(\mathbf{q})\ddot{\mathbf{q}}. \tag{3.26}$$

With (3.17), (3.22) and (3.26), taking the time derivative of (3.25) results in

$$\begin{aligned}
&\dot{\mathbf{z}} = \dot{\hat{\boldsymbol{\tau}}}_d - \dot{\mathbf{p}}(\mathbf{q}, \dot{\mathbf{q}}) = \dot{\hat{\boldsymbol{\tau}}}_d - \mathbf{L}(\mathbf{q}, \dot{\mathbf{q}})\hat{\mathbf{M}}(\mathbf{q})\ddot{\mathbf{q}} \Rightarrow \\
&\dot{\mathbf{z}} = -\mathbf{L}(\mathbf{q}, \dot{\mathbf{q}}) \underbrace{[\mathbf{z} + \mathbf{p}(\mathbf{q}, \dot{\mathbf{q}})]}_{\hat{\boldsymbol{\tau}}_d} + \\
&\mathbf{L}(\mathbf{q}, \dot{\mathbf{q}})\{\hat{\mathbf{M}}(\mathbf{q})\ddot{\mathbf{q}} + \hat{\mathbf{N}}(\mathbf{q}, \dot{\mathbf{q}}) - \boldsymbol{\tau} - \hat{\mathbf{M}}(\mathbf{q})\ddot{\mathbf{q}}\} \\
&\Rightarrow \dot{\mathbf{z}} = -\mathbf{L}(\mathbf{q}, \dot{\mathbf{q}})\mathbf{z} + \\
&\mathbf{L}(\mathbf{q}, \dot{\mathbf{q}})\{\hat{\mathbf{N}}(\mathbf{q}, \dot{\mathbf{q}}) - \boldsymbol{\tau} - \mathbf{p}(\mathbf{q}, \dot{\mathbf{q}})\}.
\end{aligned} \tag{3.27}$$

Therefore, the modified disturbance observer, which does not need acceleration measurement due to cancellation of the term $\hat{\mathbf{M}}(\mathbf{q})\ddot{\mathbf{q}}$, takes the following form:

$$\begin{aligned}
\dot{\mathbf{z}} &= -\mathbf{L}(\mathbf{q},\dot{\mathbf{q}})\mathbf{z} + \mathbf{L}(\mathbf{q},\dot{\mathbf{q}})\{\hat{\mathbf{N}}(\mathbf{q},\dot{\mathbf{q}}) - \boldsymbol{\tau} - \mathbf{p}(\mathbf{q},\dot{\mathbf{q}})\} \\
\hat{\boldsymbol{\tau}}_d &= \mathbf{z} + \mathbf{p}(\mathbf{q},\dot{\mathbf{q}}) \\
\frac{d}{dt}\mathbf{p}(\mathbf{q},\dot{\mathbf{q}}) &= \mathbf{L}(\mathbf{q},\dot{\mathbf{q}})\hat{\mathbf{M}}(\mathbf{q})\ddot{\mathbf{q}}.
\end{aligned} \tag{3.28}$$

From (3.28), the error dynamics becomes

$$\begin{aligned}
&\Delta\dot{\boldsymbol{\tau}}_d = \dot{\boldsymbol{\tau}}_d - \dot{\hat{\boldsymbol{\tau}}}_d = \dot{\boldsymbol{\tau}}_d - \dot{\mathbf{z}} - \frac{d}{dt}\mathbf{p}(\mathbf{q},\dot{\mathbf{q}}) \\
&= \dot{\boldsymbol{\tau}}_d + \mathbf{L}(\mathbf{q},\dot{\mathbf{q}})\underbrace{[\hat{\boldsymbol{\tau}}_d - \mathbf{p}(\mathbf{q},\dot{\mathbf{q}})]}_{\mathbf{z}} - \mathbf{L}(\mathbf{q},\dot{\mathbf{q}})\{\underbrace{-\hat{\mathbf{M}}(\mathbf{q})\ddot{\mathbf{q}} + \boldsymbol{\tau}_d}_{\hat{\mathbf{N}}(\mathbf{q},\dot{\mathbf{q}})-\boldsymbol{\tau}} \\
&-\mathbf{p}(\mathbf{q},\dot{\mathbf{q}})\} - \mathbf{L}(\mathbf{q},\dot{\mathbf{q}})\hat{\mathbf{M}}(\mathbf{q})\ddot{\mathbf{q}} = \dot{\boldsymbol{\tau}}_d - \mathbf{L}(\mathbf{q},\dot{\mathbf{q}})(\boldsymbol{\tau}_d - \hat{\boldsymbol{\tau}}_d).
\end{aligned}$$

Therefore, we get

$$\Delta\dot{\boldsymbol{\tau}}_d = \dot{\boldsymbol{\tau}}_d - \mathbf{L}(\mathbf{q},\dot{\mathbf{q}})\Delta\boldsymbol{\tau}_d. \tag{3.29}$$

Note that the modified disturbance observer, which does not need acceleration measurement, has a similar error dynamics to the basic disturbance observer error dynamics (3.24).

In order to complete the disturbance observer design, we should determine the vector $\mathbf{p}(\mathbf{q},\dot{\mathbf{q}})$ and the matrix $\mathbf{L}(\mathbf{q},\dot{\mathbf{q}})$. This is the topic of the next section.

3.5 Nonlinear Disturbance Observer Design

In this section, we will present the main results of the chapter, namely a systematic method for the disturbance observer design and the formulation of disturbance observer design problem in the form of a linear matrix inequality (LMI).

3.5.1 Disturbance observer design method

Given the disturbance observer (3.28), we should determine $\mathbf{p}(\mathbf{q},\dot{\mathbf{q}})$ and $\mathbf{L}(\mathbf{q},\dot{\mathbf{q}})$ to complete the disturbance observer design. We propose the following disturbance observer gain matrix:

$$\mathbf{L}(\mathbf{q}) = \mathbf{X}^{-1}\hat{\mathbf{M}}^{-1}(\mathbf{q}) \tag{3.30}$$

where $\mathbf{X}$ is a constant invertible $n \times n$ matrix to be determined. Note that we have chosen the estimate of the robot inertia matrix to be symmetric and positive definite and thus invertible. According to (3.26), we have

$$\mathbf{p}(\dot{\mathbf{q}}) = \mathbf{X}^{-1}\dot{\mathbf{q}}. \tag{3.31}$$

In this way, our nonlinear disturbance observer is given by (3.28) with the disturbance observer gain matrix $\mathbf{L}(\mathbf{q})$ in (3.30) and the disturbance observer auxiliary vector $\mathbf{p}(\dot{\mathbf{q}})$ in (3.31).

First, we will assume that the rate of change of the lumped disturbance is negligible in comparsion with the disturbance estimation error dynamics, i.e., $\dot{\boldsymbol{\tau}}_d \approx \mathbf{0}$. This assumption is not overly restrictive and is commonly encountered in the robotics literature (see, for example, [12]). Next, we will consider the case when the robotic manipulator is experiencing fast-varying disturbances. The following theorem states the sufficient conditions for asymptotic and exponential disturbance tracking when the robotic manipulator is subject to slow-varying disturbances.

Theorem 3.1. *Consider the serial robotic manipulator subject to disturbances described by* (3.17)*. The disturbance observer is given in* (3.28) *with the disturbance observer gain matrix* $\mathbf{L}(\mathbf{q})$ *defined in* (3.30) *and the disturbance observer auxiliary vector* $\mathbf{p}(\dot{\mathbf{q}})$ *defined in* (3.31)*. The disturbance tracking error* $\Delta\boldsymbol{\tau}_d$ *converges exponentially to zero for* $\forall \Delta\boldsymbol{\tau}_d(0) \in \mathcal{R}^n$ *if the following conditions hold:*

1. *The matrix* $\mathbf{X}$ *is invertible,*
2. *There exists a positive definite and symmetric matrix* $\boldsymbol{\Gamma}$ *such that*

$$\mathbf{X} + \mathbf{X}^T - \mathbf{X}^T\dot{\hat{\mathbf{M}}}(\mathbf{q})\mathbf{X} \geq \boldsymbol{\Gamma}. \tag{3.32}$$

3. $\dot{\boldsymbol{\tau}}_d \approx \mathbf{0}$*, i.e., the rate of change of the lumped disturbance acting on the manipulator is negligible in comparison with the estimation error dynamics* (3.29)*.*

Under the above conditions, the minimum rate of exponential convergence is $\frac{\lambda_{min}(\boldsymbol{\Gamma})}{2\sigma_2|\mathbf{X}|^2}$*, where* σ_2 *is defined in* (3.19)*. If* $\boldsymbol{\Gamma} = 0$ *in* (3.32)*, the disturbance tracking error will converge asymptotically to zero.*

■

Proof. Consider the following candidate Lyapunov function:

$$\begin{aligned} W(\Delta\boldsymbol{\tau}_d, \mathbf{q}) &= \Delta\boldsymbol{\tau}_d^T \mathbf{X}^T \hat{\mathbf{M}}(\mathbf{q}) \mathbf{X} \Delta\boldsymbol{\tau}_d \\ &= (\mathbf{X}\Delta\boldsymbol{\tau}_d)^T \hat{\mathbf{M}}(\mathbf{q})(\mathbf{X}\Delta\boldsymbol{\tau}_d). \end{aligned} \tag{3.33}$$

Since $\hat{\mathbf{M}}(\mathbf{q})$ is symmetric and positive definite and the matrix $\mathbf{X}$ is invertible, the matrix $\mathbf{X}^T\hat{\mathbf{M}}(\mathbf{q})\mathbf{X}$ is also positive definite. Thus, the scalar function W is positive definite. Also, W is radially unbounded. Taking the time-derivative of W and using (3.29), (3.30) and (3.31) when $\dot{\boldsymbol{\tau}}_d \approx \mathbf{0}$, yields

$$\begin{aligned} &\dot{W}(\Delta\boldsymbol{\tau}_d, \mathbf{q}) = \Delta\dot{\boldsymbol{\tau}}_d^T \mathbf{X}^T \hat{\mathbf{M}}(\mathbf{q}) \mathbf{X} \Delta\boldsymbol{\tau}_d + \\ &\Delta\boldsymbol{\tau}_d^T \mathbf{X}^T \hat{\mathbf{M}}(\mathbf{q}) \mathbf{X} \Delta\dot{\boldsymbol{\tau}}_d + \Delta\boldsymbol{\tau}_d^T \mathbf{X}^T \dot{\hat{\mathbf{M}}}(\mathbf{q}) \mathbf{X} \Delta\boldsymbol{\tau}_d = \\ &-\Delta\boldsymbol{\tau}_d^T \hat{\mathbf{M}}^{-T}(\mathbf{q}) \mathbf{X}^{-T} \mathbf{X}^T \hat{\mathbf{M}}(\mathbf{q}) \mathbf{X} \Delta\boldsymbol{\tau}_d \\ &-\Delta\boldsymbol{\tau}_d^T \mathbf{X}^T \hat{\mathbf{M}}(\mathbf{q}) \mathbf{X} \mathbf{X}^{-1} \hat{\mathbf{M}}^{-1}(\mathbf{q}) \Delta\boldsymbol{\tau}_d \\ &+\Delta\boldsymbol{\tau}_d^T \mathbf{X}^T \dot{\hat{\mathbf{M}}}(\mathbf{q}) \mathbf{X} \Delta\boldsymbol{\tau}_d \Rightarrow \\ &\dot{W}(\Delta\boldsymbol{\tau}_d, \mathbf{q}) = -\Delta\boldsymbol{\tau}_d^T [\mathbf{X} + \mathbf{X}^T - \mathbf{X}^T \dot{\hat{\mathbf{M}}}(\mathbf{q}) \mathbf{X}] \Delta\boldsymbol{\tau}_d. \end{aligned} \tag{3.34}$$

According to Condition 2 and (3.34), $\dot{W}$ is negative definite for all $\Delta\boldsymbol{\tau}_d \in \mathcal{R}^n$. Therefore, the disturbance tracking error asymptotically converges to zero: $\lim_{t\to\infty} \Delta\boldsymbol{\tau}_d = 0$ for $\forall \Delta\boldsymbol{\tau}_d \in \mathcal{R}^n$.

Again consider the candidate Lyapunov function in (3.33). Condition 2 and (3.34) yield

$$\dot{W} \leq -\Delta\boldsymbol{\tau}_d^T \boldsymbol{\Gamma} \Delta\boldsymbol{\tau}_d, \;\; \forall \Delta\boldsymbol{\tau}_d \in \mathcal{R}^n. \tag{3.35}$$

Therefore, the disturbance observer tracking error converges exponentially to zero for $\forall \Delta\boldsymbol{\tau}_d \in \mathcal{R}^n$ when $\boldsymbol{\Gamma} \neq 0$.

On the other hand, using Rayleigh Inequality, we get

$$\begin{aligned} &\lambda_{min}(\mathbf{X}^T \hat{\mathbf{M}}(\mathbf{q}) \mathbf{X}) |\Delta\boldsymbol{\tau}_d|^2 \leq W \leq \\ &\lambda_{max}(\mathbf{X}^T \hat{\mathbf{M}}(\mathbf{q}) \mathbf{X}) |\Delta\boldsymbol{\tau}_d|^2, \; \forall \Delta\boldsymbol{\tau}_d \in \mathcal{R}^n. \end{aligned} \tag{3.36}$$

Since $\mathbf{X}^T\hat{\mathbf{M}}(\mathbf{q})\mathbf{X}$ is a symmetric matrix, we have

$$\lambda_{max}(\mathbf{X}^T\hat{\mathbf{M}}(\mathbf{q})\mathbf{X}) = |\mathbf{X}^T\hat{\mathbf{M}}(\mathbf{q})\mathbf{X}| \leq$$
$$|\mathbf{X}^T|.|\hat{\mathbf{M}}(\mathbf{q})|.|\mathbf{X}| = |\hat{\mathbf{M}}(\mathbf{q})|.|\mathbf{X}|^2. \tag{3.37}$$

So, $W \leq |\hat{\mathbf{M}}(\mathbf{q})|.|\mathbf{X}|^2.|\Delta\boldsymbol{\tau}_d|^2$. According to (3.19), we have

$$W \leq \sigma_2|\mathbf{X}|^2.|\Delta\boldsymbol{\tau}_d|^2. \tag{3.38}$$

The above inequality results in $|\Delta\boldsymbol{\tau}_d|^2 \geq \frac{W}{\sigma_2|\mathbf{X}|^2}$. On the other hand, the Rayleigh Inequality along with (3.35) results in

$$\dot{W} \leq -\lambda_{min}(\boldsymbol{\Gamma})|\Delta\boldsymbol{\tau}_d|^2. \tag{3.39}$$

Also note that $\lambda_{min}(\boldsymbol{\Gamma}) > 0$ because $\boldsymbol{\Gamma}$ is positive definite. Therefore, from (3.38) and (3.39) we have

$$\dot{W} \leq -\frac{\lambda_{min}(\boldsymbol{\Gamma})}{\sigma_2|\mathbf{X}|^2}W \Rightarrow W(t) \leq W(t_0)\exp[-\frac{\lambda_{min}(\boldsymbol{\Gamma})}{\sigma_2|\mathbf{X}|^2}t]. \tag{3.40}$$

Also note that (3.19), (3.33) and Rayleigh Inequality yield

$$W \geq \sigma_1\Delta\boldsymbol{\tau}_d^T\mathbf{X}^T\mathbf{X}\Delta\boldsymbol{\tau}_d$$
$$\geq \sigma_1\lambda_{min}(\mathbf{X}^T\mathbf{X})|\Delta\boldsymbol{\tau}_d|^2. \tag{3.41}$$

From (3.40) and (3.41), we get

$$|\Delta\boldsymbol{\tau}_d|^2 \leq \frac{W(t_0)}{\sigma_1\lambda_{min}(\mathbf{X}^T\mathbf{X})}\exp[-\frac{\lambda_{min}(\boldsymbol{\Gamma})}{\sigma_2|\mathbf{X}|^2}t]. \tag{3.42}$$

Thus, the minimum convergence rate of the disturbance tracking error is $\frac{\lambda_{min}(\boldsymbol{\Gamma})}{2\sigma_2|\mathbf{X}|^2}$. □

Having addressed the case of slow-varying disturbances, we now consider the case where the robot is experiencing fast-varying disturbances. The following theorem addresses the case where the robotic manipulator is subject to fast-varying disturbances.

Theorem 3.2. *Consider the robotic manipulator subject to disturbances described by* (3.17)*. The disturbance observer is given in* (3.28) *with the disturbance observer gain matrix* $\mathbf{L}(\mathbf{q})$ *defined in* (3.30) *and the disturbance observer auxiliary vector* $\mathbf{p}(\dot{\mathbf{q}})$

defined in (3.31). *The disturbance tracking error* $\boldsymbol{\tau}_d$ *is globally uniformly ultimately bounded if:*

- *The first two conditions of the Theorem 3.1 hold,*
- *The rate of change of the lumped disturbance is bounded, i.e.,* $\exists \kappa > 0$ *such that* $|\dot{\boldsymbol{\tau}}_d(t)| \leq \kappa$ *for* $\forall t > 0$.

Under the above conditions and for $\forall \Delta\boldsymbol{\tau}_d(0) \in \mathcal{R}^n$, *the tracking error converges with an exponential rate, equal to* $\frac{(1-\theta)\lambda_{min}(\boldsymbol{\Gamma})}{2\sigma_2|\mathbf{X}|^2}$, *to the ball with radius* $\frac{2\kappa\sigma_2|\mathbf{X}|^2}{\theta\lambda_{min}(\boldsymbol{\Gamma})}$ *where* $0 < \theta < 1$.

■

Proof. Again, consider the Lyapunov Candidate function in (3.33). According to (3.38) and (3.41), we have

$$\sigma_1\lambda_{min}(\mathbf{X}^T\mathbf{X})|\Delta\boldsymbol{\tau}_d|^2 \leq W \leq \sigma_2|\mathbf{X}|^2|\Delta\boldsymbol{\tau}_d|^2. \tag{3.43}$$

Note that W is a positive definite and radially unbounded function. Taking the time derivative of the Lyapunov function and using (3.29), we get

$$\begin{aligned}\dot{W}(\Delta\boldsymbol{\tau}_d, \mathbf{q}) &= -\Delta\boldsymbol{\tau}_d^T[\mathbf{X} + \mathbf{X}^T - \mathbf{X}^T\dot{\hat{\mathbf{M}}}(\mathbf{q})\mathbf{X}]\Delta\boldsymbol{\tau}_d \\ &+\dot{\boldsymbol{\tau}}_d^T\mathbf{X}^T\hat{\mathbf{M}}(\mathbf{q})\mathbf{X}\Delta\boldsymbol{\tau}_d + \Delta\boldsymbol{\tau}_d^T\mathbf{X}^T\hat{\mathbf{M}}(\mathbf{q})\mathbf{X}\dot{\boldsymbol{\tau}}_d.\end{aligned} \tag{3.44}$$

On the other hand, according to Schwarz Inequality (see, for example, [77]) and (3.19) and since $|\dot{\boldsymbol{\tau}}_d(t)| \leq \kappa$ we have

$$\dot{\boldsymbol{\tau}}_d^T\mathbf{X}^T\hat{\mathbf{M}}(\mathbf{q})\mathbf{X}\Delta\boldsymbol{\tau}_d \leq \kappa\sigma_2|\mathbf{X}|^2|\Delta\boldsymbol{\tau}_d|. \tag{3.45}$$

Using the inequality (3.32) and (3.44), we get

$$\begin{aligned}\dot{W} &\leq -\lambda_{min}(\boldsymbol{\Gamma})|\Delta\boldsymbol{\tau}_d|^2 + 2\kappa\sigma_2|\mathbf{X}|^2|\Delta\boldsymbol{\tau}_d| \\ &= -(1-\theta)\lambda_{min}(\boldsymbol{\Gamma})|\Delta\boldsymbol{\tau}_d|^2 - \theta\lambda_{min}(\boldsymbol{\Gamma})|\Delta\boldsymbol{\tau}_d|^2 \\ &+2\kappa\sigma_2|\mathbf{X}|^2|\Delta\boldsymbol{\tau}_d|\end{aligned} \tag{3.46}$$

where $\theta \in (0, 1)$. Therefore, we have

$$\dot{W} \leq -(1-\theta)\lambda_{min}(\mathbf{\Gamma})|\Delta\boldsymbol{\tau}_d|^2, \forall|\Delta\boldsymbol{\tau}_d| \geq \frac{2\kappa\sigma_2|\mathbf{X}|^2}{\theta\lambda_{min}(\mathbf{\Gamma})}. \tag{3.47}$$

According to (3.43), (3.47) and the uniform ultimate boundedness theorems (see, for example, Theorem 5.1 and Corollary 5.1 in [79]), we conclude that the tracking error is globally uniformly ultimately bounded. Similar to (3.40), we have

$$\begin{aligned}
&\dot{W} \leq -\frac{(1-\theta)\lambda_{min}(\mathbf{\Gamma})}{\sigma_2|\mathbf{X}|^2}W \Rightarrow \\
&W(t) \leq W(t_0)\exp[-\frac{(1-\theta)\lambda_{min}(\mathbf{\Gamma})}{\sigma_2|\mathbf{X}|^2}t] \\
&\forall|\Delta\boldsymbol{\tau}_d| \geq \frac{2\kappa\sigma_2|\mathbf{X}|^2}{\theta\lambda_{min}(\mathbf{\Gamma})}.
\end{aligned} \tag{3.48}$$

From (3.43) and (3.48), we get

$$\begin{aligned}
&|\Delta\boldsymbol{\tau}_d|^2 \leq \frac{W(t_0)}{\sigma_1\lambda_{min}(\mathbf{X}^T\mathbf{X})}\exp[-\frac{(1-\theta)\lambda_{min}(\mathbf{\Gamma})}{\sigma_2|\mathbf{X}|^2}t] \\
&\forall|\Delta\boldsymbol{\tau}_d| \geq \frac{2\kappa\sigma_2|\mathbf{X}|^2}{\theta\lambda_{min}(\mathbf{\Gamma})}.
\end{aligned} \tag{3.49}$$

Therefore, we will have

$$\begin{aligned}
&|\Delta\boldsymbol{\tau}_d(t)| \leq \sqrt{\frac{W(t_0)}{\sigma_1\lambda_{min}(\mathbf{X}^T\mathbf{X})}}\exp[-\frac{(1-\theta)\lambda_{min}(\mathbf{\Gamma})}{2\sigma_2|\mathbf{X}|^2}t] \\
&+\frac{2\kappa\sigma_2|\mathbf{X}|^2}{\theta\lambda_{min}(\mathbf{\Gamma})}, \forall t \geq 0.
\end{aligned} \tag{3.50}$$

Therefore, the tracking error converges with an exponential rate, equal to $\frac{(1-\theta)\lambda_{min}(\mathbf{\Gamma})}{2\sigma_2|\mathbf{X}|^2}$ to the ball with radius $\frac{2\kappa\sigma_2|\mathbf{X}|^2}{\theta\lambda_{min}(\mathbf{\Gamma})}$ where $0 < \theta < 1$ for $\forall\Delta\boldsymbol{\tau}_d(0) \in \mathcal{R}^n$.

□

Remark. Conventional linear disturbance observers and nonlinear disturbance observers proposed by [12, 13] are special cases of our disturbance observer in (3.28), disturbance observer gain matrix (3.30), and disturbance observer auxiliary vector (3.31) in the following ways:

- In the conventional linear disturbance observers [3], the robot inertia matrix estimate $\hat{\mathbf{M}}(\mathbf{q})$ is represented by a constant diagonal matrix of the form $\mathbf{diag}\{m_i\}$ where $m_i > 0,\ i = 1, \ldots, n$ are positive real constants. Also, the vector $\hat{\mathbf{N}}(\mathbf{q}, \dot{\mathbf{q}})$ is chosen to be zero and the matrix $\mathbf{X}$ is taken to be a constant diagonal matrix $\mathbf{diag}\{x_i\}$ with $x_i > 0$.
- In [12, 13], a nonlinear disturbance observer was designed for a serial planar robot with 2 and n revolute joints, respectively. In both of these, it was assumed that the exact dynamic model of the robotic manipulator is available, i.e., they took $\hat{\mathbf{M}}(\mathbf{q}) = \mathbf{M}(\mathbf{q})$ and $\hat{\mathbf{N}}(\mathbf{q}, \dot{\mathbf{q}}) = \mathbf{N}(\mathbf{q}, \dot{\mathbf{q}})$. Also, the vector $\mathbf{p}(\mathbf{q}, \dot{\mathbf{q}})$ was considered to be

$$\mathbf{p}(\dot{\mathbf{q}}) = c \begin{bmatrix} \dot{q}_1 \\ \dot{q}_1 + \dot{q}_2 \\ \vdots \\ \dot{q}_1 + \dot{q}_2 + \cdots + \dot{q}_n \end{bmatrix}. \tag{3.51}$$

  This is clearly a special case of our proposed vector $\mathbf{p}(\dot{\mathbf{q}})$ in (3.31), when $\mathbf{X}^{-1}$ is chosen to be

$$\mathbf{X}^{-1} = c \begin{bmatrix} 1 & 0 & \ldots & 0 \\ 1 & 1 & \ddots & \vdots \\ \vdots & \vdots & \ddots & 0 \\ 1 & 1 & \ldots & 1 \end{bmatrix}. \tag{3.52}$$

♢

3.5.2 LMI formulation of the design method

According to Theorems 3.1 and 3.2, the disturbance observer design problem reduces to finding a constant invertible matrix $\mathbf{X}$ such that the inequality (3.32) is satisfied. The following theorem shows how (3.32) can be formulated as a linear matrix inequality.

Theorem 3.3. *Define the matrix* $\mathbf{Y} = \mathbf{X}^{-1}$ *and assume that an upper bound of* $|\dot{\hat{\mathbf{M}}}(\mathbf{q})|$ *is* ζ. *The inequality* (3.32) *holds if the following LMI is satisfied:*

$$\begin{bmatrix} \mathbf{Y} + \mathbf{Y}^T - \zeta \mathbf{I} & \mathbf{Y}^T \\ \mathbf{Y} & \mathbf{\Gamma}^{-1} \end{bmatrix} \geq 0. \tag{3.53}$$

Proof. Multiply (3.32) by $\mathbf{Y}$ and $\mathbf{Y}^T$ from right and left, respectively to get

$$\mathbf{Y} + \mathbf{Y}^T - \mathbf{Y}^T\mathbf{\Gamma}\mathbf{Y} \geq \dot{\hat{\mathbf{M}}}(\mathbf{q}). \tag{3.54}$$

Since $|\dot{\hat{\mathbf{M}}}(\mathbf{q})| \leq \zeta$, we have $\zeta\mathbf{I} \geq \dot{\hat{\mathbf{M}}}(\mathbf{q})$ where $\mathbf{I}$ is the identity matrix. Therefore, (3.54) holds if

$$\mathbf{Y} + \mathbf{Y}^T - \mathbf{Y}^T\mathbf{\Gamma}\mathbf{Y} \geq \zeta\mathbf{I}. \tag{3.55}$$

The above inequality is equivalent to $\mathbf{Y} + \mathbf{Y}^T - \zeta\mathbf{I} - \mathbf{Y}^T\mathbf{\Gamma}\mathbf{Y} \geq 0$. Note that $\mathbf{\Gamma}$ is a positive definite matrix. According to the Schur Complement Inequality, this inequality holds if and only if the LMI (3.53) holds. □

Note that LMI software packages have the ability to solve (3.53) simultaneously for $\mathbf{Y}$ and $\mathbf{\Gamma}$ when $\mathbf{\Gamma}$ is not known.

3.6 Practical Considerations in the Design of Disturbance Observers

In this section, we will address practical issues in the design of disturbance observers. Also, we will present an analytical solution to the observer design problem.

3.6.1 Rate of convergence of the disturbance observer and the sensitivity to measurement noise

As we saw in Theorems 3.1 and 3.2, the rate of convergence of the tracking error is proportional to $\frac{1}{|\mathbf{Y}^{-1}|^2}$, where $\mathbf{X}^{-1} = \mathbf{Y}$. Also, the radius of the ball that the tracking errors converge to, in the case of fast-varying disturbances, is proportional to $|\mathbf{Y}^{-1}|^2$ (see Theorem 3.2). Since a smaller $|\mathbf{Y}^{-1}|$ implies a larger disturbance observer gain $|\mathbf{L}|$ due to (3.30), we need to have a large observer gain in order to increase the rate of convergence and the accuracy of the disturbance observer. On the other hand, large disturbance observer gains will increase the sensitivity of the observer to measurement noise by amplifying this noise. From this perspective, it is desirable to choose the disturbance observer gain $|\mathbf{L}|$ to be small. Thus, there exists a trade-off between the rate of convergence and the accuracy of the estimations and the noise amplification. According to (3.30), we have

$$|\mathbf{L}| \leq |\mathbf{Y}|.|\hat{\mathbf{M}}^{-1}(\mathbf{q})|. \tag{3.56}$$

Since the disturbance observer gain directly depends on the matrix $\mathbf{Y}$, we cannot choose this matrix to be very large. Assume that we want to limit the matrix $\mathbf{Y}$

to $\nu\mathbf{I}$ to reduce the noise amplification. Then, we need to solve the following set of LMIs:

$$\begin{aligned} \begin{bmatrix} \mathbf{Y}+\mathbf{Y}^T-\zeta\mathbf{I} & \mathbf{Y}^T \\ \mathbf{Y} & \mathbf{\Gamma}^{-1} \end{bmatrix} &\geq 0 \\ \mathbf{Y} &\leq \nu\mathbf{I}. \end{aligned} \tag{3.57}$$

LMI software packages such as MATLAB LMI Control Toolbox have the ability to solve a set of LMIs, such as the one in (3.57), simultaneously [78].

3.6.2 Analytical solution to the disturbance observer design problem

When the matrix $\mathbf{Y}$ is chosen to be $y\mathbf{I}$ [3], where $\mathbf{I}$ is the identity matrix, the LMI used for observer design in (3.53) will have an explicit analytical solution. Assume that we want the minimum convergence rate of the disturbance tracking error to be equal to β. Also assume that $\mathbf{\Gamma}=\gamma\mathbf{I}$. According to Theorem 3.1, we have

$$\gamma = \frac{2\beta\sigma_2}{y^2}. \tag{3.58}$$

And, the LMI (3.53) turns into

$$\begin{bmatrix} (2y-\zeta)\mathbf{I} & y\mathbf{I} \\ y\mathbf{I} & \frac{y^2}{2\beta\sigma_2}\mathbf{I} \end{bmatrix} \geq 0. \tag{3.59}$$

According to Schur Complement Inequality, the above LMI is equivalent to

$$\begin{aligned} &(2y-\zeta)\mathbf{I}-(y\mathbf{I})^T(\frac{y^2}{2\beta\sigma_2}\mathbf{I})^{-1}(y\mathbf{I}) \geq 0 \\ &\Leftrightarrow (2y-\zeta-2\beta\sigma_2) \geq 0 \Leftrightarrow y \geq \frac{1}{2}\zeta+\beta\sigma_2. \end{aligned} \tag{3.60}$$

The above inequality clearly depicts the trade-off existing between the minimum convergence rate and the noise amplification. Note that ζ and σ_2 are constants and

[3] Note that the matrix $\mathbf{Y}$ is a diagonal matrix with equal elements on its diagonal. The units of these diagonal elements are not necessarily the same. In fact, if the i^{th} joint of the robot is revolute (prismatic) the unit of the i^{th} element will be $\frac{rad}{sec}$ ($\frac{m}{sec}$)).

depend on the robot dynamic parameters and the maximum joint velocities of the robot. Faster convergence rates and better accuracy require larger values of β. This, in turn, means larger values of y and thus results in more sensitivity to noise. Since we want to reduce the sensitivity to noise in disturbance rejection applications and at the same time guarantee the minimum convergence rate of tracking error to be equal to β, we can choose $\mathbf{Y}$ to be

$$\mathbf{Y}_{optimal} = \frac{1}{2}(\zeta + 2\beta\sigma_2)\mathbf{I}. \tag{3.61}$$

Then, based on (3.30) and $\mathbf{X}^{-1} = \mathbf{Y}$, $\mathbf{L}$ is found.

3.7 Simulation Study

SCARA (Selective Compliance Assembly Robot Arm) is an industrial 4-DOF robotic arm, which is widely used in the assembly of electronic circuits and devices. The first two joints of the arm, which are used to generate motion in a horizontal plane, are revolute and have parallel axes of rotation. The third joint of the arm is a prismatic joint, which controls the vertical motion (z-axis) of the end-effector. Finally, the last joint is revolute and is used to orient the gripper about the z-axis. Do not confuse this with the auxiliary vector of the disturbance observer given in (3.28). Figure 3.3 depicts a schematic digram of this manipulator. The dynamics of the SCARA manipulator is [87]:

$$\begin{aligned}
\mathbf{M}(\mathbf{q}) &= \begin{bmatrix} p_1 + p_2c_2 & p_3 + 0.5p_2c_2 & 0 & -p_5 \\ p_3 + 0.5p_2c_2 & p_3 & 0 & -p_5 \\ 0 & 0 & p_4 & 0 \\ -p_5 & -p_5 & 0 & p_5 \end{bmatrix} \\
\mathbf{C}(\mathbf{q}, \dot{\mathbf{q}}) &= \begin{bmatrix} -p_2s_2\dot{q}_2 & -0.5p_2s_2\dot{q}_2 & 0 & 0 \\ 0.5p_2s_2\dot{q}_1 & 0 & 0 & 0 \\ 0 & 0 & 0 & 0 \\ 0 & 0 & 0 & 0 \end{bmatrix} \\
\mathbf{G}(\mathbf{q}) &= \begin{bmatrix} 0 \\ 0 \\ -p_4g \\ 0 \end{bmatrix}.
\end{aligned} \tag{3.62}$$

The SCARA arm parameters are defined as

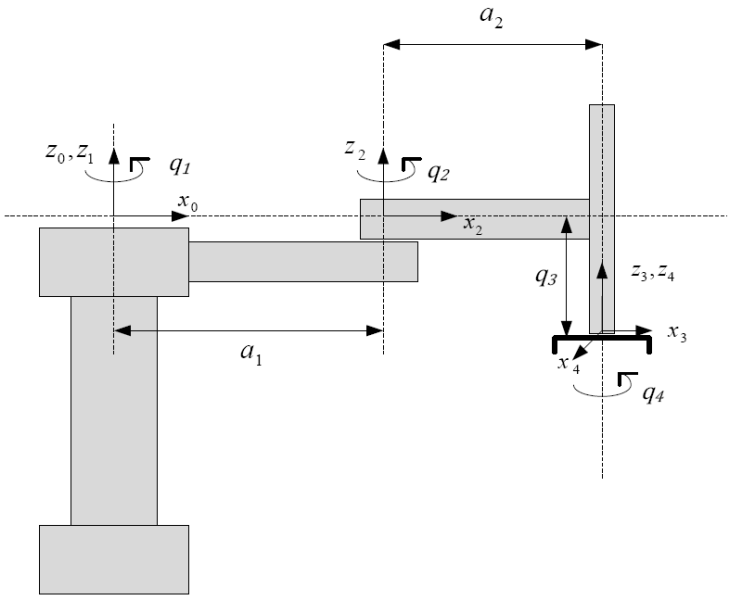

Figure 3.3: SCARA robotic arm

$$\begin{aligned} p_1 &= \sum_{i=1}^{4} I_i + m_1 x_1^2 + m_2(x_2^2 + a_1^2) + \\ &\quad (m_3 + m_4)(a_1^2 + a_2^2) \\ p_2 &= 2a_1[x_2 m_2 + a_2(m_3 + m_4)] \\ p_3 &= \sum_{i=2}^{4} I_i + m_2 x_2^2 + a_2^2(m_3 + m_4) \\ p_4 &= m_3 + m_4 \\ p_5 &= I_4 \end{aligned} \tag{3.63}$$

where I_i is the moment of inertia around the centriod, m_i is the mass, x_i is the mass center, and a_i is the length for link i. The Jacobian of the SCARA manipulator, with respect to the robot base frame, is [88]:

$$\mathbf{J}(\mathbf{q}) = \begin{bmatrix} -a_1 s_1 - a_2 s_{12} & -a_2 s_{12} & 0 & 0 \\ a_1 c_1 + a_2 c_{12} & a_2 c_{12} & 0 & 0 \\ 0 & 0 & -1 & 0 \\ 1 & 1 & 0 & 1 \end{bmatrix}. \tag{3.64}$$

In the above, $s_2 = \sin(q_2)$, $c_2 = \cos(q_2)$, $s_{12} = \sin(q_1 + q_2)$, $c_{12} = \cos(q_1 + q_2)$

Two types of disturbances are exerted to the robot, namely friction and external payload. We adopt computed-torque scheme for position control [80]:

$$\begin{aligned}\boldsymbol{\tau} &= \mathbf{M}(\mathbf{q})\{\ddot{\mathbf{q}}_{ref} + \mathbf{K}_v(\dot{\mathbf{q}}_{ref} - \dot{\mathbf{q}}) + \mathbf{K}_p(\mathbf{q}_{ref} - \mathbf{q})\} \\ &+\mathbf{C}(\mathbf{q}, \dot{\mathbf{q}})\dot{\mathbf{q}} + \mathbf{G}(\mathbf{q}) \end{aligned} \tag{3.65}$$

where $\mathbf{q}_{ref}$ is the vector of desired joint positions as a function of time. The external end-effector payload is chosen to be a weight exerted to the robot end-effector in the z direction. This weight is equal to 10^N from $t = 0^{sec}$ to $t = 7^{sec}$ and is then reduced to 5^N at $t = 7^{sec}$. The friction torques acting on the joints of the robots are generated based on the model in [89, 90]. For the $i - th$ joint of the robot, $i = 1, 2, 3, 4$, we have the friction modeled as

$$\begin{aligned}\tau_{i_{friction}} &= F_{ci}\text{sgn}(\dot{q}_i)[1 - \exp(\frac{-\dot{q}_i^2}{v_{si}^2})] \\ &\quad +F_{si}\text{sgn}(\dot{q}_i)\exp(\frac{-\dot{q}_i^2}{v_{si}^2}) + F_{vi}\dot{q}_i \end{aligned} \tag{3.66}$$

where F_{ci}, F_{si}, F_{vi} are the Coulomb, static, and viscous friction coefficients, respectively. The parameter v_{si} is the Stribeck parameter. Table 3.1 gives the simulation parameters.

The total disturbance vector acting on the joints of the robot can be computed by

$$\boldsymbol{\tau}_d = \boldsymbol{\tau}_{friction} + \mathbf{J}^T\mathbf{F}_{payload}. \tag{3.67}$$

Square-wave commands are supplied as the reference trajectory for all joints of the robot. In the first case, no disturbance observer is used with the computed torque controller. In the second case, a disturbance observer is used to estimate and suppress the joint frictions and the external payload together with computed torque law. The block diagram of the control system is similar to Figure 2.1. The designed observer has a structure given by (3.28), (3.30) and (3.31). We consider the matrix $\mathbf{Y} = \mathbf{X}^{-1} = y\mathbf{I}$ to design our disturbance observer. Based on the parameters provided in Table 3.1 we have

$$|\mathbf{M}(\mathbf{q})| \leq 15. \tag{3.68}$$

Table 3.1: Simulation parameters for disturbance observer based control of SCARA manipulator

Parameter	Value	Parameter	Value
m_1	15 kg	m_2	12 kg
m_3	3 kg	m_4	3 kg
I_1	$0.02087m_1$ kg.m^2	I_2	$0.08m_2$ kg.m^2
I_3	0.05 kg.m^2	I_4	$0.02m_4$ kg.m^2
a_1	0.5 m	a_2	0.4 m
x_1	0.25 m	x_2	0.2 m
F_{c1}	0.49 N.m	F_{c2}	0.31 N.m
F_{c3}	0.1 N	F_{c4}	0.1 N.m
F_{s1}	3.5 N.m	F_{s2}	2.8 N.m
F_{s3}	0.7 N	F_{s4}	0.7 N.m
F_{v1}	0.15 $\frac{kg.m}{s}$	F_{v2}	0.12 $\frac{kg.m}{s}$
F_{v3}	0.03 $\frac{kg}{s}$	F_{v4}	0.03 $\frac{kg.m}{s}$
v_{s1}	0.19 $\frac{rad}{s}$	v_{s2}	0.15 $\frac{rad}{s}$
v_{s3}	0.03 $\frac{m}{s}$	v_{s4}	0.03 $\frac{rad}{s}$
$\mathbf{K}_v$	$6\mathbf{I}$	$\mathbf{K}_p$	$16\mathbf{I}$
$\mathbf{Y} = \mathbf{X}^{-1}$	$95.8\mathbf{I}$	g	9.8 $\frac{N}{kg}$

Eigenvalues of the matrix $\dot{\mathbf{M}}(\mathbf{q})$ are 0, 0, $\frac{1}{2}(-1+\sqrt{2})p_2\dot{q}_2\sin(q_2)$ and $\frac{1}{2}(-1-\sqrt{2})p_2\dot{q}_2\sin(q_2)$, respectively. We have

$$|\dot{\mathbf{M}}(\mathbf{q})| \leq \frac{1}{2}(1+\sqrt{2})p_2\dot{q}_{2max} = 5.8\dot{q}_{2max}. \tag{3.69}$$

Assuming the maximum velocity of the second joint to be $\dot{q}_{2max} = 2\frac{rad}{sec}$ and the minimum convergence rate to be $\beta = 6$ and according to (3.61), we will have

$$\mathbf{Y}_{optimal} = \frac{1}{2}(5.8\dot{q}_{2max} + 2\beta\sigma_2) \Rightarrow \mathbf{Y}_{optimal} = 95.8\mathbf{I}. \tag{3.70}$$

Figure 3.4 illustrates the time profiles of the positions of the joints of the robot. As it can be observed, the computed-torque control law fails to track the position commands accurately when no disturbance observer is used. On the other hand, when the disturbance observer is used, the robot performs the position commands accurately. Figure 3.5 depicts the actual and estimated disturbances. Despite the fast time-varying disturbances, the estimated disturbance is able to track these disturbances and tends towards the actual disturbances in the steady state.

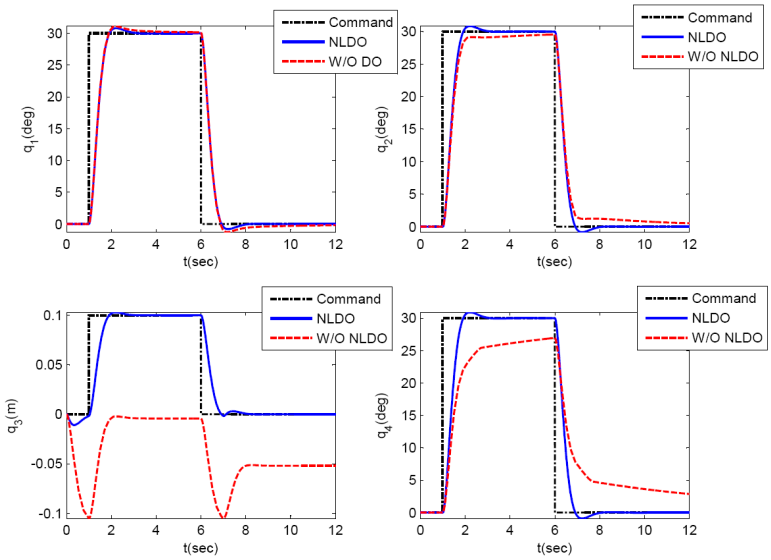

Figure 3.4: Position of the joints of the SCARA robot

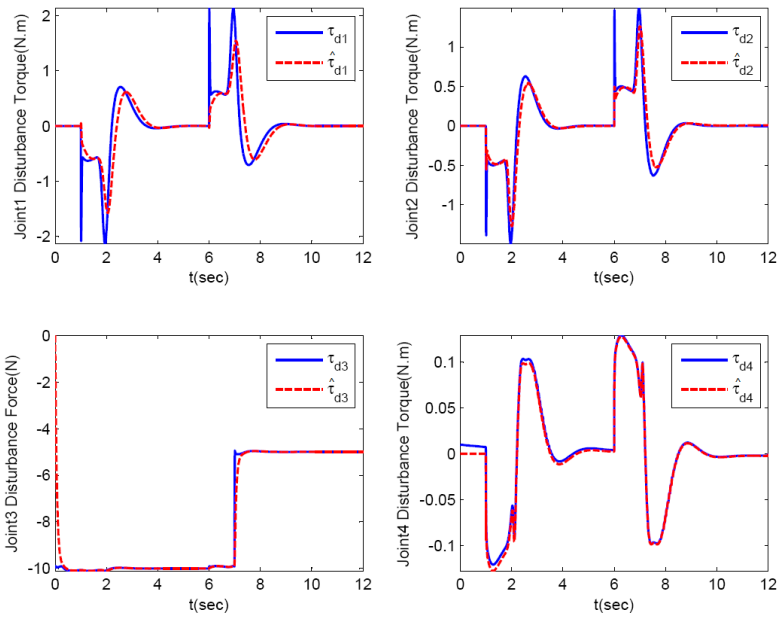

Figure 3.5: Disturbance tracking of the SCARA robot NLDO

Chapter 4

Nonlinear Disturbance Observer Based Control of Bilateral Teleoperation Systems with Variable Time Delay

4.1 Introduction

In this chapter, we will provide an extension to [59] by slight modification of the nonlinear disturbance observers proposed in the previous chapter and incorporating them into the framework of variable time delay teleoperation. By taking the Lyapunov approach in [59, 82], we will develop a disturbance observer based control scheme that is able to guarantee asymptotic disturbance tracking, position tracking of the master and the slave robots in free motion, and overall stability of the teleoperation system in the presence of variable time delays and disturbances.

This chapter is organized in the following way. We first introduce the notation and several lemmas that will be used throughout the chapter. Next, dynamics of teleoperation systems is presented. Thereafter, the disturbance observer based control laws for variable time delay teleoperation and the main theorem of this chapter are given. Lastly, simulations are performed for a nonlinear 2-DOF teleoperation system subject to disturbances and variable time delays to show the effectiveness of the proposed approach.

4.2 Mathematical Preliminaries

This section contains the concepts and lemmas used throughout the chapter. The lemmas presented in this section will serve as our main tools for analyzing the stability of teleoperation systems subject to disturbances and variable time delays.

Notation. We will use the following notation throughout this chapter:

- We denote the space of signals with bounded energy and the $\mathcal{L}_2$ norm of vector signals by $\mathcal{L}_2$ and $||.||_2$, respectively, thus

$$\mathbf{f}(.) \in \mathcal{L}_2 \Longleftrightarrow ||\mathbf{f}||_2^2 = \int_0^\infty |\mathbf{f}(\sigma)|^2 \, d\sigma < \infty.$$

- We denote the space of bounded signals and the $\mathcal{L}_\infty$ norm of vector signals by $\mathcal{L}_\infty$ and $||.||_\infty$, respectively, thus

$$\mathbf{f}(.) \in \mathcal{L}_\infty \Longleftrightarrow ||\mathbf{f}||_\infty = \sup_{t \geq 0} |\mathbf{f}(t)| < \infty, \ \forall t \geq 0.$$

- We denote the the set of real numbers, positive real numbers, and positive real numbers and zero by $\mathcal{R}$, $\mathcal{R}^+$, and $\mathcal{R}_0^+$, respectively.

Mathematical Lemmas. Here, we present lemmas needed throughout the chapter. First, we will present two different versions of the Barbalat's Lemma.

Lemma 4.1. *(Barbalat's Lemma) [91] Consider the vector signal* $\mathbf{f}(.) : \mathcal{R}_0^+ \to \mathcal{R}^n$.

- *Version 1: If* $\dot{\mathbf{f}}(.) \in \mathcal{L}_\infty$ *and* $\mathbf{f}(.) \in \mathcal{L}_\infty \cap \mathcal{L}_2$, *then* $\lim_{t \to \infty} \mathbf{f}(t) = 0$.
- *Version 2: If* $\dot{\mathbf{f}}(.)$ *is uniformly continuous,* k *is a scalar constant, and* $\lim_{t \to \infty} \mathbf{f}(t) = k$, *then* $\lim_{t \to \infty} \dot{\mathbf{f}}(t) = 0$.

■

The following lemma will be helpful in checking the uniform continuity of a signal.

Lemma 4.2. *(Uniform Continuity of a Signal) [77]* $\mathbf{f}(.)$ *is uniformly continuous if* $\dot{\mathbf{f}}(.) \in \mathcal{L}_\infty$.

■

The following lemmas are quite useful in our later analysis of the stability of teleoperation systems subject to variable time delays.

Lemma 4.3. *(Schwarz Inequality) [77] For any two vector signals* $\mathbf{f}(.), \mathbf{g}(.) : \mathcal{R}_0^+ \to \mathcal{R}^n$, *we have*

$$\int_0^t \mathbf{f}^{\mathbf{T}}(\sigma)\mathbf{g}(\sigma)\,d\sigma \leq (\int_0^t |\mathbf{f}(\sigma)|^2\,d\sigma)^{\frac{1}{2}}(\int_0^t |\mathbf{g}(\sigma)|^2\,d\sigma)^{\frac{1}{2}}. \tag{4.1}$$

■

Lemma 4.4. *(Bound on Delayed-Signals) [82] Consider the vector signals* $\mathbf{f}(.)$, $\mathbf{g}(.) : \mathcal{R}_0^+ \to \mathcal{R}^n$ *and assume that* $0 \leq T(t) \leq T_{max} < \infty$. *For* $\forall \alpha > 0$, *we have*

$$-\int_0^t \mathbf{f}^T(\sigma) \int_{-T(\sigma)}^0 \mathbf{g}(\sigma+\theta)\,d\theta\,d\sigma \leq \frac{\alpha}{2}||\mathbf{f}||_2^2 + \frac{T_{max}^2}{2\alpha}||\mathbf{g}||_2^2. \tag{4.2}$$

■

Lemma 4.5. *[82] Consider the vector signal* $\mathbf{x}(.) : \mathcal{R}_0^+ \to \mathcal{R}^n$ *and assume that* $0 \leq T(t) \leq T_{max} < \infty$. *We have*

$$\mathbf{x}(t - T(t)) - \mathbf{x} = -\int_{-T(t)}^0 \dot{\mathbf{x}}(t+\theta)\,d\theta \tag{4.3}$$

$$\mathbf{x} - \mathbf{x}(t - T(t)) = \int_0^{T(t)} \dot{\mathbf{x}}(t-\theta)\,d\theta \leq T_{max}^{\frac{1}{2}}||\dot{\mathbf{x}}||_2. \tag{4.4}$$

■

4.3 Dynamics of a Teleoperation System

In this section, we will present the dynamic equations of a teleoperation system consisting of a master and a slave manipulator in the presence of disturbances. Similar to Chapter 3, we will lump the effect of all dynamic uncertainties, joint frictions and external disturbances of the master and the slave into single disturbance terms.

4.3.1 Dynamics of the master and the slave manipulators

Similar to (3.17), we have the following dynamics for a teleoperation system consisting of a master and a slave manipulator:

$$\hat{\mathbf{M}}_m(\mathbf{q}_m)\ddot{\mathbf{q}}_m + \hat{\mathbf{C}}_m(\mathbf{q}_m, \dot{\mathbf{q}}_m)\dot{\mathbf{q}}_m + \hat{\mathbf{G}}_m(\mathbf{q}_m) = \boldsymbol{\tau}_{cm} - \boldsymbol{\tau}_h + \boldsymbol{\tau}_{dm} \tag{4.5}$$

$$\hat{\mathbf{M}}_s(\mathbf{q}_s)\ddot{\mathbf{q}}_s + \hat{\mathbf{C}}_s(\mathbf{q}_s, \dot{\mathbf{q}}_s)\dot{\mathbf{q}}_s + \hat{\mathbf{G}}_s(\mathbf{q}_s) = -\boldsymbol{\tau}_{cs} + \boldsymbol{\tau}_e + \boldsymbol{\tau}_{ds} \tag{4.6}$$

where $\boldsymbol{\tau}_h$ and $\boldsymbol{\tau}_e$ are the torques exerted by the human operator and the remote environment, $\boldsymbol{\tau}_{cm}$ and $\boldsymbol{\tau}_{cs}$ are the control troques applied to the master and the slave, and $\boldsymbol{\tau}_{dm}$ and $\boldsymbol{\tau}_{ds}$ are the disturbances, lumping the effect of all dynamic uncertainties, joint frictions and external disturbances, exerted to the master and the slave, respectively. We have

$$\boldsymbol{\tau}_{di} = \boldsymbol{\tau}_{ext,i} - \Delta\mathbf{M}_i\ddot{\mathbf{q}}_i - \Delta\mathbf{C}_i\dot{\mathbf{q}}_i - \Delta\mathbf{G}_i - \mathbf{F}_i(\dot{\mathbf{q}}_i),\ i = m, s \tag{4.7}$$

where the external disturbances, $\boldsymbol{\tau}_{ext,i}$, $i = m, s$, the robot model uncertainties, $\Delta\mathbf{M}_i$, $\Delta\mathbf{C}_i$, $\Delta\mathbf{G}_i$, $i = m, s$, and the joint friction vectors, $\mathbf{F}_i(\dot{\mathbf{q}}_i)$, $i = m, s$ are defined as in (3.12)–(3.17). Also, $\hat{\mathbf{M}}_i(\mathbf{q}_i)$, $i = m, s$ are the symmetric and positive definite estimates of the inertia matrices of the master and the slave, and satisfy

$$\mu_m\mathbf{I} \leq \hat{\mathbf{M}}_m(\mathbf{q}_m) \leq \mu_M\mathbf{I} \tag{4.8}$$

$$\mu_s\mathbf{I} \leq \hat{\mathbf{M}}_s(\mathbf{q}_s) \leq \mu_S\mathbf{I}. \tag{4.9}$$

Similarly, $\hat{\mathbf{C}}_i(\mathbf{q}_i, \dot{\mathbf{q}}_i)$, $i = m, s$ and $\hat{\mathbf{G}}_i(\mathbf{q}_i)$ represent the centrifugal/Coriolis matrix and the gravity vector estimates, respectively.

We will apply the following control torques to the master and the slave robots:

$$\boldsymbol{\tau}_{cm} = \hat{\mathbf{G}}_m(\mathbf{q}_m) - \hat{\boldsymbol{\tau}}_{dm} + \boldsymbol{\tau}_m \tag{4.10}$$

$$\boldsymbol{\tau}_{cs} = -\hat{\mathbf{G}}_s(\mathbf{q}_s) + \hat{\boldsymbol{\tau}}_{ds} + \boldsymbol{\tau}_s \tag{4.11}$$

where $\hat{\boldsymbol{\tau}}_{dm}$ and $\hat{\boldsymbol{\tau}}_{ds}$ are the estimates of the master and the slave disturbances provided by the disturbance observers that will be introduced later in this chapter. Also, $\boldsymbol{\tau}_m$ and $\boldsymbol{\tau}_s$ are the synchronizing torques applied to the master and the slave, respectively [59]. We have

$$\boldsymbol{\tau}_m = k_m[\mathbf{q}_s(t - T_s(t)) - \mathbf{q}_m] - b_m\dot{\mathbf{q}}_m \tag{4.12}$$

$$\boldsymbol{\tau}_s = k_s[\mathbf{q}_s - \mathbf{q}_m(t - T_m(t))] + b_s\dot{\mathbf{q}}_s \tag{4.13}$$

where $\mathbf{q}_m(t - T_m(t))$ and $\mathbf{q}_s(t - T_s(t))$ are the delayed positions of the joints of the master and the slave that have been transmitted through the communication channel. The parameters $k_i, b_i, i = m, s$ are positive real constants to be determined. Note that the synchronizing torques $\boldsymbol{\tau}_m$ and $\boldsymbol{\tau}_s$ consist of two terms, namely, a term proportional to the position error modelling a spring and a velocity term modelling a damper. This is shown schematically in Figure 4.1. As it will be seen later,

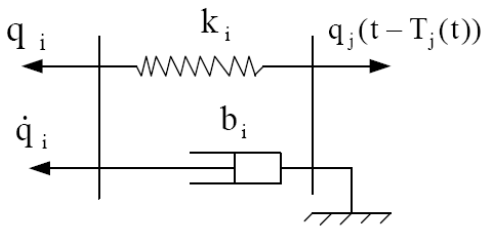

Figure 4.1: Physical interpretation of the synchronizing torques.

the synchronizing torques make the master and the slave robots follow each other's positions.

Remark. There are two other synchronizing control torques, namely, a *PD*-like and a scattering-based controller for teleoperation systems with variable time delays [59, 82]. However, the rate of change of time delays should be known in these two schemes. Also, the absolute value of the rate of change of time delays in these two schemes should be less than unity, which is not the case in packet switched communication networks, such as the Internet [59]. Moreover, as shown by [59], these two schemes result in an inferior performance in comparison with the proportional-damping scheme. Therefore, we will only address the proportional-damping scheme and use it in the disturbance observer based control of teleoperation system of (4.5)–(4.6) with variable time delays.

♢

Applying the control torques (4.10)–(4.11) to the teleoperation system (4.5)–(4.6) yields

$$\hat{\mathbf{M}}_m(\mathbf{q}_m)\ddot{\mathbf{q}}_m + \hat{\mathbf{C}}_m(\mathbf{q}_m, \dot{\mathbf{q}}_m)\dot{\mathbf{q}}_m = \boldsymbol{\tau}_m - \boldsymbol{\tau}_h + \Delta\boldsymbol{\tau}_{dm} \tag{4.14}$$

$$\hat{\mathbf{M}}_s(\mathbf{q}_s)\ddot{\mathbf{q}}_s + \hat{\mathbf{C}}_s(\mathbf{q}_s, \dot{\mathbf{q}}_s)\dot{\mathbf{q}}_s = -\boldsymbol{\tau}_s + \boldsymbol{\tau}_e + \Delta\boldsymbol{\tau}_{ds} \tag{4.15}$$

where $\Delta\boldsymbol{\tau}_{di} = \boldsymbol{\tau}_{di} - \hat{\boldsymbol{\tau}}_{di}$, $i = m, s$ is the disturbance tracking error. Determining the disturbance estimates $\hat{\boldsymbol{\tau}}_{dm}$ and $\hat{\boldsymbol{\tau}}_{ds}$ is the subject of the next section. Figure 4.2 represents a schematic diagram of the teleoperation system with disturbance observers incorporated into it.

To conclude this section, we will present a lemma for teleoperation systems in free motion, i.e., when $\boldsymbol{\tau}_h = \boldsymbol{\tau}_e = \mathbf{0}$.

Lemma 4.6. *(Teleoperator's Zero-convergence Lemmas) [82] Consider the teleoperation system subject to disturbances as described by* (4.14)–(4.15)*, in free motion (i.e., when* $\boldsymbol{\tau}_h = \boldsymbol{\tau}_e = \mathbf{0}$*). We have*

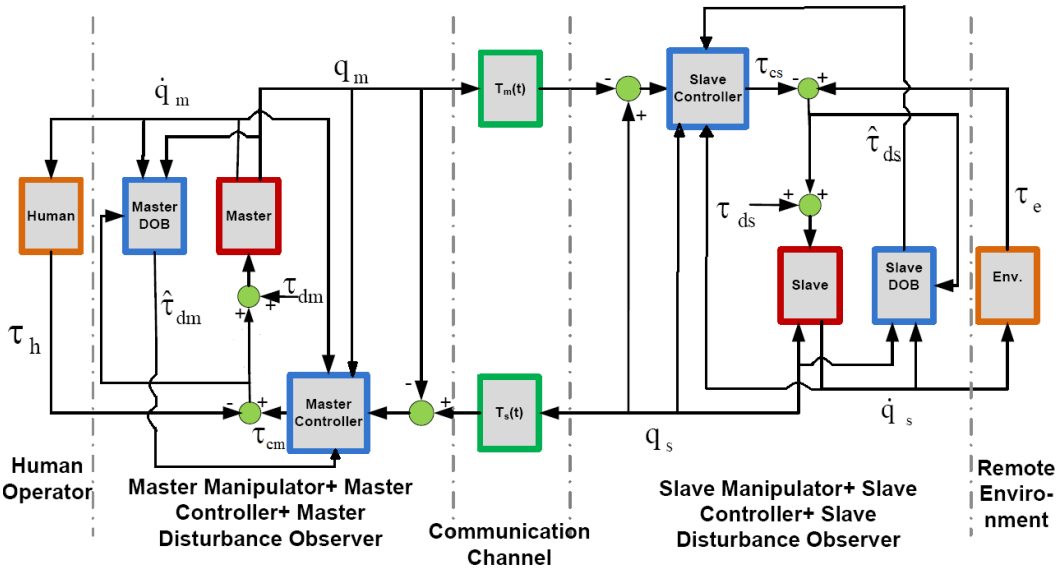

Figure 4.2: Disturbance observer based control of a teleoperation system with variable time delays.

- ***Velocity Zero-convergence.*** *Assume that* $\dot{\mathbf{q}}_i \in \mathcal{L}_2 \cap \mathcal{L}_\infty$ *and* $\boldsymbol{\tau}_i \in \mathcal{L}_\infty$, *and* $\Delta\boldsymbol{\tau}_{di} \in \mathcal{L}_\infty$ *for* $i = m, s$. *Then* $\lim_{t\to\infty} |\dot{\mathbf{q}}_i| = 0$.
- ***Acceleration Zero-convergence.*** *In addition to the previous assumptions, assume that* $\dot{\boldsymbol{\tau}}_i \in \mathcal{L}_\infty$, *and*$\Delta\dot{\boldsymbol{\tau}}_{di} \in \mathcal{L}_\infty$ *for*$i = m, s$. *Then,* $\ddot{\mathbf{q}}_i$ *is uniformly continuous and* $\lim_{t\to\infty} |\ddot{\mathbf{q}}_i| = 0$.

■

4.4 Disturbance Observer Based Control Laws

In this section, we will present our disturbance observer based control laws. The previous work by [59] can only address the case when the teleoperation system is subject to variable time delays. We will extend past work on variable time delay teleoperation by considering the disturbances acting on the master and the slave robots. Our stability and performance goals are:

- Ensuring boundedness of the master and the slave position trajectories, in both free and constrained motions, independent of the variable time delays present in the communication channel and in the presence of disturbances,
- Synchronizing the positions of the master and the slave manipulators when the teleoperation system is in free motion.

The disturbance observer based control laws are given in (4.10)–(4.11) with the synchronizing torques given in (4.12)–(4.13). First, we will propose the disturbance observers to be used in the disturbance observer based control laws (4.10)–(4.11). Next, we will introduce candidate Lyapunov functions for different parts of the teleoperation system. Finally, we will present one main result in the form of a theorem.

Disturbance observers

Inspired by the nonlinear disturbance observer in (3.28), we propose the following disturbance observer to be employed at the master side of the teleoperation system:

$$\begin{aligned}\dot{\mathbf{z}}_m &= -\alpha_m \hat{\mathbf{M}}_m^{-1}(\mathbf{q}_m)\mathbf{z}_m + \alpha_m \hat{\mathbf{M}}_m^{-1}(\mathbf{q}_m)[\hat{\mathbf{C}}_m(\mathbf{q}_m,\dot{\mathbf{q}}_m)\dot{\mathbf{q}}_m + \hat{\mathbf{G}}_m(\mathbf{q}_m) + \boldsymbol{\tau}_h - \boldsymbol{\tau}_{cm} \\ &\quad -\alpha_m \dot{\mathbf{q}}_m] + \dot{\mathbf{q}}_m \\ \hat{\boldsymbol{\tau}}_{dm} &= \mathbf{z}_m + \alpha_m \dot{\mathbf{q}}_m \end{aligned} \tag{4.16}$$

where α_m is a positive real constant. Note that the disturbance observer gain in this case is $\mathbf{L}_m(\mathbf{q}_m) = \alpha_m \hat{\mathbf{M}}_m^{-1}(\mathbf{q}_m)$ (see (3.30)). Also, we have $\mathbf{p}_m(\dot{\mathbf{q}}_m) = \alpha_m \dot{\mathbf{q}}_m$ (see (3.31)).

Remark. The last term $\dot{\mathbf{q}}_m$ in (4.16) does not exist in the nonlinear disturbance observer in (3.28). This new term will help to achieve desired stability and performance goals in the proposed disturbance observer based control of teleoperation systems with variable time delays.

$\diamondsuit$

Here, we assume that the rate of change of the lumped disturbance is neglibgible in comparsion with the disturbance estimation error dynamics, i.e., $\dot{\boldsymbol{\tau}}_{dm} \approx \mathbf{0}$. This assumption is not overly restrictive and is commonly encountered in the robotics literature (see, for example, [12, 13]). The error dynamics of the disturbance observer under this assumption and according to (4.5), (4.10), (4.14), and (4.16) will be:

$$\Delta\dot{\boldsymbol{\tau}}_{dm} = -\dot{\hat{\boldsymbol{\tau}}}_{dm} = -\dot{\mathbf{z}}_m - \alpha_m \ddot{\mathbf{q}}_m = \alpha_m \hat{\mathbf{M}}_m^{-1}(\mathbf{q}_m)\underbrace{(\hat{\boldsymbol{\tau}}_{dm} - \alpha_m \dot{\mathbf{q}}_m)}_{\mathbf{z}_m}$$
$$-\alpha_m \hat{\mathbf{M}}_m^{-1}(\mathbf{q}_m)[\underbrace{\hat{\mathbf{C}}_m(\mathbf{q}_m,\dot{\mathbf{q}}_m)\dot{\mathbf{q}}_m + \hat{\mathbf{G}}_m(\mathbf{q}_m) + \boldsymbol{\tau}_h - \boldsymbol{\tau}_{cm}}_{-\hat{\mathbf{M}}_m(\mathbf{q}_m)\ddot{\mathbf{q}}_m + \boldsymbol{\tau}_{dm}} - \alpha_m \dot{\mathbf{q}}_m] - \dot{\mathbf{q}}_m - \alpha_m \ddot{\mathbf{q}}_m.$$

Therefore, we have

$$\Delta\dot{\boldsymbol{\tau}}_{dm} = -\dot{\mathbf{q}}_m - \alpha_m \hat{\mathbf{M}}_m^{-1}(\mathbf{q}_m)\Delta\boldsymbol{\tau}_{dm}. \tag{4.17}$$

Similar to the disturbance observer at the master side, we employ the following disturbance observer at the slave side of the teleoperation sytem:

$$\begin{aligned} \dot{\mathbf{z}}_s &= -\alpha_s \hat{\mathbf{M}}_s^{-1}(\mathbf{q}_s)\mathbf{z}_s + \alpha_s \hat{\mathbf{M}}_s^{-1}(\mathbf{q}_s)[\hat{\mathbf{C}}_s(\mathbf{q}_s,\dot{\mathbf{q}}_s)\dot{\mathbf{q}}_s + \hat{\mathbf{G}}_s(\mathbf{q}_s) - \boldsymbol{\tau}_e + \boldsymbol{\tau}_{cs} - \alpha_s\dot{\mathbf{q}}_s] \\ &\quad +\dot{\mathbf{q}}_s \\ \hat{\boldsymbol{\tau}}_{ds} &= \mathbf{z}_s + \alpha_s\dot{\mathbf{q}}_s \end{aligned} \tag{4.18}$$

where α_s is a positive real constant. Again, under the assumption of slow-varying disturbances, the error dynamics of the disturbance observer will be

$$\Delta\dot{\boldsymbol{\tau}}_{ds} = -\dot{\mathbf{q}}_s - \alpha_s \hat{\mathbf{M}}_s^{-1}(\mathbf{q}_s)\Delta\boldsymbol{\tau}_{ds}. \tag{4.19}$$

4.4.1 Candidate Lyapunov functions

Every teleoperation system consists of five subsystems, namely, the human operator, the master, the communication channel and the controllers, the slave, and the remote environment. We will assume that the human operator and the remote environment are passive systems. This is a common assumption that is frequently encountered in the teleoperation literature and is the basis of the passivity-based control of teleoperation systems with time delay [15, 37]. This assumption enables us to analyze the (absolute) stability and performance of teleoperation systems independent of the dynamic models of the human operator and the remote environment [37]. The assumption of a passive environment is reasonable as many environments consist of passive objects. There is ample research that shows that the human arm displays passive dynamics while it maintains stable contact with any strictly passive object (see, for example, [92, 93]) despite active control by the central nervous system [94]. Let us introduce candidate Lyapunov functions that will be used in the analysis of stability of teleoperation systems with variable time delays and disturbances.

- *Human operator:* We assume that the human operator defines a passive velocity to torque/force mapping, i.e.,

$$\exists\, \nu_m > 0 \,\text{such that}\, \int_0^t \dot{\mathbf{q}}_m^T \boldsymbol{\tau}_h \, d\sigma \geq -\nu_m \;, \forall t \geq 0. \tag{4.20}$$

We define the following candidate Lyapunov function for the human operator:

$$V_{human} = \int_0^t \dot{\mathbf{q}}_m^T \boldsymbol{\tau}_h \, d\sigma + \nu_m. \tag{4.21}$$

Taking the time-derivative of (4.21) yields

$$\dot{V}_{human} = \dot{\mathbf{q}}_m^T \boldsymbol{\tau}_h. \tag{4.22}$$

- *Master manipulator:* We define the following candidate Lyapunov function for the master manipulator and its associated disturbance observer:

$$V_{master} = \frac{1}{2}\dot{\mathbf{q}}_m^T \hat{\mathbf{M}}_m(\mathbf{q}_m)\dot{\mathbf{q}}_m + \frac{1}{2}\Delta\boldsymbol{\tau}_{dm}^T \Delta\boldsymbol{\tau}_{dm}. \tag{4.23}$$

The first and the second terms of this Lyapunov function can be considered as the kinetic energy of the master and the energy of its disturbance observer, respectively. Taking the time-derivative of (4.23) and according to (3.20), (4.14), and (4.17), we get

$$\begin{aligned}
\dot{V}_{master} = \dot{\mathbf{q}}_m^T \underbrace{[-\hat{\mathbf{C}}_m(\mathbf{q}_m, \dot{\mathbf{q}}_m)\dot{\mathbf{q}}_m + \boldsymbol{\tau}_m - \boldsymbol{\tau}_h + \Delta\boldsymbol{\tau}_{dm}]}_{\hat{\mathbf{M}}_m(\mathbf{q}_m)\ddot{\mathbf{q}}_m} + \frac{1}{2}\dot{\mathbf{q}}_m^T \dot{\hat{\mathbf{M}}}_m(\mathbf{q}_m)\dot{\mathbf{q}}_m \\
+\Delta\boldsymbol{\tau}_{dm}^T \underbrace{[-\dot{\mathbf{q}}_m - \alpha_m \hat{\mathbf{M}}_m^{-1}(\mathbf{q}_m)\Delta\boldsymbol{\tau}_{dm}]}_{\Delta\dot{\boldsymbol{\tau}}_{dm}} = \dot{\mathbf{q}}_m^T(\boldsymbol{\tau}_m - \boldsymbol{\tau}_h) - \alpha_m \Delta\boldsymbol{\tau}_{dm}^T \hat{\mathbf{M}}_m^{-1}(\mathbf{q}_m) \\
\Delta\boldsymbol{\tau}_{dm} + \frac{1}{2}\underbrace{\dot{\mathbf{q}}_m^T[\dot{\hat{\mathbf{M}}}_m(\mathbf{q}_m) - 2\hat{\mathbf{C}}_m(\mathbf{q}_m, \dot{\mathbf{q}}_m)]\dot{\mathbf{q}}_m}_{0}.
\end{aligned}$$

Therefore, we have

$$\dot{V}_{master} = \dot{\mathbf{q}}_m^T(\boldsymbol{\tau}_m - \boldsymbol{\tau}_h) - \alpha_m \Delta\boldsymbol{\tau}_{dm}^T \hat{\mathbf{M}}_m^{-1}(\mathbf{q}_m)\Delta\boldsymbol{\tau}_{dm}. \tag{4.24}$$

- *Communication channel:* We make the following assumptions about the variable time delay in the communication channel [59, 82]:

– There exist a known upper bound on the variable time delay:

$$0 \leq T_i(t) \leq T_{max\_i} < \infty, \forall t \geq 0 \,\text{and}\, i = m, s. \tag{4.25}$$

– The rate of change of the variable time delay is bounded:

$$|\dot{T}_i(t)| \leq \zeta_{T\_i} < \infty, \forall t \geq 0 \,\text{and}\, i = m, s. \tag{4.26}$$

Remark. The assumptions (4.25)–(4.26) are frequently encountered in network-based control (see, for example, [95]). Also, note that we do not need to know ζ_{T_i}, $i = m, s$, i.e., an upper bound of the rate of change of the communication time delays to design the controllers.

♢

Let us define the following candidate Lyapunov function for the communication channel:

$$V_{comm.} = \frac{1}{2}|\mathbf{q}_m - \mathbf{q}_s|^2. \tag{4.27}$$

Taking the time-derivative of (4.27), we get

$$\dot{V}_{comm.} = (\mathbf{q}_m - \mathbf{q}_s)^T(\dot{\mathbf{q}}_m - \dot{\mathbf{q}}_s). \tag{4.28}$$

- *Slave manipulator:* We define the following candidate Lyapunov function for the slave manipulator:

$$V_{slave} = \frac{1}{2}\dot{\mathbf{q}}_s^T\hat{\mathbf{M}}_s(\mathbf{q}_s)\dot{\mathbf{q}}_s + \frac{1}{2}\Delta\boldsymbol{\tau}_{ds}^T\Delta\boldsymbol{\tau}_{ds}. \tag{4.29}$$

Similar to the calculations for the master, we get

$$\dot{V}_{slave} = \dot{\mathbf{q}}_s^T(-\boldsymbol{\tau}_s + \boldsymbol{\tau}_e) - \alpha_s\Delta\boldsymbol{\tau}_{ds}^T\hat{\mathbf{M}}_s^{-1}(\mathbf{q}_s)\Delta\boldsymbol{\tau}_{ds}. \tag{4.30}$$

- *Remote environment:* We assume that the remote environment defines a passive velocity to torque/force mapping, i.e.,

$$\exists\, \nu_s > 0 \,\text{such that}\, -\int_0^t \dot{\mathbf{q}}_s^T \boldsymbol{\tau}_e \, d\sigma \geq -\nu_s \;, \forall t \geq 0. \tag{4.31}$$

We define the following candidate Lyapunov function for the remote environment:

$$V_{environment} = -\int_0^t \dot{\mathbf{q}}_s^T \boldsymbol{\tau}_e \, d\sigma + \nu_s. \tag{4.32}$$

Taking the time-derivative of (4.32), we get

$$\dot{V}_{environment} = -\dot{\mathbf{q}}_s^T \boldsymbol{\tau}_e. \tag{4.33}$$

4.4.2 Main theorem

Now, we are ready to state the main result of this chapter in the form of the following theorem.

Theorem 4.1. *Consider the teleoperation system described by* (4.5) *and* (4.6)*. This teleoperation system is subject to variable time delays satisfying* (4.25) *and* (4.26)*. The master and the slave disturbance observers are given in* (4.16) *and* (4.18)*. The disturbance observer based control laws are given in* (4.10) *and* (4.11) *with the synchronization torques* $\boldsymbol{\tau}_m$ *and* $\boldsymbol{\tau}_s$ *given in* (4.12) *and* (4.13)*. Assume that the disturbance observer gains and the controller gains satisfy* $\alpha_i > 0, k_i > 0, b_i > 0,$ *for* $i = m, s$*. Also, assume that the controller gains are set such that the following inequality is satisfied:*

$$4 b_m b_s > (T_{max\_m}^2 + T_{max\_s}^2) k_m k_s. \tag{4.34}$$

Then:

- *The velocities and position error are bounded, i.e.,* $\{\dot{\mathbf{q}}_i, \mathbf{q}_m - \mathbf{q}_s\} \in \mathcal{L}_\infty$ *and* $\dot{\mathbf{q}}_i \in \mathcal{L}_2$*. Moreover,* $\{\mathbf{q}_m - \mathbf{q}_s(t - T_s(t)), \mathbf{q}_s - \mathbf{q}_m(t - T_m(t))\} \in \mathcal{L}_\infty$ *and* $\lim_{t\to\infty} \Delta\boldsymbol{\tau}_{di}(t) = 0.$
- *In the case of free motion, i.e., when* $\boldsymbol{\tau}_h = \boldsymbol{\tau}_e = \mathbf{0}$*, velocities asymptotically converge to zero and position tracking is achieved, i.e.,* $\lim_{t\to\infty} |\mathbf{q}_m - \mathbf{q}_s(t - T_s(t))| = \lim_{t\to\infty} |\mathbf{q}_s - \mathbf{q}_m(t - T_m(t))| = 0.$

Proof. Let us define the following candidate Lyapunov function for the teleoperation system:

$$V_{teleop.} = V_{human} + V_{master} + k_m V_{comm.} + \frac{k_m}{k_s} V_{slave} + \frac{k_m}{k_s} V_{environment} \tag{4.35}$$

where V_{human}, V_{master}, $V_{comm.}$, V_{slave}, and $V_{environment}$ are defined in (4.21), (4.23), (4.27), (4.29), and (4.32), respectively. This candidate Lyapunov function is positive definite and radially unbounded, i.e., $V_{teleop.} > 0$ and $V_{teleop.} \to \infty$, if $\{\dot{\mathbf{q}}_i, \Delta\boldsymbol{\tau}_{di}, \mathbf{q}_m - \mathbf{q}_s\} \to \infty$. Taking the time derivative of (4.35), we get

$$\dot{V}_{teleop.} = \dot{V}_{human} + \dot{V}_{master} + k_m \dot{V}_{comm.} + \frac{k_m}{k_s} \dot{V}_{slave} + \frac{k_m}{k_s} \dot{V}_{environment}. \tag{4.36}$$

Using (4.22), (4.24), (4.28), (4.30), and (4.33) in (4.36), we get

$$\begin{aligned}
\dot{V}_{teleop.} &= -b_m|\dot{\mathbf{q}}_m|^2 - \frac{k_m b_s}{k_s}|\dot{\mathbf{q}}_s|^2 + k_m \dot{\mathbf{q}}_m^T[\mathbf{q}_s(t - T_s(t)) - \mathbf{q}_s] \\
&+ k_m \dot{\mathbf{q}}_s^T[\mathbf{q}_m(t - T_m(t)) - \mathbf{q}_m] - \alpha_m \Delta\boldsymbol{\tau}_{dm}^T \hat{\mathbf{M}}_m^{-1}(\mathbf{q}_m)\Delta\boldsymbol{\tau}_{dm} \\
&- \frac{k_m \alpha_s}{k_s} \Delta\boldsymbol{\tau}_{ds}^T \hat{\mathbf{M}}_s^{-1}(\mathbf{q}_s)\Delta\boldsymbol{\tau}_{ds}.
\end{aligned} \tag{4.37}$$

Employing (4.3) in (4.37), we get

$$\begin{aligned}
\dot{V}_{teleop.} &= -b_m|\dot{\mathbf{q}}_m|^2 - \frac{k_m b_s}{k_s}|\dot{\mathbf{q}}_s|^2 - k_m \dot{\mathbf{q}}_m^T \int_{-T_s(t)}^{0} \dot{\mathbf{q}}_s(t + \theta)\, d\theta \\
&- k_m \dot{\mathbf{q}}_s^T \int_{-T_m(t)}^{0} \dot{\mathbf{q}}_m(t + \theta)\, d\theta - \alpha_m \Delta\boldsymbol{\tau}_{dm}^T \hat{\mathbf{M}}_m^{-1}(\mathbf{q}_m)\Delta\boldsymbol{\tau}_{dm} \\
&- \frac{k_m \alpha_s}{k_s} \Delta\boldsymbol{\tau}_{ds}^T \hat{\mathbf{M}}_s^{-1}(\mathbf{q}_s)\Delta\boldsymbol{\tau}_{ds}.
\end{aligned} \tag{4.38}$$

Using (4.8) and (4.9) in (4.38), we get

$$\begin{aligned}
\dot{V}_{teleop.} &\leq -b_m|\dot{\mathbf{q}}_m|^2 - \frac{k_m b_s}{k_s}|\dot{\mathbf{q}}_s|^2 - \frac{\alpha_m}{\mu_M}|\Delta\boldsymbol{\tau}_{dm}|^2 - \frac{k_m \alpha_s}{k_s \mu_S}|\Delta\boldsymbol{\tau}_{ds}|^2 \\
&- k_m \dot{\mathbf{q}}_m^T \int_{-T_s(t)}^{0} \dot{\mathbf{q}}_s(t + \theta)\, d\theta - k_m \dot{\mathbf{q}}_s^T \int_{-T_m(t)}^{0} \dot{\mathbf{q}}_m(t + \theta)\, d\theta.
\end{aligned} \tag{4.39}$$

Let us integrate (4.39) from 0 to ∞ to get

$$V_{teleop.}(\infty) - V_{teleop.}(0) \leq -b_m \int_0^\infty |\dot{\mathbf{q}}_m|^2 \, d\sigma - \frac{k_m b_s}{k_s} \int_0^\infty |\dot{\mathbf{q}}_s|^2 \, d\sigma$$
$$-\frac{\alpha_m}{\mu_M} \int_0^\infty |\Delta\boldsymbol{\tau}_{dm}|^2 \, d\sigma - \frac{k_m \alpha_s}{k_s \mu_S} \int_0^\infty |\Delta\boldsymbol{\tau}_{ds}|^2 \, d\sigma$$
$$-k_m \int_0^\infty \dot{\mathbf{q}}_m^T \int_{-T_s(t)}^0 \dot{\mathbf{q}}_s(t+\theta) \, d\theta \, d\sigma - k_m \int_0^\infty \dot{\mathbf{q}}_s^T \int_{-T_m(t)}^0 \dot{\mathbf{q}}_m(t+\theta) \, d\theta \, d\sigma. \tag{4.40}$$

Now, we use (4.2) to get

$$V_{teleop.}(\infty) - V_{teleop.}(0) \leq -b_m ||\dot{\mathbf{q}}_m||_2^2 - \frac{k_m b_s}{k_s} ||\dot{\mathbf{q}}_s||_2^2 - \frac{\alpha_m}{\mu_M} ||\Delta\boldsymbol{\tau}_{dm}||_2^2 - \frac{k_m \alpha_s}{k_s \mu_S}$$
$$||\Delta\boldsymbol{\tau}_{ds}||_2^2 + \frac{k_m}{2}\{\alpha_m ||\dot{\mathbf{q}}_m||_2^2 + \frac{T_{max\_s}^2}{\alpha_m} ||\dot{\mathbf{q}}_s||_2^2\} + \frac{k_m}{2}\{\alpha_s ||\dot{\mathbf{q}}_s||_2^2 + \frac{T_{max\_m}^2}{\alpha_s} ||\dot{\mathbf{q}}_m||_2^2\}. \tag{4.41}$$

Further simplification yields

$$V_{teleop.}(\infty) - V_{teleop.}(0) \leq -\underbrace{\{b_m - \frac{k_m}{2}(\alpha_m + \frac{T_{max\_m}^2}{\alpha_s})\}}_{\kappa_m} ||\dot{\mathbf{q}}_m||_2^2 -$$
$$\underbrace{\{\frac{k_m b_s}{k_s} - \frac{k_m}{2}(\alpha_s + \frac{T_{max\_s}^2}{\alpha_m})\}}_{\kappa_s} ||\dot{\mathbf{q}}_s||_2^2 - \frac{\alpha_m}{\mu_M} ||\Delta\boldsymbol{\tau}_{dm}||_2^2 - \frac{k_m \alpha_s}{k_s \mu_S} ||\Delta\boldsymbol{\tau}_{ds}||_2^2. \tag{4.42}$$

If (4.34) holds, it can be easily observed that $\kappa_m, \kappa_s > 0$, for $\forall \alpha_m, \alpha_s > 0$. Since $V_{teleop.}$ is positive definite and from (4.42), we have

$$V_{teleop.}(0) \geq \kappa_m ||\dot{\mathbf{q}}_m||_2^2 + \kappa_s ||\dot{\mathbf{q}}_s||_2^2 + \frac{\alpha_m}{\mu_M} ||\Delta\boldsymbol{\tau}_{dm}||_2^2 + \frac{k_m \alpha_s}{k_s \mu_S} ||\Delta\boldsymbol{\tau}_{ds}||_2^2. \tag{4.43}$$

Therefore, the signals $\dot{\mathbf{q}}_i(.), \Delta\boldsymbol{\tau}_{di}(.)$, $i = m, s$ belong to $\mathcal{L}_2$. Now, we integrate (4.39) from 0 to t to get

$$V_{teleop.}(t) - V_{teleop.}(0) \leq -\kappa_m ||\dot{\mathbf{q}}_m||_2^2 - \kappa_s ||\dot{\mathbf{q}}_s||_2^2 - \frac{\alpha_m}{\mu_M} ||\Delta\boldsymbol{\tau}_{dm}||_2^2 - \frac{k_m \alpha_s}{k_s \mu_S} ||\Delta\boldsymbol{\tau}_{ds}||_2^2 + \psi(t) \tag{4.44}$$

where $\psi(t) = b_m \int_t^\infty |\dot{\mathbf{q}}_m|^2 \, d\sigma + \frac{k_m b_s}{k_s} \int_t^\infty |\dot{\mathbf{q}}_s|^2 \, d\sigma + \frac{\alpha_m}{\mu_M} \int_t^\infty |\Delta\boldsymbol{\tau}_{dm}|^2 \, d\sigma + \frac{k_m \alpha_s}{k_s \mu_S} \int_t^\infty |\Delta\boldsymbol{\tau}_{ds}|^2 \, d\sigma < \infty$. Also, we have $V_{teleop.}(t) \leq V_{teleop.}(0) + \psi(t) < \infty$. Since $V_{teleop.}$ is positive definite and radially unbounded, $\{\dot{\mathbf{q}}_i(.), \Delta\boldsymbol{\tau}_{di}(.), \mathbf{q}_m - \mathbf{q}_s\} \in \mathcal{L}_\infty$. Let us rewrite $\mathbf{q}_m - \mathbf{q}_s(t - T_s(t))$ as

$$\mathbf{q}_m - \mathbf{q}_s(t - T_s(t)) = \underbrace{\mathbf{q}_m - \mathbf{q}_s}_{\in \mathcal{L}_\infty} + \underbrace{\mathbf{q}_s - \mathbf{q}_s(t - T_s(t))}_{\leq T_{max\_s}^{\frac{1}{2}} ||\dot{\mathbf{q}}_s||_2 \text{ according to (4.4)}} . \tag{4.45}$$

Hence, $\mathbf{q}_m - \mathbf{q}_s(t - T_s(t)) \in \mathcal{L}_\infty$. Similarly, we can prove that $\mathbf{q}_s - \mathbf{q}_m(t - T_m(t)) \in \mathcal{L}_\infty$.

Now consider the derivative of the disturbance tracking errors in (4.17) and (4.19). Since $\{\dot{\mathbf{q}}_i, \Delta\boldsymbol{\tau}_{di}\} \in \mathcal{L}_\infty$, we have $\Delta\dot{\boldsymbol{\tau}}_{di} \in \mathcal{L}_\infty$. According to the first version of the Barbalat's Lemma, we have $\lim_{t\to\infty} \Delta\boldsymbol{\tau}_{di} = 0$. This concludes the first part of our proof.

Now, consider the teleoperation system in free motion, i.e., $\boldsymbol{\tau}_h = \boldsymbol{\tau}_e = \mathbf{0}$. We have proved that $\dot{\mathbf{q}}_i \in \mathcal{L}_2 \cap \mathcal{L}_\infty$, and $\{\Delta\boldsymbol{\tau}_{di}, \Delta\dot{\boldsymbol{\tau}}_{di}\} \in \mathcal{L}_\infty$. Since $\{\mathbf{q}_m - \mathbf{q}_s(t - T_s(t)), \mathbf{q}_s - \mathbf{q}_m(t - T_m(t))\} \in \mathcal{L}_\infty$, $\{\dot{\mathbf{q}}_m - \dot{T}_s(t)\dot{\mathbf{q}}_s(t - T_s(t)), \dot{\mathbf{q}}_s - \dot{T}_m(t)\dot{\mathbf{q}}_m(t - T_m(t))\} \in \mathcal{L}_\infty$ and according to (4.10) and (4.11), we conclude that $\{\boldsymbol{\tau}_i, \dot{\boldsymbol{\tau}}_i\} \in \mathcal{L}_\infty$. According to the Zero-convergence Lemma, we conclude that the velocities and the accelerations asymptotically converge to zero. According to (4.14)–(4.15) and in free motion, we have

$$\ddot{\mathbf{q}}_m = -\hat{\mathbf{M}}_m^{-1}(\mathbf{q}_m)\{\hat{\mathbf{C}}_m(\mathbf{q}_m, \dot{\mathbf{q}}_m)\dot{\mathbf{q}}_m + k_m[\mathbf{q}_s(t - T_s(t)) - \mathbf{q}_m] - b_m\dot{\mathbf{q}}_m + \Delta\boldsymbol{\tau}_{dm}\} \tag{4.46}$$

$$\ddot{\mathbf{q}}_s = -\hat{\mathbf{M}}_s^{-1}(\mathbf{q}_s)\{\hat{\mathbf{C}}_s(\mathbf{q}_s, \dot{\mathbf{q}}_s)\dot{\mathbf{q}}_s - k_s[\mathbf{q}_s - \mathbf{q}_m(t - T_m(t))] - b_s\dot{\mathbf{q}}_s + \Delta\boldsymbol{\tau}_{ds}\}. \tag{4.47}$$

Since the velocities, the accelerations, and the disturbance tracking errors asymptotically converge to zero, position tracking is achieved, i.e., $\lim_{t\to\infty} |\mathbf{q}_m - \mathbf{q}_s(t - T_s(t))| = \lim_{t\to\infty} |\mathbf{q}_s - \mathbf{q}_m(t - T_m(t))| = 0$. □

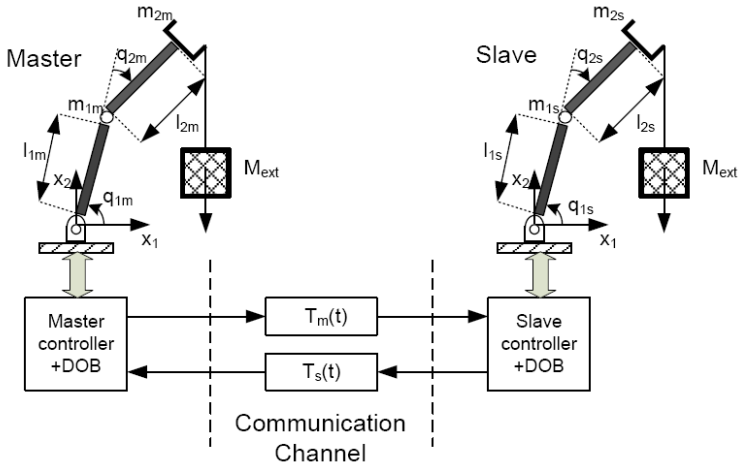

Figure 4.3: Schematic diagram of the teleoperation system used in simulation study.

Remark. The inequality (4.34) indicates a tradeoff between the damping gains, the proportional gains and the maximum time delays, i.e., the larger the proportional gains or the maximum communication time delays, the larger the damping gains to guarantee the stability of the teleoperation system. On the other hand, larger damping gains imply more sluggish responses and thus inferior performance of the teleoperation system. Therefore, given the proportional gains and maximum communication time delays, it is desirable to choose the minimum possible values of damping coefficients based on (4.34) to have better performance, i.e., less sluggish responses.

♢

4.5 Simulation Study

In this section, computer simulations will illustrate the effectiveness of the proposed control scheme. Both the master and the slave robots are considered to be planar two-link manipulators with revolute joints. The schematic diagram of the teleoperation system is shown in Figure 4.3.

The dynamics of the manipulators are [83]

$$\mathbf{M}(\mathbf{q}) = \begin{bmatrix} l_2^2 m_2 + 2l_1 l_2 m_2 c_2 + l_1^2(m_1+m_2) & l_2^2 m_2 + l_1 l_2 m_2 c_2 \\ l_2^2 m_2 + l_1 l_2 m_2 c_2 & l_2^2 m_2 \end{bmatrix} \tag{4.48}$$

$$\mathbf{V}(\mathbf{q},\dot{\mathbf{q}}) = \mathbf{C}(\mathbf{q},\dot{\mathbf{q}})\dot{\mathbf{q}} = \begin{bmatrix} -m_2 l_1 l_2 s_2 \dot{q}_2^2 - 2m_2 l_1 l_2 s_2 \dot{q}_1 \dot{q}_2 \\ m_2 l_1 l_2 s_2 \dot{q}_1^2 \end{bmatrix}$$

$$\mathbf{G}(\mathbf{q}) = \begin{bmatrix} m_2 l_2 g c_{12} + (m_1 + m_2) l_1 g c_1 \\ m_2 l_2 g c_{12} \end{bmatrix}. \tag{4.49}$$

Also, the forward kinematics, $\mathbf{h}(\mathbf{q})$, and the Jacobian matrix, $\mathbf{J}(\mathbf{q})$, are [1]

$$\mathbf{h}(\mathbf{q}) = \begin{bmatrix} l_1 c_1 + l_2 c_{12} \\ l_1 s_1 + l_2 s_{12} \end{bmatrix} \tag{4.50}$$

$$\mathbf{J}(\mathbf{q}) = \begin{bmatrix} l_1 s_2 & 0 \\ l_1 c_2 + l_2 & l_2 \end{bmatrix} \tag{4.51}$$

where l_1 and l_2 are the lengths of the links and m_1 and m_2 are the point masses of the links. Also, we have $s_1 = \sin(q_1)$, $s_2 = \sin(q_2)$, $c_1 = \cos(q_1)$, $c_2 = \cos(q_2)$, $s_{12} = \sin(q_1 + q_2)$ and $c_{12} = \cos(q_1 + q_2)$.

We take the dynamic parameter values of the master and the slave robots to be

$$\begin{aligned} m_{1m} = 2.3kg,\ m_{2m} = 2.3kg,\ l_{1m} = 0.5m,\ l_{2m} = 0.5m \\ m_{1s} = 2.3kg,\ m_{2s} = 2.3kg,\ l_{1s} = 0.5m,\ l_{2s} = 0.5m. \end{aligned} \tag{4.52}$$

In this simulation study, we consider the teleoperation system in free motion, i.e., no forces/torques are applied to the manipulators by the human operator or the remote environment. We will consider two types of disturbances acting on the manipulators, namely, joint frictions and end-effector payloads. We do not consider dynamic uncertainties in this simulation study. Therefore, the total disturbance vector acting on the joints of each of the manipulators can be computed by

[1] Given the joint positions $\mathbf{q}$ and the joint velocities $\dot{\mathbf{q}}$ of a manipulator, the following equations can be used to find the position $\mathbf{x}$ and the velocity $\dot{\mathbf{x}}$ of the manipulator's end-effector:

$$\begin{aligned} \mathbf{x} &= \mathbf{h}(\mathbf{q}) \\ \dot{\mathbf{x}} &= \mathbf{J}(\mathbf{q})\dot{\mathbf{q}} \end{aligned}$$

$$\boldsymbol{\tau}_d = \boldsymbol{\tau}_{friction} + \mathbf{J}^T \mathbf{F}_{payload} \tag{4.53}$$

where $\boldsymbol{\tau}_{friction}$ and $\mathbf{F}_{payload}$ represent the friction torque and the end-effector payload force vectors, respectively.

The friction torques acting on the joints of the robots are generated based on the model in [90]. For the $i-th$ joint of the robot, $i = 1, 2$, we have the frictions modeled as

$$\begin{aligned} \tau_{i_{friction}} &= F_{ci}\text{sgn}(\dot{q}_i)[1 - \exp(\frac{-\dot{q}_i^2}{v_{si}^2})] \\ &\quad + F_{si}\text{sgn}(\dot{q}_i)\exp(\frac{-\dot{q}_i^2}{v_{si}^2}) + F_{vi}\dot{q}_i \end{aligned} \tag{4.54}$$

where F_{ci}, F_{si}, F_{vi} are the Coulomb, static, and viscous friction coefficients, respectively. The parameter v_{si} is the Stribeck parameter. In the simulations, the friction coefficients and the Stribeck parameter for the master and the slave are chosen as follows [96]:

$$\begin{aligned} F_{ci} &= 0.49,\ F_{si} = 3.5,\ F_{vi} = 0.15,\ v_{si} = 0.189 \\ i &= 1, 2. \end{aligned} \tag{4.55}$$

The end-effector payloads (see Figure (4.3)) are chosen to be masses equal to $4kg$ connected to the end-effectors of the robots. Therefore, we have

$$\mathbf{F}_{payload} = \begin{bmatrix} 0 \\ M_{ext}g \end{bmatrix}. \tag{4.56}$$

The one-way variable time delay in the communication channel is modelled by a random signal with shifted gamma distribution. This distribution has been used to model the internet-based teleoperation time delays [97, 98]. The probability density function of shifted gamma is [97]:

$$f(x) = \frac{(\frac{x-\gamma}{\beta})^{\alpha-1}.\exp(-\frac{x-\gamma}{\beta})}{\beta.\Gamma(\alpha)}. \tag{4.57}$$

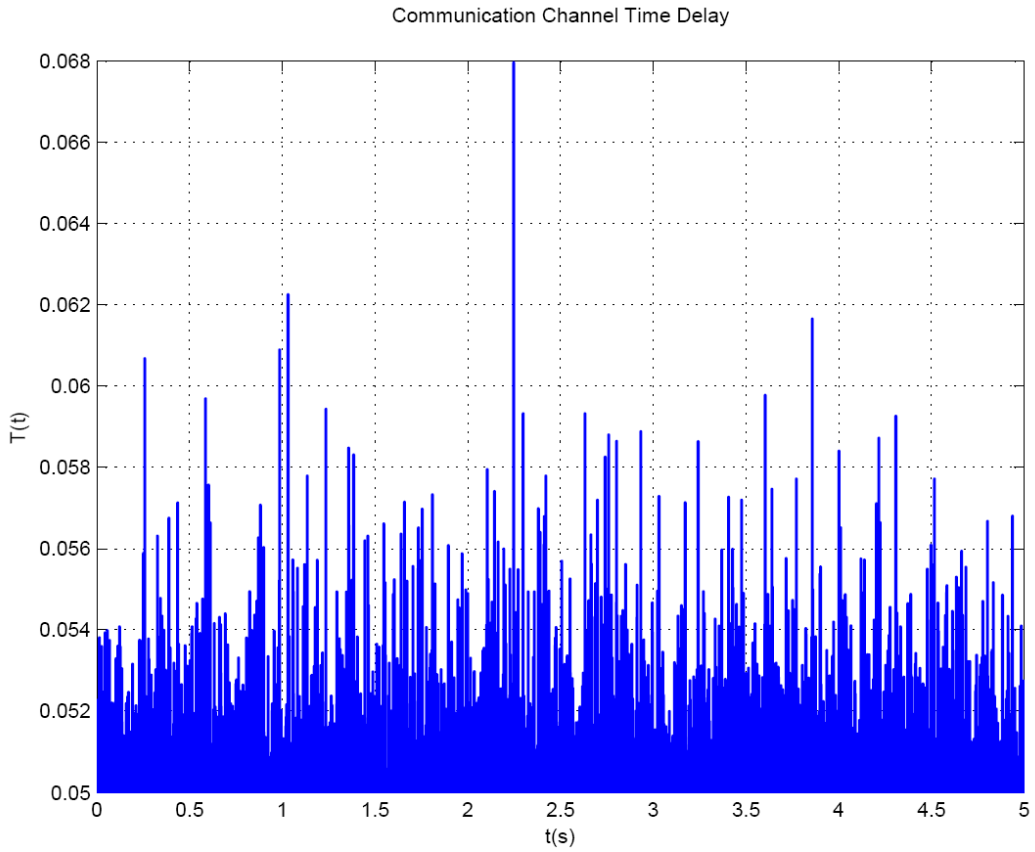

Figure 4.4: Communication channel time delay.

We have chosen $\alpha = \beta = 2.5 \times 10^{-3}$ and $\gamma = 5 \times 10^{-3}$ in the simulation. For the sake of simplicity, we consider the same variable time delay in both directions, i.e., $T_m(t) = T_s(t)$. Figure 4.4 shows the time history of the variable time delay. As it can be observed, the time delay varies between 50^{ms} and 68^{ms}.

In this simulation study, the parameters of the synchronizing torques, given in (4.12) and (4.13), are considered to be $k_i = 2$ and $b_i = 0.8$, $i = m, s$. Note that these gains satisfy the inequality (4.34) of Theorem 4.1. The disturbance observers are given by (4.16) and (4.18) with $\alpha_i = 20$, $i = m, s$. The teleoperation control torques are given by (4.10) and (4.11).

We choose different values for initial joint positions of the master and the slave while assuming that both robots are initially at rest. We take the initial joint position vectors to be

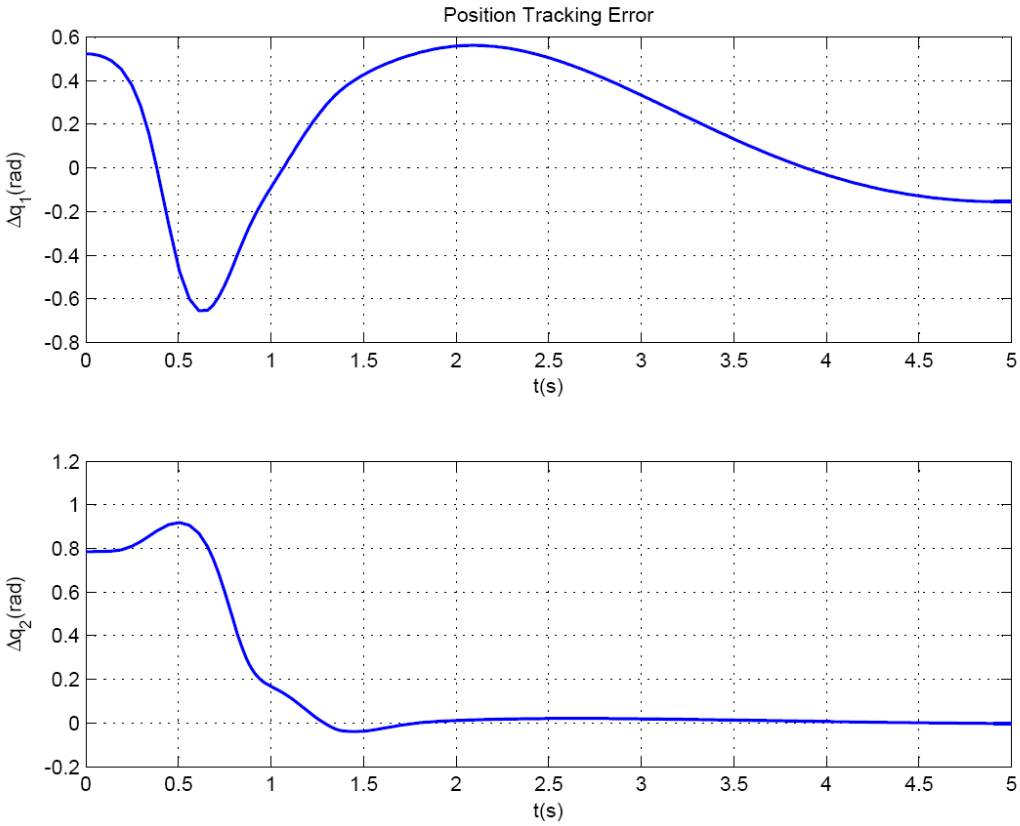

Figure 4.5: Position tracking response of the teleoperation system without disturbance observers.

$$\begin{aligned} \mathbf{q}_{0m} &= [30^\circ, 135^\circ]^T \\ \mathbf{q}_{0s} &= [0, 90^\circ]^T. \end{aligned}$$

Figure 4.5 shows the position tracking response of the teleoperation system when no disturbance observer is used, i.e., when the control law proposed by [59] is used. Because of the friction torques and the external payloads exerted to the master and the slave, the control law without using disturbance observers fails to achieve good position tracking when the teleoperation system is in free motion.

Now, we employ disturbance observers at the master and the slave sides of the teleoperation system. Figures 4.6 and 4.7 show the disturbance tracking response of the disturbance observers at the master and the slave sides, respectively. As it was also indicated by Theorem 4.1, the disturbance observers are able to acheive perfect disturbance tracking. Figure 4.8 shows the position tracking response of the

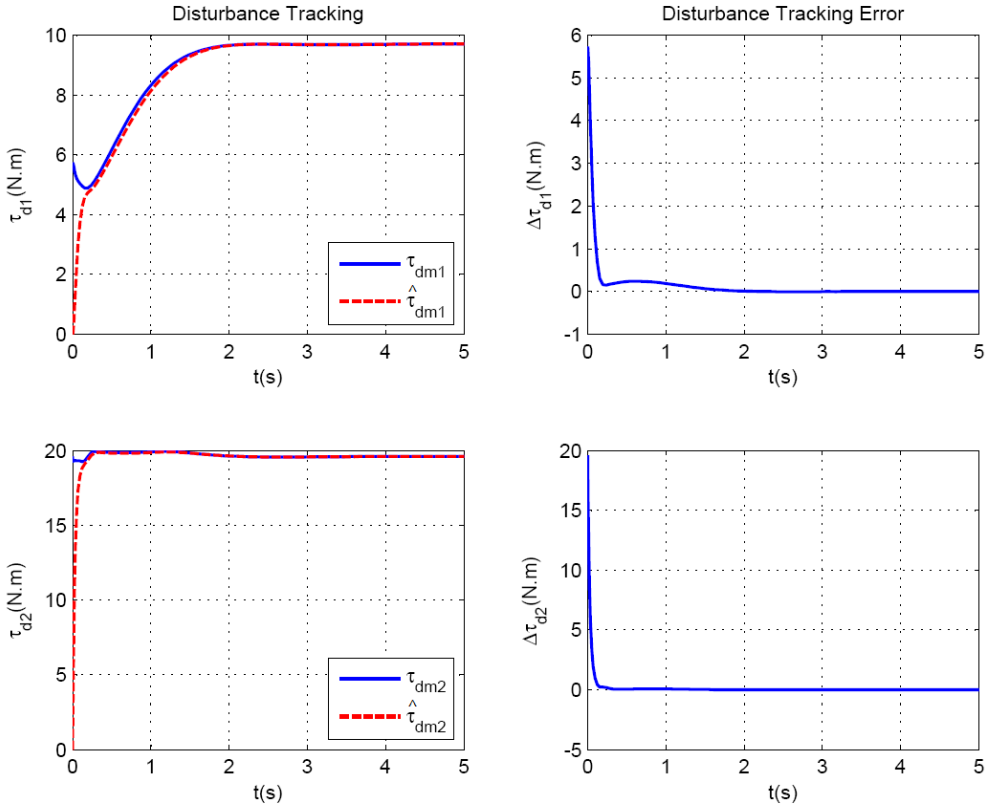

Figure 4.6: Disturbance tracking at the master side.

teleoperation system when disturbance observers are employed at the master and the slave sides of the teleoperation system. The position tracking error goes to zero according to Theorem 4.1.

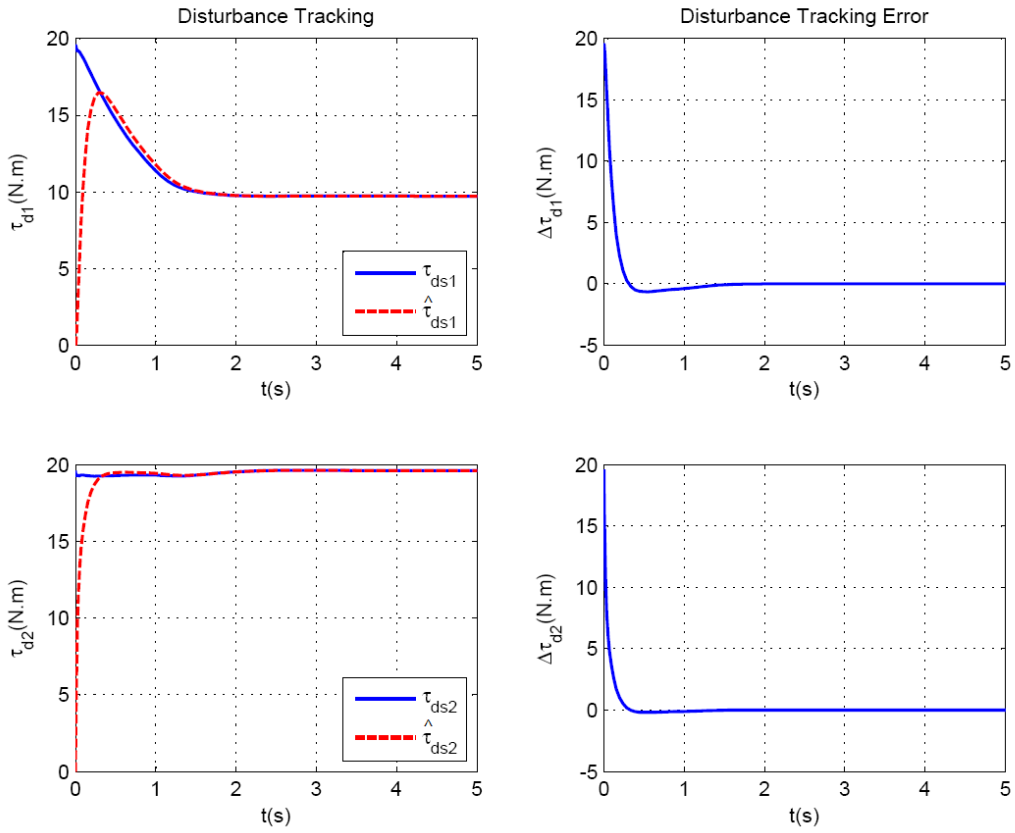

Figure 4.7: Disturbance tracking at the slave side.

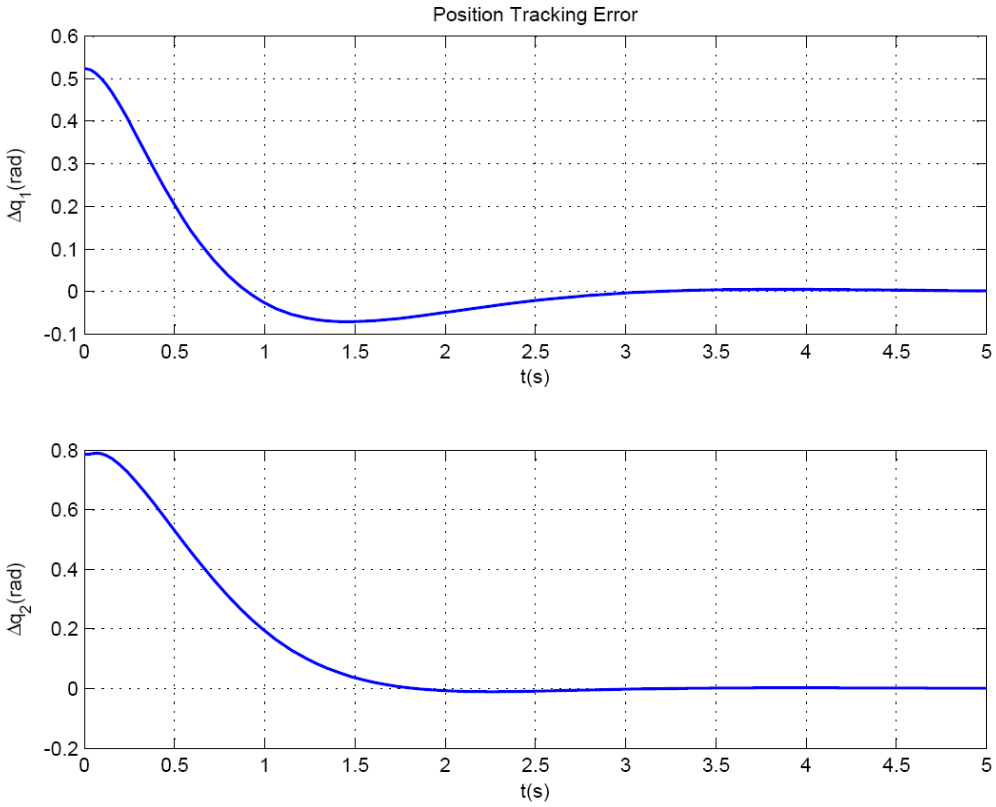

Figure 4.8: Position tracking response of the teleoperation system with disturbance observers.

Chapter 5

Experiments

5.1 Introduction

In this chapter[1], we present the experimental setup, the developed software and the experiments. We demonstrate the effectiveness of the proposed design methods developed throughout the thesis by performing experiments using PHANToM Omni® haptic device.

This chapter is organized in the following way. First, we will introduce the PHANToM Omni robot (haptic device) and its dynamics. Next, we will introduce the PHANSIM Toolkit which has been developed to control the PHANToM haptic devices from MATLAB/Simulink. Thereafter, we will perform experiments to show the efficiency of the disturbance observer design method and disturbance observer based control of bilateral teleoperation systems with variable time delays that are proposed in Chapters 2 and 3, respectively.

5.2 Introduction to PHANToM Omni Haptic Device

5.2.1 Overview of the PHANToM haptic devices

The word *haptic*, from the Greek origin *haptikus*, means of/related to the sense of touch. Haptic technology enables the users to touch and manipulate remote or virtual objects in remote or virtual environments. This technology has found applications in a wide variety of areas such as video games, medical training, scientific visualization, computer animation, remote vehicle and robot control, and medical

[1] A version of the second section of this chapter has been published in the Proceedings of the 23rd Canadian Congress of Applied Mechanics [99].

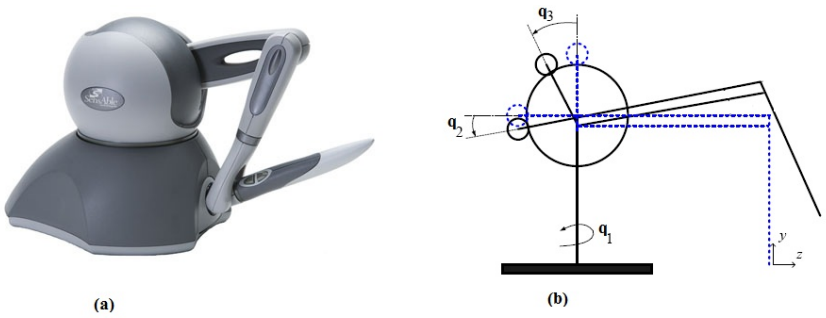

Figure 5.1: (a) PHANToM Omni haptic device, ©Copyright SensAble Technologies, Inc., (b) PHANToM Omni schematic diagram.

rehabilitation. The SensAble™ PHANToM® haptic devices (SenSable Technologies, MA, USA, `www.sensable.com`) are among the most popular commercial haptic devices that provide the users with an opportunity for research and education in haptic technology and its applications. The PHANToM® product line includes a large variety of haptic devices, from the Premium models with high-precision, large workspaces and high forces to the Omni model that is one of the most cost-effective haptic devices available in the market. These haptic devices have been used in various applications that provide the user with the sense of touch such as computer games [100], surgical simulators [101], virtual rehabilitation excercise systems [102] and teleoperation systems [103].

5.2.2 PHANToM Omni dynamics

The PHANToM Omni haptic device is a small robot arm that has three actuated revolute joints which provide the user with force feedback information. The active joints of the Omni robot are actuated by computer-controlled electric DC motors. In addition to the actuated joints, the PHANToM robot has 3 wrist joints that are passive. We will use the first three joints of the device, i.e., the actuated joints, in our experiments. Figure 5.1 depicts a PHANToM Omni haptic device and its schmeatic diagram.

The following equation gives the dynamics of an n-DOF, n is equal to 3 in the case of the Omni robot, rigid manipulator [80]:

$$\mathbf{M}(\mathbf{q})\ddot{\mathbf{q}} + \mathbf{C}(\mathbf{q}, \dot{\mathbf{q}})\dot{\mathbf{q}} + \mathbf{G}(\mathbf{q}) = \boldsymbol{\tau} \tag{5.1}$$

where $\mathbf{q}$,$\dot{\mathbf{q}}$ and $\ddot{\mathbf{q}}$ are the $n \times 1$ vectors of joint positions, velocities and accelerations, respectively. Here, $\mathbf{M}(\mathbf{q})$ is the $n \times n$ inertia matrix, $\mathbf{C}(\mathbf{q}, \dot{\mathbf{q}})$ is the $n \times n$ Coriolis/-centrifugal matrix, $\mathbf{G}(\mathbf{q})$ is the $n \times 1$ vector of gravitational forces, and $\boldsymbol{\tau}$ is the $n \times 1$

vector of input control torques. The inertia matrix of the Omni robot is [104]:

$$\mathbf{M}(\mathbf{q}) = \begin{bmatrix} M_{11} & M_{12} & 0 \\ M_{21} & M_{22} & M_{23} \\ 0 & M_{32} & M_{33} \end{bmatrix} \tag{5.2}$$

where,

$$\begin{aligned} M_{11} &= \alpha_{D1} + \alpha_{D2}\cos(2q_2) + \alpha_{D3}\cos(2q_3) + \alpha_{D4}\sin(2q_3) + \\ &\alpha_{D5}\cos(q_2)\sin(q_3) + \alpha_{D6}\cos(q_2)\cos(q_3) \\ M_{12} &= M_{21} = \alpha_{D7}\sin(q_2) \\ M_{22} &= \alpha_{D8} \\ M_{23} &= M_{32} = -0.5\alpha_{D5}\sin(q_2 - q_3) + 0.5\alpha_{D6}\cos(q_2 - q_3) \\ M_{33} &= \alpha_{D9}. \end{aligned} \tag{5.3}$$

We define the vector $\mathbf{V}(\mathbf{q}, \dot{\mathbf{q}})$ as the sum of the Coriolis, centrifugal and gravity forces. We have [104]:

$$\mathbf{V}(\mathbf{q}, \dot{\mathbf{q}}) = [V_1, V_2, V_3]^T = \mathbf{C}(\mathbf{q}, \dot{\mathbf{q}})\dot{\mathbf{q}} + \mathbf{G}(\mathbf{q}) \tag{5.4}$$

where,

$$\begin{aligned} V_1 &= -2\alpha_{D2}\dot{q}_1\dot{q}_2\sin(2q_2) - 2\alpha_{D3}\dot{q}_1\dot{q}_3\sin(2q_3) + 2\alpha_{D4}\dot{q}_1\dot{q}_3\cos(2q_3) - \alpha_{D5}\dot{q}_1\dot{q}_2\sin(q_2)\sin(q_3) \\ &+\alpha_{D5}\dot{q}_1\dot{q}_3\cos(q_2)\cos(q_3) - \alpha_{D6}\dot{q}_1\dot{q}_2\sin(q_2)\cos(q_3) - \alpha_{D6}\dot{q}_1\dot{q}_3\cos(q_2)\sin(q_3) + \alpha_{D7}\dot{q}_2^2\cos(q_2) \\ V_2 &= 2\alpha_{D2}\dot{q}_1^2\cos(q_2)\sin(q_2) + 0.5\alpha_{D5}\dot{q}_1^2\sin(q_2)\sin(q_3) + 0.5\alpha_{D5}\dot{q}_3^2\cos(q_2 - q_3) \\ &0.5\alpha_{D6}\dot{q}_1^2\sin(q_2)\cos(q_3) + 0.5\alpha_{D6}\dot{q}_3^2\sin(q_2 - q_3) + \alpha_{D10}\cos(q_2) + \alpha_{D13}(q_2 - \frac{\pi}{2}) \\ V_3 &= 2\alpha_{D3}\dot{q}_1^2\cos(q_3)\sin(q_3) - \alpha_{D4}\dot{q}_1^2\cos(2q_3) - 0.5\alpha_{D5}\dot{q}_1^2\cos(q_2)\cos(q_3) - 0.5\alpha_{D5}\dot{q}_2^2\cos(q_2 - q_3) \\ &+0.5\alpha_{D6}\dot{q}_1^2\cos(q_2)\sin(q_3) - 0.5\alpha_{D6}\dot{q}_2^2\sin(q_2 - q_3) + \alpha_{D11}\sin(q_3) + \alpha_{D12}\cos(q_3). \end{aligned} \tag{5.5}$$

5.3 Software Development

The OpenHaptics® Software Development Kit, provided by the SensAble Technologies, Inc. (`www.sensable.com`), enables the users to develop C/C++ programs to work with the PHANToM haptic devices. However, it does not provide easy access to the device inputs and outputs, easy integration with external hardware such

as cameras, and advanced mathematical functions such as matrix operations and filtering tasks. On the other hand, MATLAB/Simulink software package, which supports external hardware integration and a large variety of mathematical functions, has been used to develop versatile real-time interface for motion control of different robots such as KUKA and PUMA 560 manipulators [105, 106]. Quanser Inc. has developed a commercial software package, QUARC®, which integrates with the MATLAB/Simulink and provides real-time access to many different hardware platforms including the PHANToM Omni. However, it is a relatively costly software package. A noncommercial interface has also been developed for the PHANToM Omni [107]. However, it requires dismantling the haptic device and using an additional hardware system, i.e. dSPACE system, in order to use this interface. This serves as the motivation to develop an academic/non-commercial Simulink toolkit for the PHANToM haptic devices.

The PHANSIM Toolkit uses C/C++ S-functions along with the OpenHaptics toolkit to make an interface that provides the users with access to the PHANToM torque/-force inputs, the Cartesian pose (position and orientation) of the gimbal and the joint angles of the device in the Simulink environment. The toolkit supports the operation of a single haptic device as well as the teleoperation of a master-slave system consisting of two haptic devices. This toolkit enables the users to implement and test their designed controllers on the PHANToM devices in a fast and easy way. The toolkit can be downloaded from the webpage: `http://www.ece.ualberta.ca/\textasciitildealireza3/Research.html`.

In this section, we will introduce the PHANSIM Toolkit and its capabilites. We will explain how this toolkit works. Also, we will provide an overview on the Simulink blocks which are provided in the PHANSIM Toolkit library. Finally, we show the usefulness of the toolkit by an illustrative experiment, namely a circle drawing task using an Omni robot.

5.3.1 Overview of the PHANSIM Toolkit

The PHANSIM Toolkit builds up a Simulink interface/block on top of the OpenHaptics Toolkit. The OpenHaptics HDAPI (Haptic Device Application Programming Interface) functions included in the OpenHaptics Toolkit enable the programmers to access and manipulate the low-level signals of the haptic devie (e.g., joint torque commands and joint position readings) using C/C++. One important component of the HDAPI is the scheduler component which enables the developer to communicate with the underlying servo-loop thread without using platform specific synchronization and thread related system calls. In order to create an interface for the haptic device, which enables the users to set the input force/torque of the haptic device and to read the device states in the Simulink environment, we have used C/C++ S-functions to access the OpenHaptics HDAPI functions from Simulink. Figure 5.2 depicts how the Simulink communicates with the physical device by using the toolkit

S-functions and the OpenHaptics HDAPI functions.

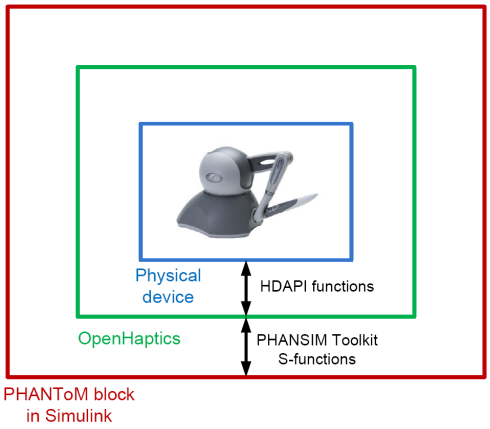

Figure 5.2: PHANSIM Toolkit hierarchy.

In order to work with a haptic device using the OpenHaptics Toolkit, the HDAPI functions should be called according to the following pattern (the readers are referred to the OpenHaptics Toolkit guide , provided with the software, for a thorough explanation):

1. The device should be initialized.
2. The force outputs should be activated and the device scheduler function should be defined and started.
3. The force outputs should be disabled and the scheduler should be cleaned up.

The PHANSIM Toolkit S-functions use the above pattern to invoke the HDAPI functions and manipulate the haptic device. Figure 5.3 depicts the flow chart of the PHANSIM interface. As it can be observed, when the user starts the Simulink model, the haptic device will be initialized, device force outputs will be activated and the device scheduler function will be started. The scheduler function is called every 1 millisecond and applies the force or torque inputs, which are provided by the Simulink S-functions, to the device and reads the states (e.g., joint angles and gimbal position) of the device, which are reported to the Simulink S-functions. The Simulink should be able to update the inputs provided for the haptic device with a rate faster than or equal to 1 kHz if a smooth motion is required. The rate at which the inputs of the device are updated in the Simulink can be set through the Configuration Parameters dialog box of the Simulink model. In fact, one can consider the scheduler function as a sample-and-hold device which reads the inputs and reports the outputs at a rate of 1 kHz. When the user terminates running the Simulink model, the haptic device scheduler will be stopped and the device force outputs will be disabled. In short, the PHANSIM Simulink interface initialzes the

device, provides input for the scheduler function, reads the device output and stops the device at the end by using the HDAPI functions.

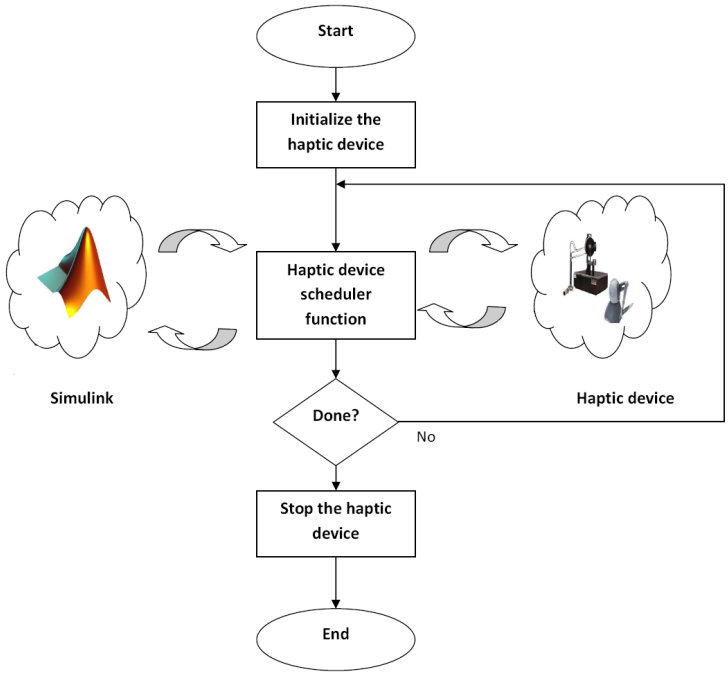

Figure 5.3: Flow chart of the PHANSIM interface.

The PHANSIM library consists of the following blocks:

- PHANToM Block: This block can be used when only one haptic device is used. Force or torque inputs may be applied to the device. The user can determine the domain of the inputs (joint-level vs. Cartesian-level) in the block dialog box. Gimbal coordinates and angles and the angles of the first three actuated joints (q_1, q_2 and q_3) can be read from the device. If more than one haptic device is connected to the PC, the user can choose the desired device by typing its name in the block dialog box. The device name is the name by which the SenSable's PHANTOM Test program recognizes the haptic device. Figure 5.4 shows the PHANTOM Block.
- PHANTOM Teleoperation Block: This block can be used when two haptic devices are used simultaneously. Again, force or torque inputs may be applied to the devices; the user can determine the type of inputs in the block dialog box. Gimbal coordinates and angles and the angles of the first three actuated joints of the robots can be read. The user can identify each device by typing its name in the block dialog box. Figure 5.5 shows this block.
- PHANTOM Clock Generator Block: Since Simulink's simulation time is not

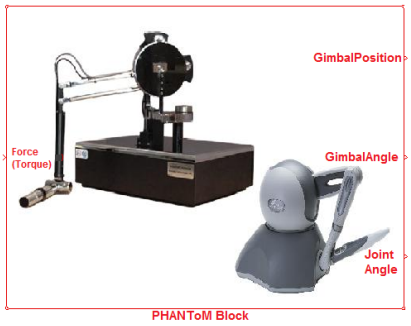

Figure 5.4: PHANSIM Library: PHANTOM Block.

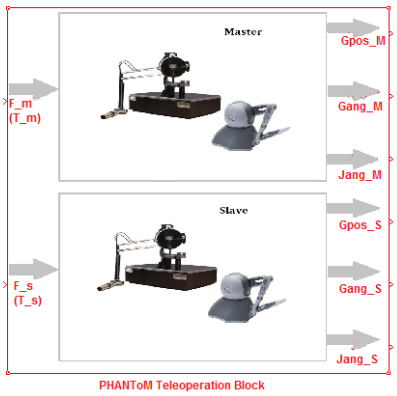

Figure 5.5: PHANSIM Library: PHANTOM Teleoperation Block.

representative of the actual time elapsed during an experiment, a block is needed to synchronize the simulation with the actual time. The PHANTOM Clock Generator Block generates a real-time clock signal by reading the CPU time. This block can be used to generate real-time signals. For instance, if we want to record the time passed during a teleoperation task, we should use this block's output to record the time. Figure 5.6 shows this block.

5.3.2 Illustrative experiment: Circle drawing task

This section illustrates the effectiveness of the toolkit by an experiment, namely, a circle drawing task. In the experiment, a PHANToM Omni haptic device is connected to a PC through the IEEE 1394 port. The following software programs were installed on the PC:

- Microsoft Windows® XP (service pack 2),
- MATLAB® R2009a (32-bit version),

Figure 5.6: PHANSIM Library: PHANTOM Clock Generator Block.

- OpenHaptics® 3.0 academic edition.

A PHANToM Omni haptic device is used to draw a circle with a radius of 30 mm on a horizontal plane. Proportional-derivative (PD) control laws are used as control schemes at each joint with proportional and derivative gains equal to 0.25 and 0.7, respectively. Through the PHANTOM Block, a force input (i.e., PD controller output) was applied to the device, and the Cartesian coordiantes of the device gimbal were read. The reference trajectory was:

$$x(t) = 30\sin(\frac{\pi}{2}t),\ y(t) = 0,\ z(t) = 30\cos(\frac{\pi}{2}t). \tag{5.6}$$

Figure 5.7 shows the block diagram used to run the experiment in the Simulink environment. The Simulink PID controller block from *Simulink Extras/Additional Linear library* was used to implement the PD control law. Note that the output of the PHANToM Clock Generator Block is used to synchronize the *sine wave* sources with the actual time which is read from the PC's CPU. Figure 5.8 depicts the gimbal's x and z coordinates time-histories and the final trajectory of the device gimbal.

5.4 Experiments

In this section, we will perform two experiments in order to demonstrate the effectiveness of the methods developed throughout the thesis. In the first experiment, we will design a disturbance observer for a single Omni robot. In the second experiment, we will design a disturbance observer based control law for a bilateral teleoperation system that consists of two Omni robots.

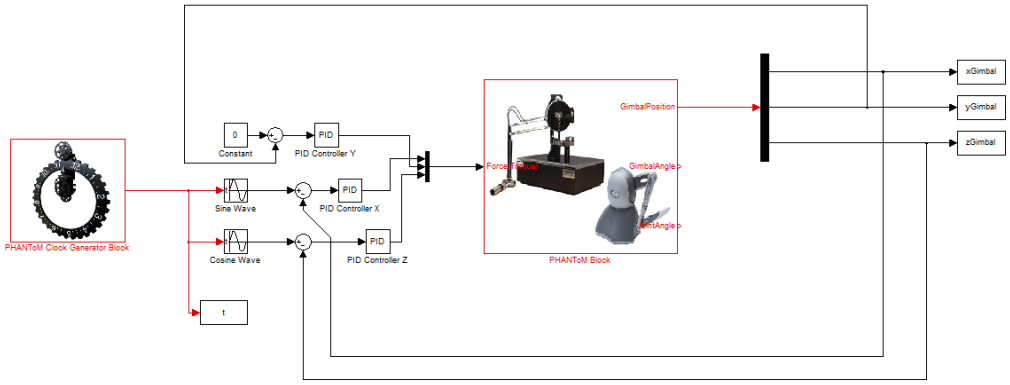

Figure 5.7: Simulink block diagram of the control system in the first experiment.

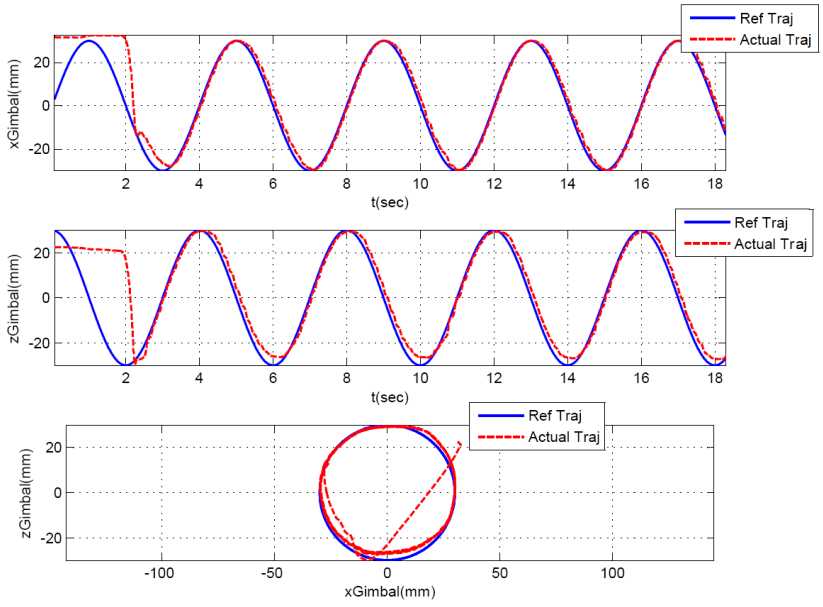

Figure 5.8: Illustrative experiment: Circle drawing task.

5.4.1 Experiment 1: Disturbance observer design for a non-planar 2-DOF robot

In this section, we will design a disturbance observer for a single non-planar 2-DOF robot and use it with a computed-torque controller to show the effectiveness of the disturbance observer design method proposed in Chapter 3.

Experimental setup

We will use the first and the third actuated joints of the Omni robot in this experiment while the second actuated joint is locked at 0°. Note that this mechanism is not confined to a constant 2-D plane and moves in three-dimensional space. Therefore, the nonlinear disturbance observer proposed by [12] cannot be employed here. Figure 5.9 shows the PHANToM Omni setup that was used in our experiments. The disturbance observer is used to estimate and compensate for the joint frictions and an external unknown payload. The payload is a metal cube that is attached to the gimbal of the robot. The Omni is connected to a PC through an IEEE 1394 port. The Omni end-effector position and orientation data are collected at a rate of 1000 Hz. We define $c_i = \cos(q_i)$, $s_i = \sin(q_i)$, $c_{2.i} = \cos(2q_i)$, and $s_{2.i} = \sin(2q_i)$. The inertia matrix of the Omni, assuming $q_2 = 0$, can be found from (5.2) and (5.3). We have

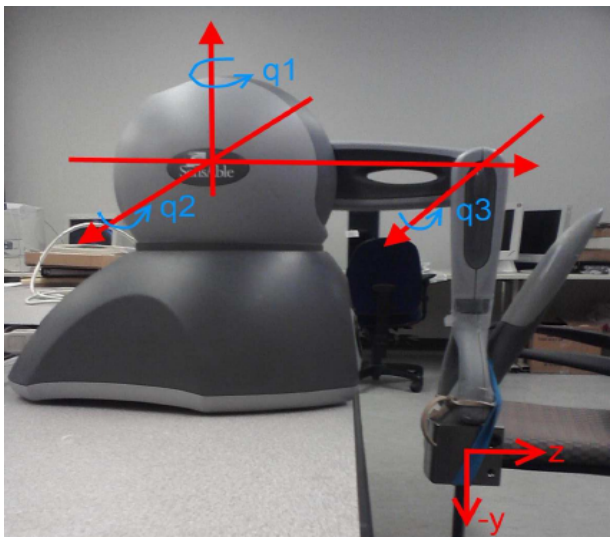

Figure 5.9: Setup used for Experiment 1.

$$\mathbf{M}(\mathbf{q}) = \begin{bmatrix} \alpha_1 + \alpha_2 c_{2.3} + \alpha_3 s_{2.3} + \alpha_4 c_3 + \alpha_5 s_3 & 0 \\ 0 & \alpha_6 \end{bmatrix}. \tag{5.7}$$

Also, defining the vector

$$\mathbf{V}(\mathbf{q},\dot{\mathbf{q}}) = [V_1, V_2]^T = \mathbf{C}(\mathbf{q},\dot{\mathbf{q}})\dot{\mathbf{q}} + \mathbf{G}(\mathbf{q}) \tag{5.8}$$

as the sum of the Coriolis, centrifugal and gravity forces, we have

$$\begin{aligned} V_1 &= -2\alpha_2\dot{q}_1\dot{q}_3\sin(2q_3) + 2\alpha_3\dot{q}_1\dot{q}_3\cos(2q_3) \\ &\quad +\alpha_4\dot{q}_1\dot{q}_3\cos(q_3) - \alpha_5\dot{q}_1\dot{q}_3\sin(q_3) \\ V_2 &= 2\alpha_2\dot{q}_1^2\cos(q_3)\sin(q_3) - \alpha_3\dot{q}_1^2\cos(2q_3) - \\ &\quad \frac{1}{2}\alpha_4\dot{q}_1^2\cos(q_3) + \frac{1}{2}\alpha_5\dot{q}_1^2\sin(q_3) \\ &\quad +\alpha_7\sin(q_3) + \alpha_8\cos(q_3). \end{aligned} \tag{5.9}$$

The Jacobian of the Omni, considering $q_2 = 0$, is:

$$\mathbf{J}(\mathbf{q}) = \begin{bmatrix} l_1 + l_2 s_3 & 0 \\ 0 & l_1 s_3 \end{bmatrix} \tag{5.10}$$

where $l_1 = l_2 = 135$ mm are the lengths of the first and the second links of the robot. Therefore, the disturbance due to the external payload that is being exerted to the first and the third joints of the robot is:

$$\boldsymbol{\tau}_{payload} = \mathbf{J}^T\mathbf{F} = \mathbf{J}^T \begin{bmatrix} 0 \\ mg \end{bmatrix} = \begin{bmatrix} 0 \\ mgl_1 s_3 \end{bmatrix}. \tag{5.11}$$

Experimental identification of the 2-DOF model parameters

We need to experimentally identify the dynamics of the Omni robot to use it in the computed-torque control law and the disturbance observer in the first experiment of this section. We identified the Omni parameters without any external payloads using the method proposed in [104] and [108]. Based on this method, we should linearly parametrize the dynamic equation of the Omni robot. An important property of the dynamical model of the robot given in (5.1) is that this model is linearly parametrizable [80]. That is, we have

$$\underbrace{\mathbf{Y}(\ddot{\mathbf{q}},\dot{\mathbf{q}},\mathbf{q})\boldsymbol{\alpha}}_{\mathbf{M}(\mathbf{q})\ddot{\mathbf{q}}+\mathbf{C}(\mathbf{q},\dot{\mathbf{q}})\dot{\mathbf{q}}+\mathbf{G}(\mathbf{q})} = \boldsymbol{\tau} \tag{5.12}$$

where $\mathbf{Y}$ is called the dynamic regressor matrix of the robot. The matrix $\mathbf{Y}$ is a matrix of known functions of $\ddot{\mathbf{q}}, \dot{\mathbf{q}}$, and $\mathbf{q}$. The vector $\boldsymbol{\alpha} = [\alpha_1, \ldots, \alpha_8]^T$ represents the vector of the unknown parameters of the robot that are to be identified. The parameters α_i, $i = 1, \ldots, 8$ are functions of the inertial and kinematic parameters of the robot such as the mass and the length of the linkages (see [109] for a detailed derivation). The significance of the approach in [104] and [108] is that we do not need to know the inertial and kinematic parameters of the robot in order to determine the parameters α_i. Note that $\mathbf{Y} \in R^{2\times 8}$ and $\boldsymbol{\alpha} \in R^{8\times 1}$ in the case of the 2-DOF mechanism given by equations (5.7)–(5.9). We have

$$\mathbf{Y}^T = \begin{bmatrix} \ddot{q}_1 & 0 \\ \ddot{q}_1 c_{2.3} - 2\dot{q}_1\dot{q}_3 s_{2.3} & 2\dot{q}_1^2 c_3 s_3 \\ \ddot{q}_1 s_{2.3} + 2\dot{q}_1\dot{q}_3 c_{2.3} & -\dot{q}_1^2 c_{2.3} \\ \ddot{q}_1 s_3 + \dot{q}_1\dot{q}_3 c_3 & -\frac{1}{2}\dot{q}_1^2 c_3 \\ \ddot{q}_1 c_3 - \dot{q}_1\dot{q}_3 s_3 & \frac{1}{2}\dot{q}_1^2 s_3 \\ 0 & \ddot{q}_3 \\ 0 & s_3 \\ 0 & c_3 \end{bmatrix}. \tag{5.13}$$

As it can be seen from (5.12), we need to know the joint velocities and accelerations in order to compute the regressor matrix $\mathbf{Y}$. However, acceleration measurements are not available and therefore we will have to use precise numerical differentiation techniques in order to obtain the joint accelerations from the noise-corrupted joint velocities. Another alternative, which is shown in Figure 5.11, is to pass the dynamic model (5.12) through a first-order stable low-pass filter of the form $L(s) = \frac{\omega_L}{s+\omega_L}$ to avoid acceleration measurements [108]. The cut-off frequency of the filter, i.e., ω_L, should be chosen to be between the robot motion frequencies and noise frequencies. Passing the dynamic model (5.12) through $L(s)$, we get

$$\mathbf{Y}_L(\dot{\mathbf{q}},\mathbf{q})\boldsymbol{\alpha} = \boldsymbol{\tau}_L \tag{5.14}$$

where $\mathbf{Y}_L$ is the filtered regressor matrix and $\boldsymbol{\tau}_L$ is the filtered torque (see [108] for a detailed derivation).

As it is shown in Figure 5.11, we perform the Omni identification in two steps. In the first step, data is collected when the robot is excited by the joint torques and

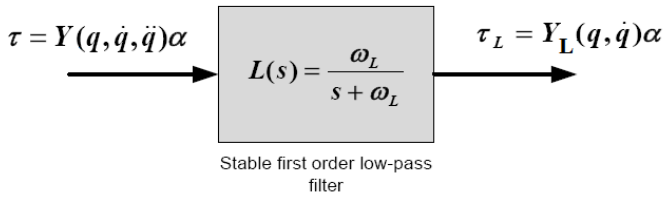

Figure 5.10: Passing the dynamic of the Omni robot through a first-order stable low-pass filter.

is moving in free space. In the second step, the parameters of the Omni robot are identified by solving a linear optimization problem.

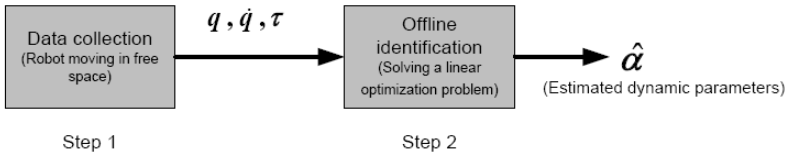

Figure 5.11: Two-step identification of the Omni parameters.

Having acquired the experimental data from the first step, we use the recursive least squares algorithm to find the dynamic parameters of the Omni robot in the second step. In the least square estimation, we would like to find an estimation of the Omni dynamic parameters such that the the sum of the squares of the difference between the actual filtered torques and the computed filtered torques is minimized [110]. Assume that the filtered torque and the filtered regressor matrix are $\boldsymbol{\tau}_L(t_k)$ and $\mathbf{Y}_L(t_k)$ at time instant t_k, respectively. The recursive least squares algorithm will have the following form [110]:

$$\hat{\boldsymbol{\alpha}}(t_k) = \hat{\boldsymbol{\alpha}}(t_{k-1}) + \mathbf{K}(t_k)[\boldsymbol{\tau}_L(t_k) - \mathbf{Y}_L(t_k)\hat{\boldsymbol{\alpha}}(t_{k-1})] \tag{5.15}$$

where $\hat{\boldsymbol{\alpha}}(t_k)$ is the estimated dynamic parameter vector of the Omni robot at time instant t_k. Also, we have

$$\mathbf{K}(t_k) = \mathbf{P}(t_{k-1})\mathbf{Y}_L^T(t_k)[\mathbf{I} + \mathbf{Y}_L^T(t_k)\mathbf{P}(t_{k-1})\mathbf{Y}_L(t_k)]^{-1} \tag{5.16}$$

where $\mathbf{I}$ is the identity matrix. Also, the covariance matrix $\mathbf{P}(t_k)$ is defined as follows:

Table 5.1: Phantom Omni identified parameters

Parameter	Value	Parameter	Value
α_1	$6.11 \times 10^{-3} \pm 0.9 \times 10^{-3}$	α_2	$-2.89 \times 10^{-3} \pm 0.43 \times 10^{-3}$
α_3	$-4.24 \times 10^{-3} \pm 1.01 \times 10^{-3}$	α_4	$3.01 \times 10^{-3} \pm 0.52 \times 10^{-3}$
α_5	$2.05 \times 10^{-3} \pm 0.15 \times 10^{-3}$	α_6	$1.92 \times 10^{-3} \pm 0.23 \times 10^{-3}$
α_7	$1.60 \times 10^{-1} \pm 0.05 \times 10^{-1}$	α_8	$-8.32 \times 10^{-3} \pm 2.78 \times 10^{-3}$

$$\mathbf{P}(t_k) = [\mathbf{I} - \mathbf{K}(t_k)\mathbf{Y}_L(t_{k-1})]\mathbf{P}(t_{k-1}). \tag{5.17}$$

The cut-off frequency of the low-pass filter $L(s)$ was chosen to be between robot motion frequencies and noise frequencies, namely equal to 8 Hz. A sum of 8 sinusoids, 4 sinusoids for each of the joints 1 and 3, with frequencies ranging from 0.2 Hz to 1 Hz were applied to the Omni. Note that the sum of n sinusoids is persistent excitation of an order no less than $2n-2$ [110]. Table 5.1 gives the Omni identified model parameters.

Trajectory following experiment

Based on the identified robot model, equation (5.7), and assuming $\dot{q}_{3max} = 1\frac{\text{rad}}{\text{sec}}$, we have

$$||\hat{\mathbf{M}}(\mathbf{q})|| \leq 0.0132 \tag{5.18}$$

and

$$||\dot{\hat{\mathbf{M}}}(\mathbf{q})|| \leq 0.0138. \tag{5.19}$$

Assuming a minimum convergence rate of $\beta = 1$ and according to (3.61), we will have

$$\mathbf{X}^{-1}_{optimal} = \frac{1}{2}(0.0138 + 2 \times 0.0132 \times \beta) \Rightarrow \mathbf{X}^{-1}_{optimal} = 0.02\mathbf{I}. \tag{5.20}$$

The matrix $\mathbf{X}^{-1}_{optimal}$ is used to design the disturbance observer given by equations (3.28), (3.30), and (3.31). Square-wave commands are supplied as the reference trajectory for the first and the third joints of the robot in the presence of the computed-torque control scheme (3.65). The block diagram of the disturbance observer based

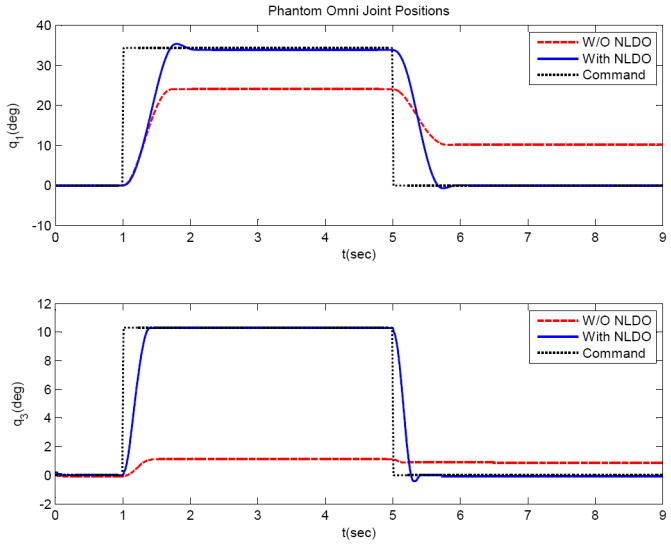

Figure 5.12: Experiment 1: Position-tracking profile of the joints of the Omni robot.

control scheme is shown in Figure 2.1. Figures 5.12 and 5.13 illustrate the time histories of joint positions and disturbances, respectively. Note that we did not know the actual values of the disturbances acting on the the first joint, namely friction and dynamic uncertainties. The upper diagram in Figure 5.13 only demonstrates the output of the disturbance observer, i.e., the estimated disturbance acting on the first joint. As it can be seen, the position tracking in the presence of the disturbance observer has been improved significantly. According to (5.11), the external force exerted to the third joint of the robot is equal to $0.21 \times 9.8 \times 0.135 \times \sin(10) = 0.05$ N when $q_3 = 10^\circ$. The disturbance observer estimates this external force to be equal to 0.058 N. Note that our identification of the dynamic model of the robot was not perfect and we have dynamic uncertainties in the model of our robot. According to Theorem 3.2, the tracking error is guaranteed to be bounded and to converge to its ultimate bound region with an exponential rate. This justifies the residual difference in the tracking error of the disturbance observer. Also, the actual rate of convergence of the tracking error can be computed from Figure 5.13 in the following way (Note that it takes approximately 0.5 second for the disturbance estimate to change from 0 N.m to 0.058 N.m and reach its steady state value.):

$$\text{rate of convergence} \approx -\frac{1}{0.5}\ln(0.058) = 5.7 \geq \beta = 1. \tag{5.21}$$

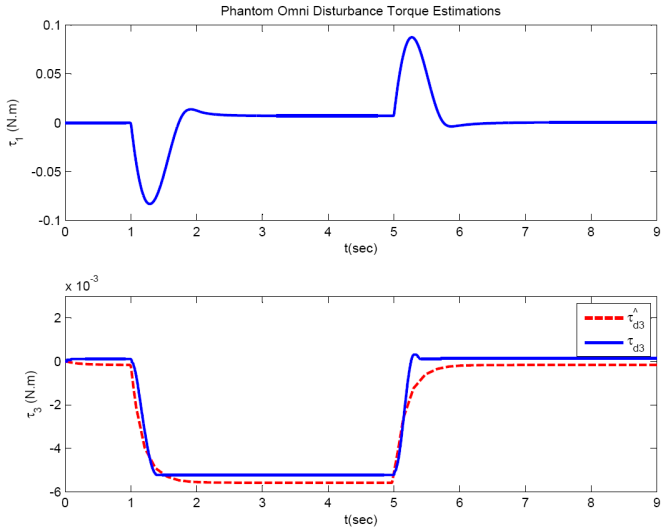

Figure 5.13: Experiment 1: Disturbances of the joints of the Phantom robot.

5.4.2 Experiment 2: Disturbance observer based control of bilateral teleoperation systems with variable time delay

In this section, two experiments are carried out using a pair of Omni robots in order to demonstrate the effectiveness of the disturbance observer based control scheme proposed in Chapter 4 for bilateral teleoperation systems with variable time delay.

Experimental setup

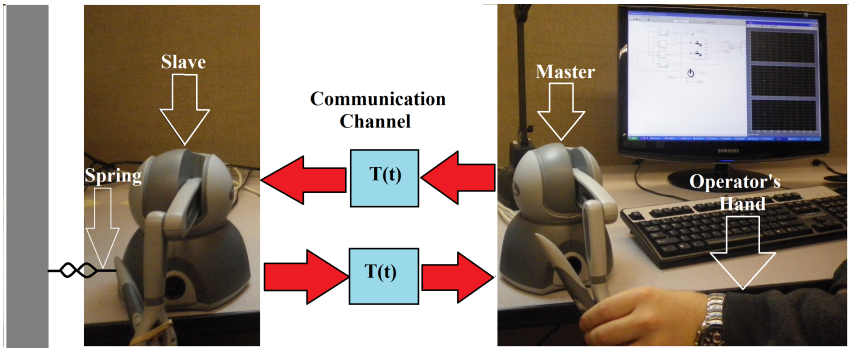

Figure 5.14: Setup used for Experiment 2.

Two PHANToM haptic devices are connected to a computer in a daisy chain configuration, i.e., the first robot's Firewire cable is plugged to the second robot, and the second robot's Firewire cable is plugged to the IEEE 1394 port of the computer.

Again, the Omnis' end-effector position and orientation data are collected at a frequency of 1000 Hz. In the first experiment, the human operator moves the first joint of the master robot while the slave robot is connected to a spring. In the second experiment, the slave robot moves in free space. Figure 5.14 depicts the experimental setup. For the sake of simplicity we consider the communication channel time delay to be the same in both directions, i.e., $T_m(t) = T_s(t) = T(t)$, and is shown in Figure 5.15.

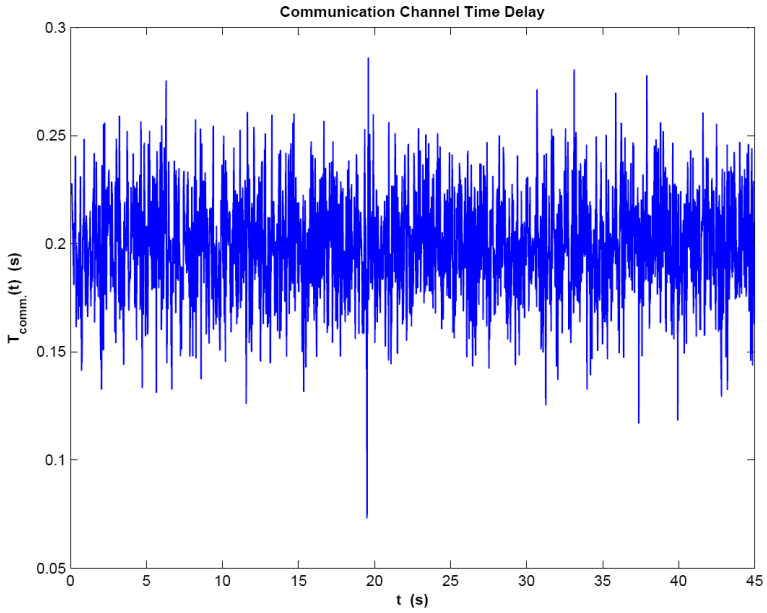

Figure 5.15: Communication channel time delay used in Experiment 2.

Experiment 2 (part. 1): Slave connected to a spring

In the first experiment, the human operator moves the first joint of the master robot. The slave robot, which follows the motion of the master robot, is connected by a rubber band to a stiff wall. The rubber band's exerted torque to the slave robot can be approximated by a linear spring with stiffness $k = 0.67\frac{\text{N.m}}{\text{rad}}$. The second and the third joints of the robots are locked at 0 rad. The parameters of the synchronizing torques, given in (4.12) and (4.13), are considered to be $k_i = 0.1$ and $b_i = 0.022$, $i = m, s$. Note that these gains satisfy the inequality (4.34) of Theorem 4.1. The teleoperation control torques are given by (4.10) and (4.11) with $\hat{\mathbf{G}}_i(\mathbf{q}_i) = 0$. Here, we consider the human operator and the remote environment torques as disturbances.

Figure 5.16 depicts the position tracking response of the teleoperation system when no disturbance observer is used, i.e., when the control law proposed by [59] is used.

Because of the rubber band's interaction with the slave robot, the control law without using disturbance observers fails to achieve good position tracking. As it can be observed from Figure 5.16, there exists a relatively large offset between the steady state position of the master and the slave.

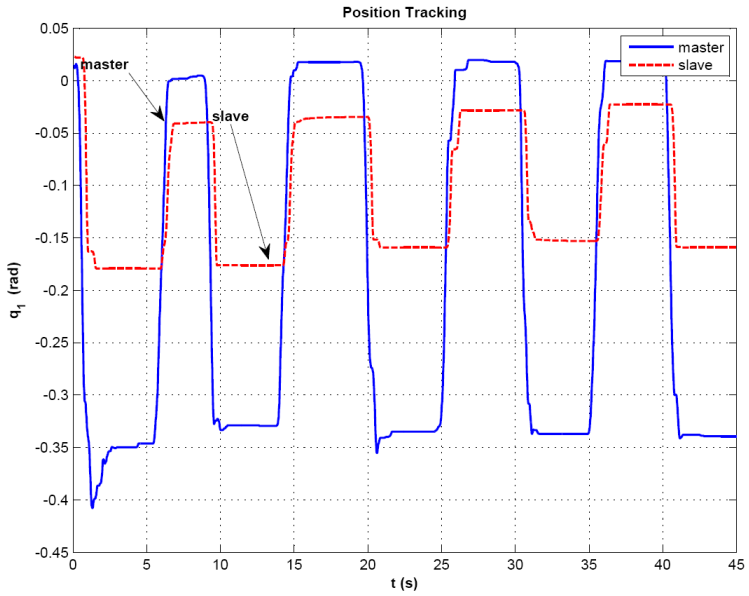

Figure 5.16: Experiment 2 (part. 1)– position tracking response of the teleoperation system without disturbance observers.

Now, we employ the disturbance observers given by (4.16) and (4.18) with $\alpha_i = 0.01$, $\hat{\mathbf{M}}_i(\mathbf{q}_i) = 0.25\mathbf{I}$, $\hat{\mathbf{C}}_i(\mathbf{q}_i, \dot{\mathbf{q}}_i) = 0$, and $\hat{\mathbf{G}}_i(\mathbf{q}_i) = 0$, where $\mathbf{I}$ is the identity matrix. Note that we have not used the exact dynamic models of the robots in implementing the disturbance observers. However, we can ignore the effect of dynamic uncertainties in the model of the robots since the master and the slave robots do not move very fast in these experiments (see equation (4.7)). Figure 5.17 depicts the position tracking response of the teleoperation system when disturbance observers are employed in the teleoperation system. As it can be observed from the figure, the slave robot closely follows the master robot.

Figure 5.18 depicts the disturbance tracking response of the disturbance observer employed at the slave side. As it can be observed, the estimated disturbance at the slave side provides a good approximation of the rubber band exerted torque. The difference, however, can be caused by several factors such as the unaccounted friction torques acting on the slave robot, the dynamic uncertainties in the model of the robot, and the nonlinear behaviour of the rubber band. Figure 5.19 depicts the disturbance estimates provided by both of the disturbance observers.

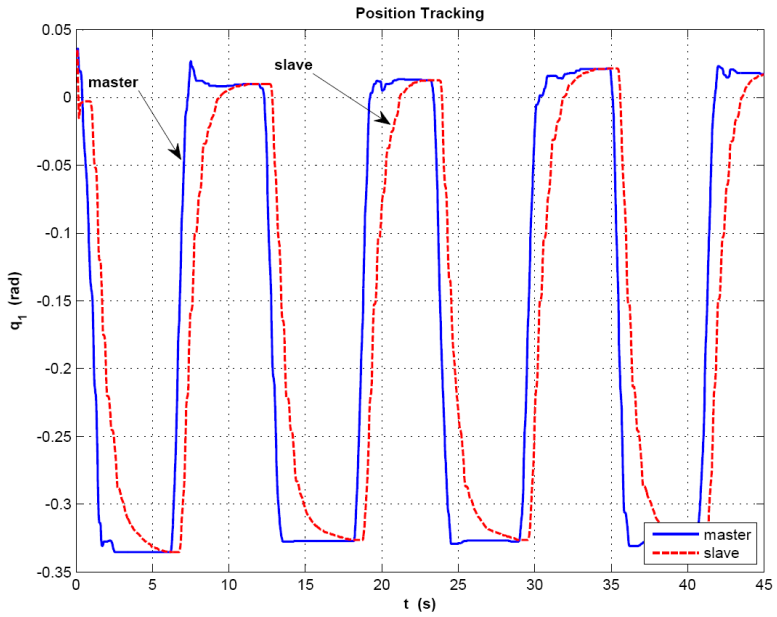

Figure 5.17: Experiment 2 (part. 1) – position tracking response of the teleoperation system with disturbance observers.

Experiment 2 (part. 2): Slave moving in free space

In the second experiment, the human operator moves the master robot and the slave robot, which is moving in free space, should follow the motions of the master robot. The parameters of the synchronizing torques and the disturbance observer are chosen to be identical to the previous experiment. The teleoperation control torques are given by (4.10) and (4.11) with $\hat{\mathbf{G}}_i(\mathbf{q}_i) = 0$. Here, we consider the gravity forces that are acting on the second and the third joints of the robots as disturbances. Also, we consider the human operator's hand force as a disturbance. Again, we can ignore the effect of dynamic uncertainties in the model of the robots since the master and the slave robots do not move very fast in these experiments (see equation (4.7)).

Figure 5.20 depicts the position tracking response of the teleoperation system when no disturbance observers are employed in the teleoperation system. The gravity forces acting on the second and the third joints of the robot cause poor tracking response of the teleoperation system.

Figure 5.21 depicts the position tracking response of the teleoperation system when disturbance observers are employed in the teleoperation system. As it can be observed from the figure, the slave robot closely follows the master robot.

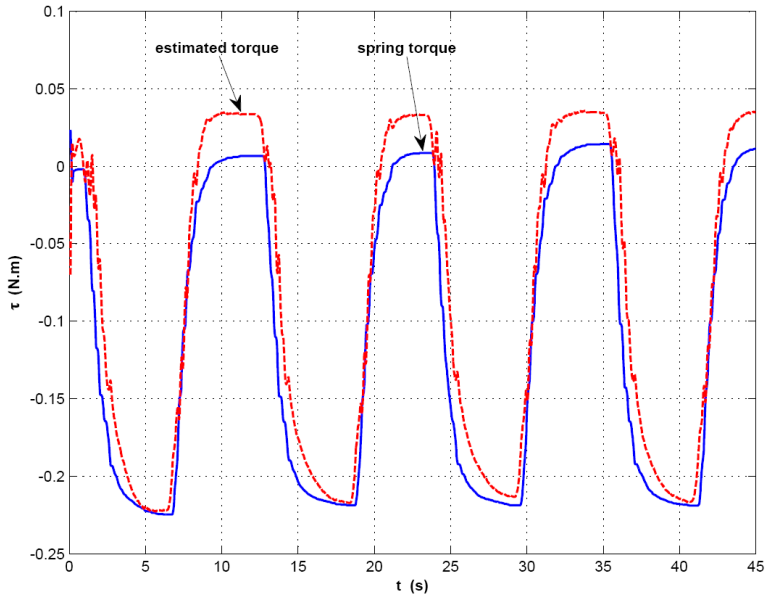

Figure 5.18: Experiment 2 (part. 1)– disturbance tracking at the slave side.

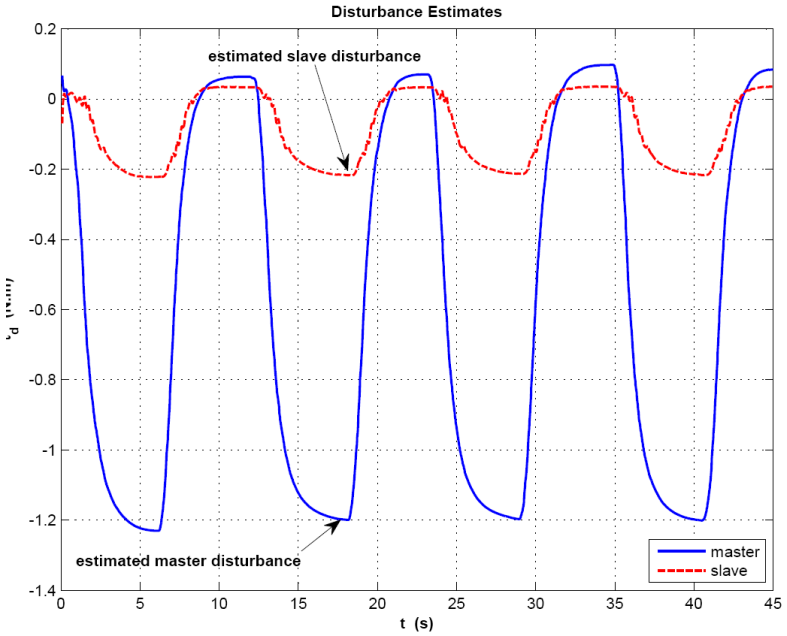

Figure 5.19: Experiment 2 (part. 1)– disturbance tracking at the master and the slave sides.

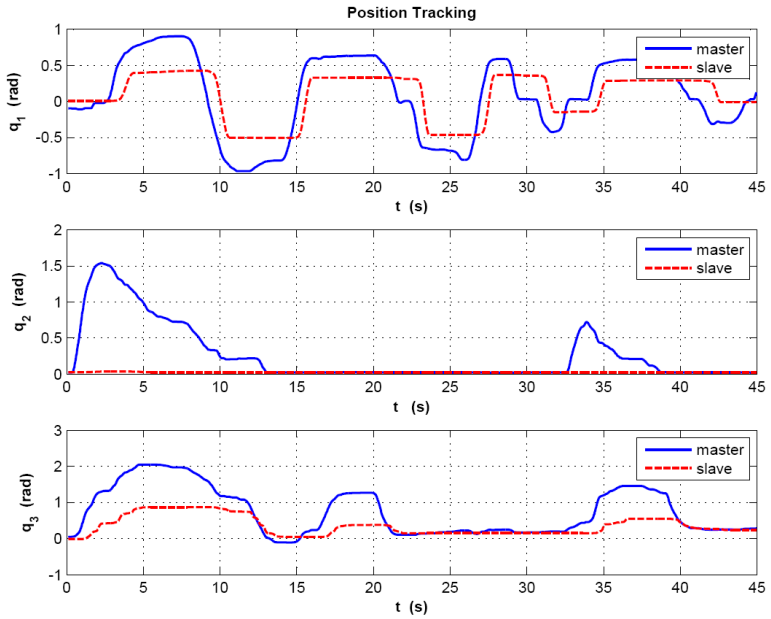

Figure 5.20: Experiment 2 (part. 2)– position tracking response of the teleoperation system without disturbance observers.

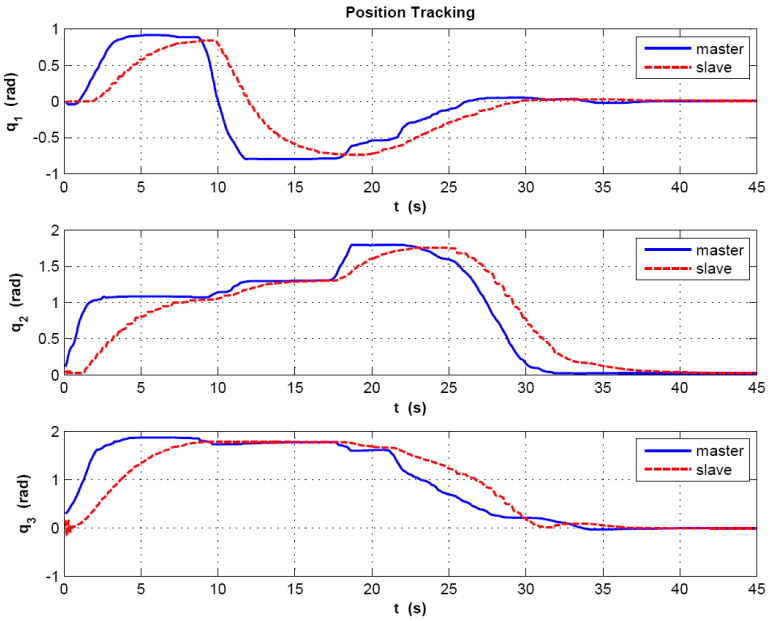

Figure 5.21: Experiment 2 (part. 2)– position tracking response of the teleoperation system with disturbance observers.

Chapter 6

Conclusions and Future Directions

6.1 Conclusions

This thesis addresses (i) the design of nonlinear disturbance observers for robotic systems and (ii) disturbance observer based control of telerobotic systems with variable time delays. The major contributions of the thesis are summarized as follows:

- A general systematic disturbance observer design method for serial robotic manipulators is proposed. The previously proposed linear and nonlinear disturbance observers can be unified in this general framework. Moreover, the proposed design method removes the previous restrictions on the number of degrees-of-freedom, the types of joints, and the manipulator configuration in the design of nonlinear disturbance observers. The observer design problem is formulated as a linear matrix inequality (LMI). The proposed design method guarantees convergence of the observer tracking error to the origin with an exponential rate in the case of slow-varying disturbances. In the case of fast-varying disturbances, the tracking error is shown to be globally uniformly ultimately bounded. The trade-off between the rate of convergence of the tracking error and the sensitivity to measurement noise has been discussed. In addition to the LMI formulation of the design problem, an analytical solution has been proposed.
- Teleoperation systems are subject to different types of disturbances. Such disturbances, when unaccounted for, may cause poor performance and even instability of the teleoperation system. This thesis presents a novel nonlinear bilateral control scheme for telerobotic systems using the concept of disturbance observer based control. Lumping the effects of dynamic uncertainties and external disturbances into a single disturbance term enables us to design

a disturbance observer in order to suppress these disturbances and alleviate their adverse effects on the teleoperation system. The proposed disturbance observer based control law guarantees stability of the teleoperation system in the presence of disturbances and variable communication time delays. Simulations and experiments are presented to verify the effectiveness of the proposed approaches.

6.2 Directions for Future Research

Several potential future research topics are proposed in the following.

1. There is a tradeoff between the performance of the disturbance observer, i.e., the rate of convergence of the disturbance tracking error and the accuracy of the disturbance estimation, and the sensitivity to measurement noise. A possible extension is to design an optimal disturbance observer for robotic manipulators to address such a tradeoff.

2. We assumed that velocity measurements of the joints of a manipulator are available for disturbance estimation. A natural extension of the proposed method is to provide the disturbance observer with the output of a velocity observer, e.g., Nicosia observer [85], when only joint position measurements are available.

3. An important class of manipulators that have not been addressed in this thesis are parallel robotic manipulators. Disturbance observer design problem for parallel robotic manipulators may be addressed as the topic for possible further research.

4. The proposed disturbance observer design method may be employed in sensorless force control of haptic interfaces.

5. The proposed disturbance observer design and the disturbance observer based control of telerobotic systems are carried out in continuous time domain. A natural extension of this work is to carry out the design in discrete time domain. It is also of great importance to address the problem of data packet loss in packet switched communications and consider its effect on the stability of the telerobotic system in the presence of disturbances and variable time delays.

6. The proposed nonlinear disturbance observer based control of telerobotic systems with variable time delays can be extended to the case of 4-channel control architecture in which the interaction forces are exchanged between the local and the remote sides of the teleoperation system in addition to the position information.

Bibliography

[1] A. Radke and Z. Gao, "A survey of state and disturbance observers for practitioners," in *Proc. American Control Conference*, 2006, pp. 5183–5188.

[2] K. Ohnishi, "A new servo method in mechatronics," *Trans. Japan Society of Electrical Engineering*, vol. 107-D, pp. 83–86, 1987.

[3] K. Ohnishi, M. Shibata, and T. Murakami, "Motion control for advanced mechatronics," *IEEE/ASME Trans. Mechatron.*, vol. 1, no. 1, pp. 56–67, Mar. 1996.

[4] S. Komada, M. Ishida, K. Ohnishi, and T. Hori, "Disturbance observer-based motion control of direct drive motors," *IEEE Trans. Energy Convers.*, vol. 6, no. 3, pp. 553–559, Sep. 1991.

[5] B. A. Guvenc, L. Guvenc, and S. Karaman, "Robust mimo disturbance observer analysis and design with application to active car steering," *Int. J. Robust Nonlinear Control*, vol. 20, pp. 873–891, 2010.

[6] T. Umeno and Y. Hori, "Robust speed control of dc servomotors using modern two degrees-of-freedom controller design," *IEEE Trans. Ind. Electron.*, vol. 38, no. 5, pp. 363–368, 1991.

[7] M. Dal and R. Teodorescu, "Disturbance observer based current controller for vector controlled im drives," in *Proc. IEEE Power Electronics Specialists Conf.*, 2008, pp. 2621–2625.

[8] C. Mitsantisuk, K. Ohishi, S. Urushihara, and S. Katsura, "Kalman filter-based disturbance observer and its applications to sensorless force control," *Advanced Robotics*, vol. 25, pp. 335–353, 2011.

[9] B. K. Kim and W. K. Chung, "Advanced disturbance observer design for mechanical positioning systems," *IEEE Trans. Ind. Electron.*, vol. 50, no. 6, pp. 1207–1216, 2003.

[10] S. Komada, N. Machii, and T. Hori, "Control of redundant manipulators considering order of disturbance observer," *IEEE Trans. Ind. Electron.*, vol. 47, no. 2, pp. 413–420, Apr. 2000.

[11] C. S. Liu and H. Peng, "Disturbance observer based tracking control," *ASME Trans. Dyn. Syst. Meas. Control*, vol. 122, no. 2, pp. 332–335, Jun. 2000.

[12] W. H. Chen, D. J. Ballance, P. J. Gawthrop, and J. O'Reilly, "A nonlinear disturbance observer for robotic manipulators," *IEEE Trans. Ind. Electron.*, vol. 47, no. 4, pp. 932–938, Aug. 2000.

[13] A. Nikoobin and R. Haghighi, "Lyapunov-based nonlinear disturbance observer for serial n-link robot manipulators," *J. Intell. Robot. Syst.*, vol. 55, no. 2-3, pp. 135–153, Jul. 2009.

[14] Y. Matsumoto, S. Katsura, and K. Ohnishi, "An analysis and design of bilateral control based on disturbance observer," in *Proc. IEEE Int. Conf. Ind. Technol.*, 2003, pp. 802–807.

[15] P. Hokayem and M. W. Spong, "Bilateral teleoperation: An historical survey," *Automatica*, vol. 42, pp. 2035–2057, 2006.

[16] C. S. Liu and H. Peng, "Disturbance estimation based tracking control for a robotic manipulator," in *Proc. American Control Conference*, 1997, pp. 92–96.

[17] C. Zhongyi, S. Fuchun, and C. Jing, "Disturbance observer-based robust control of free-floating space manipulators," *IEEE Syst. J.*, vol. 2, no. 1, pp. 114–119, Mar. 2008.

[18] S. Park and S. Lee, "Disturbance observer based robust control for industrial robots with flexible joints," in *Proc. Int. Conf. Control, Automation and Systems*, 2007, pp. 2863–2868.

[19] C. H. Choi and N. Kwak, "Robust control of robot manipulator by model-based disturbance attenuation," *IEEE/ASME Trans. Mechatron.*, vol. 8, no. 4, pp. 511–513, Dec. 2003.

[20] K. S. Eom, I. H. Suh, and W. K. Chung, "Disturbance observer based path tracking control of robot manipulator considering torque saturation," in *Proc. Int. Conf. Advanced Robot.*, 1997, pp. 651–657.

[21] B. Bona and M. Indri, "Friction compensation in robotics: an overview," in *Proc. IEEE Conf. Decision and Control*, 2005, pp. 4360–4367.

[22] U. Sawut, N. Umeda, K. Park, T. Hanamoto, and T. Tsuji, "Frictionless control of robot arm with sliding mode observer," in *Proc. Int. Conf. Vehicle Electronics*, 2001, pp. 61–66.

[23] S. H. Kang, M. L. Jin, and P. H. Chang, "A solution to the accuracy/robustness dilemma in impedance control," *IEEE/ASME Trans. Mechatron.*, vol. 14, no. 3, pp. 282–294, Jun. 2009.

[24] S. Chiaverini, B. Siciliano, and L. Villani, "A survey of robot interaction control schemes with experimental comparison," *IEEE/ASME Trans. Mechatron.*, vol. 4, no. 3, pp. 273–285, Sep. 1999.

[25] N. Shimada, K. Ohishi, S. Kumagai, and T. Miyazaki, "Smooth touch and force control to unknown environment without force sensor for industrial robot," in *Proc. IEEE Int. Workshop Advanced Motion Control*, 2010, pp. 36–41.

[26] S. Katsura, Y. Matsumoto, and K. Ohnishi, "Modeling of force sensing and validation of disturbance observer for force control," in *Proc. IEEE Conf. Ind. Electron. Society*, 2003, pp. 291–296.

[27] K. Eom, I. Suh, W. Chung, and S.-R. Oh, "Disturbance observer based force control of robot manipulator without force sensor," in *Proc. IEEE Int. Conf. Robot. Autom.*, 1998, pp. 3012–3017.

[28] Y. H. Tan, D. Sun, W. H. Huang, and S. H. Chen, "Mechanical modeling of biological cells in microinjection," *IEEE Trans. Nanobioscience*, vol. 7, no. 4, pp. 257–266, Dec. 2008.

[29] M. Rakotondrabe, C. Clevy, K. Rabenorosoa, and K. Ncir, "Presentation, force estimation and control of an instrumented platform dedicated to automated micromanipulation tasks," in *Proc. IEEE Conf. Automation Science and Engineering*, 2010, pp. 722–727.

[30] F. Caccavale, P. Cilibrizzi, F. Pierri, and L. Villani, "Actuators fault diagnosis for robot manipulators with uncertain model," *Cont. Eng. Pract.*, vol. 17, no. 1, pp. 146–157, Jan. 2009.

[31] H. Sneider and P. Frank, "Observer-based supervision and fault detection in robots using nonlinear and fuzzy logic residual evaluation," *IEEE Trans. Control Syst. Technol.*, vol. 4, no. 3, pp. 274–282, May 1996.

[32] S. P. Chan, "A disturbance Observer for robot manipulators with application to electronic components assembly," *IEEE Trans. Ind. Electron.*, vol. 42, no. 5, pp. 487–493, Oct. 1995.

[33] A. S. Smadi and F. Yasutaka, "On nonlinear disturbance observer based tracking control for euler-lagrange systems," *J. System Design and Dynamics*, vol. 3, no. 3, pp. 330–343, 2009.

[34] C. Melchiorri and P. Arcara, "Control schemes for teleoperation with time delay: A comparative study," *Robot. Auton. Syst.*, vol. 38, pp. 49–64, 2002.

[35] C. Melchiorri, "Robotic telemanipulation systems: An overview on control aspects," in *Proc. IFAC Symp. Robot Control*, 2003, pp. 707–716.

[36] T. B. Sheridan, "Telerobotics," *Automatica*, vol. 25, no. 4, pp. 487–507, Jul. 1989.

[37] G. Niemeyer, C. Preusche, and G. Hirzinger, "Telerobotics," in *Springer Handbook of Robotics*, B. Siciliano and O. Khatib, Eds. Springer-Verlag, 2008, pp. 741–757.

[38] W. Wang and K. Yuan, "Teleoperated manipulator for leak detection of sealed radioactive sources," in *Proc. IEEE Int. Conf. Robot. Autom. Proc.*, 2004, pp. 1682–1687.

[39] J. Funda and R. P. Paul, "A symbolic teleoperator interface for time-delayed underwater robot manipulation," in *Proc. Ocean Technologies and Opportunities in the Pacific for the 90s*, 1991, pp. 1526–1533.

[40] W. K. Yoon, T. Goshozono, H. Kawabe, M. Kinami, Y. Tsumaki, M. Uchiyama, M. Oda, and T. Doi, "Model-based space robot teleoperation of ets-vii manipulator," *IEEE Trans. Robot. Autom.*, vol. 20, no. 3, pp. 602–612, Jun. 2004.

[41] J. N. Lim, J. P. Ko, and J. M. Lee, "Internet-based teleoperation of a mobile robot with force-reflection," in *Proc. IEEE Conf. Control Applicat.*, 2003, pp. 680–685.

[42] H. L. Karamanoukian, R. U. Pande, Y. Patel, A. M. Freeman, P. S. Aoukar, and G. D'Ancona, "Telerobotics, telesurgery, and telementoring," *Pediatric Endosurgery & Innovative Techniques*, vol. 7, no. 4, pp. 421–425, Dec. 2003.

[43] A. J. Madhani, G. Niemeyer, and J. K. Salisbury, "The black falcon: A teleoperated surgical instrument for minimally invasive surgery," in *Proc. IEEE/RSJ Int. Conf. Intell. Robots Syst.*, 1998, pp. 936–944.

[44] G. S. Guthart and J. K. Salisbury, "The intuitive telesurgery system: Overview and application," in *Proc. IEEE Int. Conf. Robot. Autom.*, 2000, pp. 618–621.

[45] E. O. Kwon, T. C. Bautista, J. M. Blumberg, H. Jung, K. Tamaddon, S. R. Aboseif, S. G. Williams, and G. W. Chien, "Rapid implementation of a robot-assisted prostatectomy program in a large health maintenance organization setting," *J. Endourol.*, vol. 24, no. 3, pp. 461–465, Mar. 2010.

[46] Z. Nawrat, "Medical robots in cardiac surgery," *Kardiochirurgia I Torakochirurgia Polska*, vol. 5, no. 4, pp. 440–447, Dec. 2008.

[47] R. W. Holloway, S. D. Patel, and S. Ahmad, "Robotic surgery in gynecology," *Scandinavian J. Surgery*, vol. 98, no. 2, pp. 96–109, 2009.

[48] D. Repperger, C. Phillips, J. Berlin, A. Neidhard-Doll, and M. Haas, "Human-machine haptic interface design using stochastic resonance methods," *IEEE Trans. Syst., Man, Cybern. A, Syst., Humans*, vol. 35, no. 4, pp. 574–582, Jul. 2005.

[49] C. Wagner and R. D. Howe, "Mechanisms of performance enhancement with force feedback," in *Proc. World Haptics Conference*, 2005, pp. 21–29.

[50] C. M. Yip, M. Tavakoli, and R. D. Howe, "Performance analysis of a haptic telemanipulation task under time delay," *Advanced Robotics*, vol. 25, pp. 651–673, 2011.

[51] J. Cui, S. Tosunoglu, R. Roberts, C. Moore, and D. W. Repperger, "A review of teleoperation system control," in *Proc. Florida Conf. Recent Advances in Robotics*, 2003, pp. 1–12.

[52] R. J. Anderson and M. W. Spong, "Bilateral control of teleoperators with time delay," *IEEE Trans. Automat. Contr.*, vol. 34, no. 5, pp. 494–501, May 1989.

[53] T. B. Sheridan, "Space teleoperation through time delay: review and prognosis," *IEEE Trans. Robot. Autom.*, vol. 9, no. 5, pp. 592–606, Oct. 1993.

[54] A. K. Bejczy and W. S. Kim, "Predictive displays and shared compliance control for time-delayed telemanipulation," in *Proc. IEEE/IRSJ Int. Conf. Robot. Autom.*, 1990, pp. 546–551.

[55] . German Aerospace Center (DLR), "Rotex: Robot experiment technology on spacelab d2-mission," http://www.dlr.de/rm/en/desktopdefault.aspx/tabid-3827/5969_read-8744/.

[56] J. Marescaux, J. Leroy, M. Gagner, F. Rubino, D. Mutter, M. Vix, S. E. Butner, and M. K. Smith, "Transatlantic robot-assisted telesurgery," *Nature*, vol. 413, no. 6854, pp. 379–380, 2001.

[57] R. Oboe and P. Fiorini, "A design and control environment for internet-based telerobotics," *Int. J. Robot. Res.*, vol. 17, no. 4, pp. 433–499, Apr. 1998.

[58] W. R. Ferrell, "Delayed force feedback," *IEEE Trans. Human Factors*, vol. 8, no. 5, pp. 449–455, Oct. 1966.

[59] E. Nuno, L. Basanez, R. Ortega, and M. W. Spong, "Position tracking for non-linear teleoperators with variable time delay," *Int. J. Robot. Res.*, vol. 28, no. 7, pp. 895–910, Jul. 2009.

[60] G. Niemeyer and J. J. E. Slotine, "Stable adaptive teleoperation," *IEEE Trans. Ocean. Eng.*, vol. 16, no. 1, pp. 152–162, Jan. 1991.

[61] ——, "Telemanipulation with time delays," *Int. J. Robot. Res.*, vol. 23, no. 9, pp. 873–890, Sep. 2004.

[62] N. A. Tanner and G. Niemeyer, "Improving perception in time-delayed telerobotics," *Int. J. Robot. Res.*, vol. 24, no. 8, pp. 631–644, Aug. 2005.

[63] S. Munir and W. Book, "Internet-based teleoperation using wave variables with prediction," *IEEE/ASME Trans. Mechatron.*, vol. 7, no. 2, pp. 124–133, Jun. 2002.

[64] N. Chopra, M. W. Spong, R. Ortega, and N. Barbanov, "On tracking performance in bilateral teleoperation," *IEEE Trans. Robot.*, vol. 22, no. 4, pp. 844–847, Aug. 2006.

[65] T. Namerikawa and H. Kawada, "Symmetric impedance matched teleoperation with position tracking," in *Proc. IEEE Conf. Decision and Control*, 2006, pp. 4496–4501.

[66] N. Chopra, P. Berestesky, and M. W. Spong, "Bilateral teleoperation over unreliable communication networks," *IEEE Trans. Contr. Syst. Technol.*, vol. 16, no. 2, pp. 304–313, Mar. 2008.

[67] S. Munir and W. Book, "Control techniques and programming issues for time delayed internet based teleoperation," *ASME J. Dyn. Syst. Meas. Contr.*, vol. 125, no. 2, pp. 205–214, Jun. 2003.

[68] Y. Yokokohji, T. Tsujioka, and T. Yoshikawa, "Bilateral control with time-varying delay including communication blackout," in *Proc. Symp. Haptic Interfaces for Virtual Environment and Teleoperator Systems*, 2002, pp. 285–292.

[69] A. Gupta and M. K. O'Malley, "Disturbance-observer-based force estimation for haptic feedback," *J. Dyn. Syst.-T. ASME*, vol. 133, no. 1, 2011.

[70] D. S. Kwon, K. Y. Woo, and H. S. Cho, "Haptic control of the master hand controller for a microsurgical telerobot system," in *Proc. IEEE Int. Conf. Robotics and Automation*, 1999, pp. 1722–1727.

[71] S. Lichiardopol, N. van de Wouw, D. Kostic, and H. Nijmeijer, "Trajectory tracking control for a tele-operation system setup with disturbance estimation and compensation," in *Proc. IEEE Conf. Decision and Control*, 2010, pp. 1142–1147.

[72] K. Natori, T. Tsuji, K. Ohnishi, A. Hace, and K. Jezernik, "Time-delay compensation by communication disturbance observer for bilateral teleoperation under time-varying delay," *IEEE Trans. Ind. Electron.*, vol. 57, no. 3, pp. 1050–1062, Mar. 2010.

[73] K. Natori, R. Kubo, and K. Ohnishi, "Transparency of time delayed bilateral teleoperation systems with communication disturbance observer," in *Proc. IEEE Int. Conf. Mechatron.*, 2007, pp. 1–6.

[74] K. Natori, T. Tsuji, and K. Ohnishi, "Time delay compensation by communication disturbance observer in bilateral teleoperation systems," in *Proc. IEEE Int. Workshop Adv. Motion Control*, 2006, pp. 218–223.

[75] N. Iiyama, K. Natori, and K. Ohnishi, "Bilateral teleoperation under time-varying communication time delay considering contact with environment," *Electronics and Communications in Japan*, vol. 92, no. 7, pp. 38–46, 2009.

[76] A. Mohammadi, H. J. Marquez, and M. Tavakoli, "A systematic disturbance observer design method for robotic manipulators," in *Proc. IEEE Conf. Decision and Control*, 2011, submitted for publication.

[77] H. J. Marquez, *Nonlinear Control Systems*. Hoboken, NJ: John Wiley & Sons, Inc., 2003.

[78] P. Gahinet, A. Nemirovsky, and C. M. Laub, A. J., *LMI Control Toolbox: For Use With MATLAB*. Natick, MA: The Math Works, Inc., 1995.

[79] H. K. Khalil, *Nonlinear Systems*. Prentice Hall, 2nd edn., 1996.

[80] M. W. Spong, S. Hutchinson, and M. Vidyasagar, *Robot Modeling and Control*. New York: Wiley, 2005.

[81] J. I. Mulero-Martinez, "Uniform bounds of the Coriolis/centripetal matrix of serial robot manipulators," *IEEE Trans. Robot.*, vol. 23, no. 5, pp. 1083–1089, Oct. 2007.

[82] E. Nuno, L. Basanez, and R. Ortega, "Control of teleoperators with time-delay: a lyapunov approach," in *Topics in Time Delay Systems*, J. J. Loiseau, W. Michiels, N. S.-I., and R. Sipahi, Eds. Springer-Verlag, 2009, pp. 371–381.

[83] J. J. Craig, *Introduction to Robotics: Mechanics and Control*. Upper Saddle River, NJ: Pearson Prentice Hall, 2005.

[84] P. H. Chang and L. J. W., "Time delay observer: a robust observer for non-linear plants using time delayed signals," in *Proc. American Control Conf.*, 1995, pp. 1638–1642.

[85] S. Nicosia and P. Tomei, "Robot control by using only joint position measurements," *IEEE Trans. Automat. Contr.*, vol. 35, no. 9, pp. 1058–1061, Sep. 1990.

[86] A. Levant, "Robust exact differentiation via sliding mode technique," *Automatica*, vol. 34, no. 3, pp. 379–384, Mar. 1998.

[87] P. Voglewede, A. Smith, and A. Monti, "Dynamic performance of a scara robot manipulator with uncertainty using polynomial chaos theory," *IEEE Trans. Robot.*, vol. 25, no. 1, pp. 206–210, Feb. 2009.

[88] H. Liu, T. Wei, and X. Wang, "Signal decomposition and fault diagnosis of a scara robot based only on tip acceleration measurement," in *Proc. IEEE Int. Conf. Mechatron. Autom.*, 2009, pp. 4811–4816.

[89] M. R. Kermani, R. V. Patel, and M. Moallem, "Friction identification and compensation in robotic manipulators," *IEEE Trans. Instrum. Meas.*, vol. 56, no. 6, pp. 2346–2353, 2007.

[90] B. Armstrong-Hélouvry, P. Dupont, and C. Canudas de Wit, "A survey of models, analysis tools and compensation methods for the control of machines with friction," *Automatica*, vol. 30, no. 7, pp. 1083–1138, 1994.

[91] M. Hou, G. Duan, and M. Guo, "New versions of barbalat's lemma with applications," *J. Contr. Theory Appl.*, vol. 8, no. 4, pp. 545–547, 2010.

[92] J. E. Speich, L. Shao, and M. Goldfarb, "Modeling the human hand as it interacts with a telemanipulation system," *Mechatronics*, vol. 15, no. 9, pp. 1127–1142, 2005.

[93] J. Colgate and N. Hogan, "Robust control of dynamically interacting systems," *Int. J. Control*, vol. 48, no. 1, pp. 65–88, 1988.

[94] N. Hogan, "Controlling impedance at the man/machine interface," in *Proc. IEEE. Int. Conf. Robot. Autom.*, 1989, pp. 1621–1631.

[95] H. Gao, T. Chen, and J. Lam, "A new delay system approach to network-based control," *Automatica*, vol. 44, pp. 39–52, 2008.

[96] N. Hung, H. Tuan, T. Narikiyo, and P. Apkarian, "Adaptive control for nonlinearly parameterized uncertainties in robot manipulators," *IEEE Trans. Cont. Syst. Technol.*, vol. 16, no. 3, pp. 458–468, 2008.

[97] D. Chen, X. Fu, W. Ding, H. Li, N. Xi, and Y. Wang, "Shifted gamma distribution and long-range prediction of roundtrip timedelay for internet-based teleoperation," in *Proc. IEEE Int. Conf. Robotics and Biomimetics*, 2008, pp. 1261–1266.

[98] S. Kim, J. Y. Lee, and D. K. Sung, "A shifted gamma distribution model for long-range dependent internet traffic," *IEEE Commun. Lett.*, vol. 7, no. 3, pp. 124–126, Mar. 2003.

[99] A. Mohammadi, M. Tavakoli, and A. Jazayeri, "Phansim: A simulink toolkit for the sensable phantom haptic devices," in *Proc. Canadian Congress of Applied Mechanics*, Vancouver, BC, Jun. 2011, pp. 787–790.

[100] A. C. Fyans and G. McAllister, "Creating games with feelings," in *Proc. Int. Conf. Computer Games*, 2008, pp. 94–98.

[101] P. Trier, K. O. Noe, M. S. Sorenson, and J. Mosegaard, "The visilbe ear surgery simulator," in *Proc. Conf. Medicine Meets Virtual Reality*, 2008, pp. 523–525.

[102] E. J. Veras, K. J. De Laurentis, , and R. Dubey, "Design and implementation of visual-haptic assistive control system for virtual rehabilitation exercise and teleoperation manipulation," in *Proc. IEEE EMBS Conf.*, 2008, pp. 4290–4293.

[103] C. Tzafestas, S. Velanas, and G. Fakiridis, "Adaptive impedance control in haptic teleoperation to improve transparency under time-delay," in *Proc. IEEE Int. Conf. on Robot. Autom.*, 2008, pp. 212–219.

[104] E. Naerum, J. Cornella, and O. J. Elle, "Contact force estimation for back-drivable robotic manipulators with coupled friction," in *Proc. IEEE Int. Conf. Intell. Robots Syst.*, 2008, pp. 3021–3027.

[105] W. E. Dixon, D. Moses, I. D. Walker, and D. M. Dawson, "A simulink-based robotic toolkit for simulation and control of the puma 560 robot manipulator," in *Proc. IEEE/RSJ Int. Conf. Intel. Robots. Syst.*, 2001, pp. 2202–2207.

[106] F. Chinello, S. Scheggi, F. Morbidi, and D. Prattichizzo, "Kct: a matlab toolbox for motion control of kuka robot manipulators," in *Proc. IEEE Int. Conf. on Robot. Autom.*, 2010, pp. 4603–4608.

[107] M. Eriksson and J. Wikander, "A haptic interface using matlab/simulink," Sweden, Stockholm: Mechatronics Laboratory and Machine Design, KTH, Tech. Rep., 2010. [Online]. Available: http://www.md.kth.se/body/research/projects/mda/p13/AHapticInterfaceUsingMatlab.pdf

[108] B. Taati, A. M. Tahmasebi, and K. Hashtrudi-Zaad, "Experimental identification and analysis of the dynamics of a phantom premium 1.5a hatpic device," *Presence*, vol. 17, no. 4, pp. 327–342, Aug. 2008.

[109] M. C. Cavusoglu and D. Feygin, "Kinematics and dynamics of phantom model 1.5, haptic interface," EECS Department, University of California, Berkeley, Tech. Rep. UCB/ERL M01/15, 2001. [Online]. Available: http://www.eecs.berkeley.edu/Pubs/TechRpts/2001/9579.html

[110] T. Soderstrom and P. Stoica, *System Identification*. Prentice Hall International Ltd, 1989.